THESIS

USING CONTROLLED SUBSURFACE RELEASES TO INVESTIGATE THE EFFECT OF LEAK VARIATION ON ABOVE-GROUND NATURAL GAS DETECTION

Submitted by

Mercy W. Mbua

Department of Systems Engineering

In partial fulfillment of the requirements

For the Degree of Master of Science

Colorado State University

Fort Collins, Colorado

Summer 2023

Master's Committee:

Advisor: Stuart N. Riddick
Co-Advisor: Daniel J. Zimmerle

Joseph von Fischer

Copyright by Mercy Mbua 2023

All Rights Reserved

ABSTRACT

USING CONTROLLED SUBSURFACE RELEASES TO INVESTIGATE THE EFFECT OF LEAK VARIATION ON ABOVE-GROUND NATURAL GAS DETECTION

Leaks from underground natural gas (NG) pipelines pose safety and environmental concerns. Pipeline leak detection generally relies on measuring surface methane (CH_4) enhancements during walking surveys and/or mobile surveys that attempt to identify CH_4 plumes downwind of the pipeline. The likelihood of plume detection is dependent on the above-ground CH_4 plume width. The size and shape of the plume is primarily dependent on environmental conditions but could also be complicated by leak characteristics. To investigate the effect of leak characteristics on CH_4 plume width, this study uses controlled release experiments to observe above-ground plume width changes with changes in the gas composition, leak rate, and leak depth. Results show that plume width generally decreases with increased NG density, decreased leak rate and increases with depth between 0.6 and 0.9 m, but the above surface plume is undetectable above the background for leaks 1.8 m deep. The study established that the effect of adding heavy hydrocarbons to the NG mixture on plume width is equivalent to the effect of increased leak rate and depth on plume width multiplied by -0.04 and -0.89, respectively, with overall relative uncertainty of -42/ +14 %. This shows that reported leaks in areas with heavier hydrocarbons could currently be missed or underestimated. Further, this study shows that leaks from pipelines laid in covers meeting the Colorado Oil and Gas Conservation Commission minimum depth requirement of 0.9 m could be easier to detect compared to those buried at depths less than the minimum depth. Applying the findings to a real-world scenario, the study illustrates that a successful leak survey protocol tuned to NG leaks from Fayetteville shale (0.66 g/L NG density) may result in missed detections in the Permian, where NG is heavier (1.01 g/L) due to higher percentages of heavy hydrocarbons. Overall, this study illustrates that leak survey protocols for flowlines and gathering lines should be different from distribution pipelines and tailored to the compositions of the transported NG to report emissions accurately.

Keywords: natural gas; pipeline; surveys; subsurface; upstream production; flowlines; gathering lines

ACKNOWLEDGEMENTS

Professor Stuart Riddick: I'm so grateful to Dr. Stuart for taking the time to teach, train and coach me through everything I have known in this project. Thank you for your patience, mentorship, guidance, reading, and giving me feedback on my work numerous times.

Professor Daniel Zimmerle: I would like to express my most sincere gratitude for giving me a chance as a student in your Dan Zimmerle Research Group. I truly appreciate you asking me tough questions regarding my research, pushing me to work harder to produce quality work, and taking the time to give me feedback despite your busy schedule.

Professor Joseph von Fischer: Thank you for agreeing and taking the time to be part of my thesis committee despite your busy schedule, and giving me great feedback on real world application of my research.

UPSIDE/RPLUME team members: Professor Daniel Zimmerle, Professor Stuart Riddick, Professor Kate Smits, Fancy Cheptonui, Dr. Tian Shanru, Dr. Younki Cho, Cade Houlihan, Navodi Jayarathne, Richie Kolodziej, Jui Hsiang Lo, and Hartzell Wendy. Thank you for sharing with me your knowledge, and constructive criticism and for supporting me in this project.

METEC Group: Aidan Duggan, Ilonze Chiemezie, Peter Ronney, Kristine Bennett, and Andy Bollman. Thank you for supporting me in this project.

I would like to thank all members of the Zimmerle Research Group for your insightful feedback on this project and for supporting me the whole period.

Lastly, I thank the Cogen Fellowship, Department of Systems Engineering, and Mark Martinez & Joey Irwin Memorial Public Projects Fund through the Colorado Oil and Gas Conservation Commission (COGCC) for funding my studies and research project.

DEDICATION

My family: Dr. Francis Wanjala Otinga and Leo Harvey Otinga, Mbuas, Otingas, and my wonderful friends.

To all who believed in me!

TABLE OF CONTENTS

LIST OF TABLES

LIST OF FIGURES

LIST OF SYMBOLS

Bcf/d	Billion cubic feet/day
Tcf	Trillion cubic feet
ppm	Parts per million
ppb	Parts per billion
cm	Centimeters
m	Meters
Tg	Teragram
Gg	Gigagrams
kg	Kilograms
g	Grams
h	Hour
k	Kelvin
atm	Atmosphere
rms	Root mean square
slpm	Standard liters per minute

1 INTRODUCTION

1.1 US natural gas

In 2022, US natural gas (NG) production grew by 4% from 2021, averaging 119 Bcf d^{-1}, with Appalachia, Permian, and Haynesville accounting for 60% of the production (EIA, 2023b). The total NG imports increased by 7.7% from 7.7 Bcf d^{-1} in 2021 to 8.3 Bcf d^{-1} in 2022; highest total NG import since 2017 (EIA, 2023a). Natural gas consumption reached a record of 88.5 Bcf d^{-1} (since EIA began tracking in 1949), representing a 5.4% increase from 84.0 Bcf d^{-1} in 2021 (EIA, 2023a). Natural gas is transferred from production sites to consumers via pipelines, extending over 3 million miles in the US. In 2021, the NG pipeline transportation network delivered about 27.6 Tcf of NG to approximately 77.7 million consumers (EIA, 2022). Natural gas transportation network consists of a series of steps that generally are: a) gathering systems made up of small diameter, low-pressure pipelines moving NG from the wellhead to the processing plant or to a larger mainline pipeline; b) NG processing plants that separate the hydrocarbons gas/liquids, nonhydrocarbon gases and water from the NG, before transferring to a mainline transmission system; c) wide-diameter, high-pressure interstate transmission pipelines transporting NG from the processing facility to distribution centers and storage facilities; and d) local distribution pipelines that deliver NG to consumers through small-diameter, lower pressure service lines (EIA, 2022).

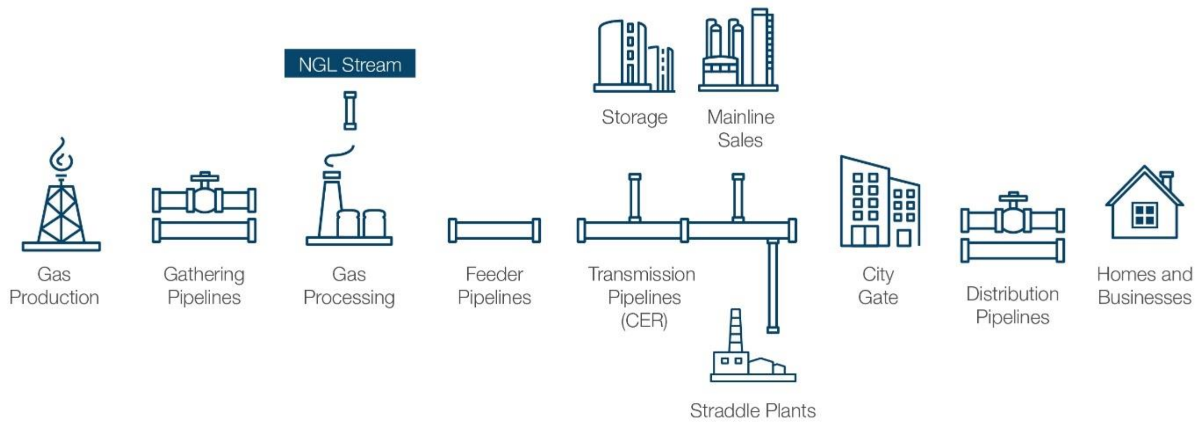

Figure 1 Overview of a gas pipeline system (Government of Canada, 2022)

1.2 Pipeline leaks

Natural gas pipeline leaks can occur due to external interference, corrosion, material failure, or earth movement. Pipeline leaks are both a climate and safety threat as methane (CH_4), the primary component of NG, is a potent greenhouse gas (GWP_{20} = 85; GWP_{100} = 27) (IEA, 2021) and combustible at concentrations between 5 and 15% in the air (National Research Council (US) Committee on Toxicology, 1984; Takahashi et al., 1998). Between 2002 and 2021 in the US, 12,793 pipeline incidents resulted in 276 fatalities, 1,144 injuries, and $10 billion in damage (PHMSA, 2022).

Various studies have reported CH_4 emission estimates in various segments of NG transportation. Zimmerle et al. (2015) estimated transmission and storage emissions at 1503 Gg yr^{-1}. Weller et al. (2020) estimated emissions from pipeline mains in distribution systems at 690 Gg yr^{-1}. The 2022 US Environmental Protection Agency inventory reported emissions from NG systems at 6478 Gg, with 1548 Gg from gathering and boosting (EPA, 2023). To accurately report emissions, especially from NG pipelines throughout the transportation network, it is crucial to understand emissions from underground pipelines. Currently, subsurface pipelines pose challenges to detection and ultimate repair of leaks due to a) the diffuse presentation of a subsurface leak as an area source, b) effects of subsurface properties such as CH_4 oxidation and soil conditions, and c) effects of atmospheric conditions such as wind speed and atmospheric stability.

1.3 Pipeline leak detection

Finding subsurface leaks falls under leak detection and quantification (LDAQ) methods that measure surface and above-ground CH_4 enhancements (henceforth, enhancement refers to concentrations above the background). The two broad LDAQ areas are survey methods and continuous monitoring.

1.3.1 Continuous monitoring

Methane or total hydrocarbon (THC) sensors are installed above or below ground. Below-ground monitoring systems are deployed during pipeline installation, internal or external to the pipeline (Fox et al., 2022). Internal systems are installed within the pipeline, measuring gas properties using volume-based, pressure-based, and mass-balance monitoring systems (Fox et al., 2022). These systems alert an operator of a leak when there is a change in gas flux between two sensor locations, and a follow-up is performed. In general, continuous monitors localize leaks coarsely, necessitating survey methods as a follow-up. LDAQ cost per unit length is a tradeoff between coverage (length of pipe covered) and survey speed and generally favors survey methods over continuous monitoring.

1.3.2 Survey methods

Above-ground leak detection methods for buried pipelines include visual, audio, and olfactory methods, where surveyors look for dead vegetation, listen for hissing sounds, or use personnel or animals to detect the smell of mercaptan (a sulfur compound added to non-industrial NG to aid leak detection). These relatively simple methods are applicable only for leaks that have persisted for a long time (dead vegetation), leaks from pipelines at shallow depths (hissing), and do not apply to upstream sectors where mercaptan has not yet been added to NG.

A walking survey is a common approach used in pipeline leak detection, particularly in distribution systems. In this method, a surveyor walks along the pipeline at approximately 1 m s^{-1} with a handheld CH_4 or THC instrument such as the HEATH Detecto Pak-Infrared (DP-IR™; detection method: infrared controlled interface polarization spectrometer; measurement range: 0-10,000 ppm; sensitivity: 1 ppm; accuracy: ± 0.5%) (HEATH, 2022). As surveyors walk, air is sampled by tapping the instrument's inlet on the ground or waving it a few centimeters above the ground. A leak is indicated when a CH_4/THC enhancement is detected.

Another commonly used approach is a ground-based mobile survey. In this approach, CH_4/THC instrument such as the ABB LGR-ICOS™ GLA131-GGA micro portable greenhouse gas analyzer (detection method: laser absorption spectrometer; measurement range: 0-100 ppm CH_4; precision: < 0.9 ppb (1 sec); frequency: 0.01-10 Hz) (ABB, 2023), is mounted on a mobile platform (e.g., car) between 0.3 and 5 m above ground level (AGL), (Caulton et al., 2018; "Discover Advanced Mobile Leak Detection (AMLD)," 2023; Jackson et al., 2014; Phillips et al., 2013) and driving at speeds of between 4 and 13 m s^{-1} (Eapi et al., 2014; von Fischer et al., 2017; Weller et al., 2019).

Other survey options include low-level unmanned aerial vehicles (UAVs) traveling at speeds between 3 and 23 m s^{-1}, between 2 and 15 m AGL (Akande et al., 2021; Barchyn et al., 2018; Bretschneider & Shetti, 2014; Castenschiold et al., 2022; Fox et al., 2022; Gas Technology Institute, 2022; Yang et al., 2018). Subsurface leak detection from remote sensing LDAQ methods, such as aircraft and satellites, is generally feasible for large leaks (100+ kg h^{-1}). Aircraft and satellite detection limits are not well understood for underground leaks, but for above-ground point sources, aircraft sensors range from 3 to 10s kg CH_4 h^{-1} (Duren et al., 2019) and 100+ kg CH_4 h^{-1} (Cooper et al., 2022) for satellites.

2 LITERATURE REVIEW

Even though most mobile leak survey methods for pipeline leaks rely on above-ground instruments for leak detection, few methods consider the dimensions of the emitted plume in survey practice, specifically how the plume changes depending on leak conditions. Natural gas properties, subsurface conditions, surface factors, and atmospheric factors influence the size of the above-ground CH_4 plume encountered during a mobile survey.

2.1 Gas properties, subsurface, and surface effects on above-ground plume

Natural gas properties such as gas density, viscosity, molecular weight, specific gravity, pressure, and temperature determine the advective and diffusive mechanisms of NG transport through soil (Scanlon et al., 2001). Subsurface and surface conditions such as soil textural configuration, soil moisture, surface cover, other underground infrastructure, and methanotrophic oxidation affect how far and how fast NG travels through the soil before venting into the atmosphere (Gao et al., 2021; Jayarathne et al., 2022; Riddick et al., 2021).

2.2 Atmospheric effects on above-ground plume

Atmospheric conditions such as wind speed, atmospheric stability, relative humidity, air pressure, and air temperature influence atmospheric gas dispersion and, thus, determine the size and height of the above-ground enhancements (commonly "plume") (Tian, 2022). Atmospheric stability is particularly applicable as it provides a multivariable way of classifying the mean atmospheric state. During unstable conditions, the environmental lapse rate is greater than the dry adiabatic lapse rate; the rising air is warmer than its surrounding; hence, the air rises and disperses (Nugent & DeCou, 2019). During stable conditions, the environmental lapse rate is lower than the moist adiabatic lapse rate; the rising air is cooler than its surrounding; hence, gas is trapped close to the ground. During neutral conditions, the environmental and dry adiabatic lapse rates are equal, and gas disperses vertically and horizontally equally from the emission area (Nugent & DeCou, 2019). Neutral conditions provide the best conditions for leak detection downwind of the leak source. Generally, the plume grows vertically and horizontally due to medium to high wind speeds > 3 m s^{-1}, slight to moderate daytime insolation, and thin overcast in night-time conditions (Kahl & Chapman, 2018), forming the emitted gas into a conical shape downwind.

2.3 Variation in leak properties

Further complicating leak detection is the need to understand the effects of gas composition, leak rate, and leak depth on the above-ground plume development under varying environmental conditions.

2.3.1 Gas composition

Understanding the effect of gas composition indicates whether leak detection methods or protocols need to be modified for use in the upstream and downstream NG supply chain sectors. Natural gas transported by flowlines/gathering lines in the upstream sector can be "wet" gas, indicating the presence of heavier hydrocarbons, non-hydrocarbon compounds such as CO_2, high water content, and residual oil or condensates in pipelines. Sectors downstream of gas processing (transmission and distribution) transport refined NG, primarily CH_4 with 3-15% ethane (C_2H_6) and smaller components of other gases. The heavy hydrocarbons in flowlines/gathering lines vary across basins. For example, NG produced from the Denver-Julesburg basin is 83% CH_4, 10% C_2H_6, and 3% propane (C_3H_8) (Howard et al., 2015), while in the Permian Basin, gas is much wetter with 66% CH_4, 13% C_2H_6, 10% C_3H_8, 5% butane (C_4H_{10}), 2% pentane (C_5H_{12}), and 1% hexane (C_6H_{14}) (Robbins et al., 2020). This study investigates how changes in the mix of hydrocarbons transported in a pipeline impact a leak's atmospheric plume, hence the detection by LDAQ methods. Hereafter, the study refers to all gas types, whether upstream (produced gas), midstream, or distribution, as 'natural gas' (NG).

Several studies have addressed the influence of gas composition on subsurface NG flow. Subsurface gas transport occurs due to pressure and concentration gradients. Pressure gradients may result from pipeline pressure, barometric pressure fluctuations, water table fluctuations, or density gradients (Falta et al., 1989; Mendoza & Frind, 1990). Gases with high molecular weight result in steeper density gradients, reducing the advective effect, thus, slowing gas migration through the soil into the atmosphere. As gas vents into the atmosphere, NG components of different densities mix with air, and the resulting density gradients influence gas transport close to the wind-exposed soil surface (Bahlmann et al., 2020). Above the surface, gas is entrained in airflow and disperses downwind of the leak point as a function of atmospheric conditions. While the physical mechanisms are reasonably understood, studies have yet to address how gas composition impacts the release of gas into the air and its 3D movement in air.

2.3.2 Leak rate and depth

In addition to gas composition, previous studies have investigated the influence of leak rates and depth on subsurface NG migration. Gao et al. (2021) reported differences in gas migration distance due to leak rate during non-steady conditions of the leak. In a steady or quasi-steady state, leaks of different sizes may result in similar diffusion distances (Gao et al., 2021). However, the leak rate influences the amount of NG escaping into the atmosphere. Above-ground surveys have reported an increase in detection probability with the increase in leak rate (Gas Technology Institute, 2022). Studies have also investigated the influence of leak depth on subsurface NG migration. Mitton (2018) reported that even though the spreading widths of leaks at different depths are similar, shallower pipelines have higher surface concentrations (Mitton, 2018).

2.4 Research objectives

Although previous studies have provided insight into subsurface NG migration, studies have not investigated the effects of gas composition, leak rate, and leak depth on the gas plume above ground, which is the critical input for most mobile or aerial leak detection methods. This study investigates variations in above-ground, in-atmosphere transport of CH_4 from pipeline leaks; and provides guidance on whether similar leak survey protocols would result in significant variations in leak detection due to variations in above-ground plume width. Specifically, this study:

1. Classifies the atmosphere into 'constant' atmospheric conditions based on atmospheric stability.
2. Investigates how the above-ground 3D CH_4 plume width changes with variation in NG composition, leak rate, and leak depth.
3. Uses a generalized linear model (GLM) to linearly correlate the effect of gas composition, leak rate, and leak depth on CH_4 plume width.
4. Uses the GLM equation to generate plume width estimates for the five major basins in the US for a 10 slpm leak at 0.9 m pipeline depth.

3 METHODS

Experiments were conducted at Colorado State University's Methane Emissions Technology and Evaluation Center (METEC) research facility in Fort Collins, Colorado, US. METEC was designed to support next-generation CH_4 LDAQ methods. Most LDAQ methods rely on downwind transport of emissions some distance from the emission point for leak detection (*METEC Facility*, 2021). To support LDAQ testing, METEC is designed to emulate emissions behavior and wind transport characteristics of operational above-ground and below-ground upstream and midstream oil and gas. METEC supports a range of well pad sizes, compressors, oil and gas tanks, and separators among other well pad equipment, and associated access roads. METEC's equipment is real, but not operational. Gas is delivered via small-diameter tubing to leak locations. Emissions are controlled and emit NG at locations that would be common in the field. The facility has approximately 200 above-ground release points which are all remotely controlled, from 6 well pads and 4 different facility types. If required, 60 release points could be initiated at any one time. In addition to above-ground equipment, METEC has an array of underground release points that simulate pipeline leaks in urban and rural settings, and rights-of-way (ROWs) with hidden leak locations. The releases at METEC are supported by analytic and practical instrumentation for NG emissions that include a mobile gas release rig, gas chromatograph, tunable wet gas mixer, CH_4 gas analyzers, and meteorological stations (fixed and mobile) (*METEC Facility*, 2021).

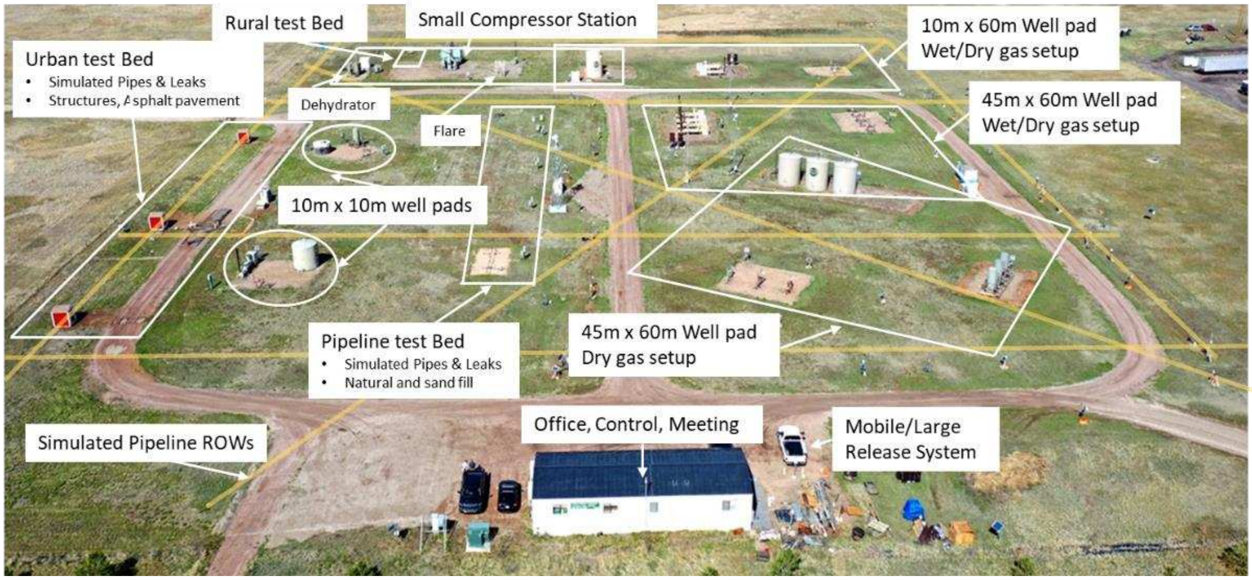

Figure 2 METEC Facility

3.1 Controlled releases

Above-ground downwind CH_4 measurements of controlled NG subsurface emissions were conducted on the 'rural testbed' at Colorado State University's METEC facility, between April and June 2022. Details of METEC's testbeds are provided by Gao et al. (2021) and Ulrich et al. (2019). METEC's rural testbed was designed to investigate leaks in flowlines, gathering, and transmission, representing a rural environment with undisturbed soil (Jayarathne et al., 2022). The testbed allows for the simulation of underground pipeline leaks at known leakage rates, at 0.6, 0.9, and 1.8 m leak depths, and varying atmospheric conditions allowing for continuously measuring subsurface, surface, and above-surface conditions (Ulrich et al., 2019). The leak depths were selected to be representative of NG pipeline depths.

Gas is supplied to the subsurface emission point by a 0.635 cm PTFE tubing and released through a 0.635 cm vent screen (model SS-MD-4, Swagelok, USA), surrounded by a 10 cm wire cube filled with gravel to prevent clogging (Jayarathne et al., 2022). The gas release rate is controlled by pressure regulators, solenoid valves, and choked flow orifices and measured using a thermal mass flow meter. Gas compositions for NG used in each experiment were determined using gas chromatography (7890B GC, Agilent Technologies) using a high split 150:1 injection method. To investigate the effects of gas composition, industrial grade 100% CH_4, C_2H_6, C_3H_8, and C_4H_{10} were mixed in varying proportions (Table 1) to simulate wetter gas compositions. In this study, the composition of 'dry' or market NG composition is nominally 85% CH_4 and 15% dry air. 'Dry air' in this study refers to air without water vapor. Experiment 1 was set as the baseline experiment for comparing leak variables. Gas was released at about 298 K, 1 atm.

Table 1 Controlled release experiments conducted at the Colorado State University's METEC site in Fort Collins in 2022

Experiment No.	Leak rate (slpm)					Leak depth (m)	Experiment dates
	CH_4	C_2H_6	C_3H_8	C_4H_{10}	dry air		
1	8.5	0	0	0	1.5	0.9	04-25 to 04-26
2	7	3	0	0	0	0.9	05-10 to 05-11
3	7	1	1	1	0	0.9	05-12 to 05-13
4	4.25	0	0	0	0.75	0.9	04-04 to 04-05
5	0.85	0	0	0	0.15	0.9	06-02 to 06-03
6	8.5	0	0	0	1.5	0.6	05-25 to 05-27
7	8.5	0	0	0	1.5	1.8	04-12 to 04-14

*Leak rates have been presented in slpm to compare NG mixture ratios easily.

3.2 Downwind methane concentration measurements

Four inlets were fixed at 0.5, 2, 5, and 7 m AGL on an 8 m stainless-steel mast 7 m northwest of the subsurface emission point. The four inlets were connected to the ABB LGR multiplexor (LGR, 2014) via 30 m lengths of PTFE tubing (1/8" ID x 1/4" OD x 1/16" Wall Tygon® 2375 Ultra Chemical Resistant Tubing) which sampled each height (z, m) for one minute sequentially. The outlet of the multiplexer was connected to a VACUUBRAND GMBH + CO KG MD1 vacuum pump and then tee-ed to an ABB LGR-ICOS GLA 132 Ultraportable Greenhouse Gas Analyzer

(UGGA). The UGGA is a laser absorption spectrometer measuring CH_4, CO_2, and H_2O mole fractions in an air sample. It reports mole fractions each second, with a stated precision of 1.4 ppb at 1 Hz, 0 to 100 ppm linear measurement range, and 0.01 – 1 Hz measurement rate (ABB, 2021).

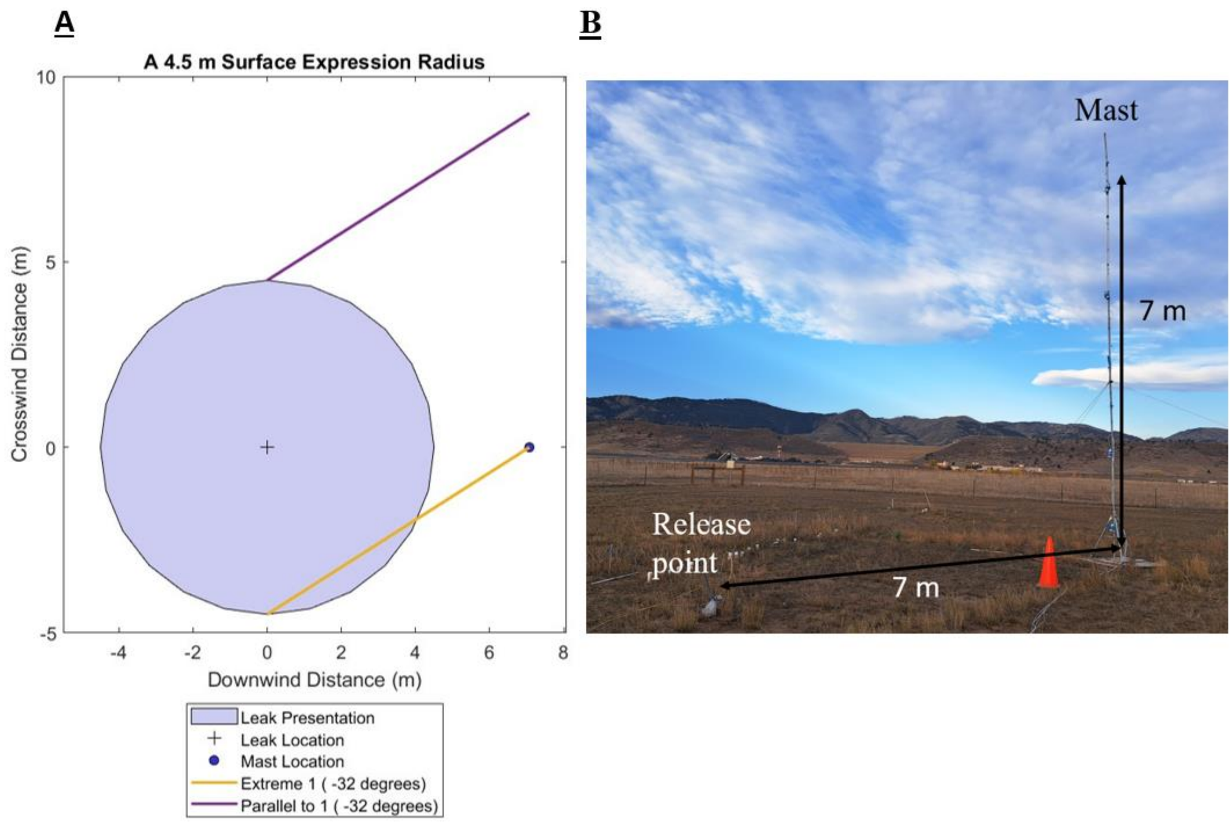

Figure 3 A is a schematic representation of the surface expression for a subsurface leak. B is the downwind measurement of above-ground CH_4 conducted at METEC's rural testbed.

3.3 Meteorological measurements

Micrometeorological data were measured at 10 Hz using RM Young 81000 ultrasonic anemometer (wind direction (*WD*) accuracy: ±2° (1 to 30 m/s) ±5° (30 to 40 m/s); wind speed accuracy: ±1% rms ±0.05 m/s (0 to 30 m/s) ±3% rms (30 to 40 m/s)) and a meteorological sensor (Met One Instruments Inc., 597A) installed 6 m above the ground. The Monin-Obukhov length (L) was calculated from the surface friction velocity (u_*, m s^{-1}), the mean absolute air temperature (T, K), the von Kármán's constant ($k_v = 0.41$), the gravitational acceleration (g = 9.8 m s^{-2}) and the 3D horizontal/vertical wind vectors (u, v, and w, m s^{-1}), respectively (Equation 1; Equation 2) (Flesch et al., 2004). For analysis, the L was converted to Pasquill-Gifford stability class (PGSC), where PGSC A is extremely unstable ($-100 \leq L < 0$), PGSC B/C is unstable ($-500 \leq L < -100$), PGSC D is neutral ($|L| > 500$), PGSC E/F is stable ($500 \leq L < 100$), and PGSC G is extremely stable ($0 < L \leq 100$) (Breedt et al., 2018; Gryning et al., 2007). A general description of the Pasquill-Gifford classification system in the Appendix (A A1).

$$L = -\frac{u_*^3 T}{k_v g \overline{w'T'}} \quad \text{Equation 1}$$

$$u_* = \left[\left(\overline{u'w'}\right)^2 + \left(\overline{v'w'}\right)^2 \right]^{1/4} \quad \text{Equation 2}$$

3.4 Determining methane plume width

3.4.1 Background concentration

Background concentration (C_b) data was collected for 2.5 hours before gas release. For each height, C_b was calculated as the average concentration for the duration (A A2.1). As all experiments were conducted at METEC exclusively, C_b was assumed to be a constant.

3.4.2 Determination of atmospheric stability (*L*)

The sampled CH_4 mixing ratios (X, ppm) were aggregated into micrometeorological data. Generally, L is determined between 15 and 30 minutes of atmospheric averaging. Averaging periods shorter than 15 minutes is likely inaccurate as it may not represent the mean atmospheric state. Averaging longer periods can be affected by changes in the surface during diurnal evolution, especially during rapid transition in weather conditions. 15-minute atmospheric averaging was selected to minimize the noise in data caused by variability in atmospheric conditions in the averaged period.

3.4.3 Binning

The data were categorized by height and PGSC and binned (Foster-Wittig et al., 2015) in increments of 4° to account for the anemometer's *WD* accuracy ±2° (1 to 30 m/s). Binned data were filtered within 90° of the mast location ensuring only downwind measurements were considered. A conditionally averaged concentration value $\langle C|WD\rangle$ for each binning was obtained as:

$$\langle C|WD\rangle = \frac{1}{n}\sum C(WD) \qquad \text{Equation 3}$$

Where n is the total number of data points within the given bin, and *C(WD)* is the concentration for each *WD*. In cases of more than one binned *WD*, the maximum CH_4 bin mean was taken as the binned concentration for that bin.

3.4.4 Plume width calculation

The mast distance from the release point (*s*, m) was constant at 7 m, and the perpendicular distance (*y*, m) for each measurement was calculated from the binned *WD* (A Figure A6) (Foster-Wittig et al., 2015; Tian, 2022). The mast location was the position when the wind was blowing directly from the center of the leak area (y = 0). Methane enhancement was calculated as the binned CH_4 concentration minus the background concentration (C_b). Enhancements were plotted against *y* and mirrored to reflect the assumption that the plume has equal width on either side of *y*, and a Gaussian model ($a*\exp(-(x/c)^2)$) fitted to the data, 95% confidence interval (A A3). Mobile survey methods have reported leak detection thresholds of 10% CH_4 concentrations above background (von Fischer et al., 2017; Weller et al., 2018) that corresponds to about 0.2 ppm enhancement for this study's C_b (A A2.1). Previous studies that have applied Gaussian plume model in leak quantification have reported a typical detection threshold of 0.1 ppm concentrations above the background (Chen et al., 2020; Riddick et al., 2021). As a result, 0.1 ppm enhancement was used as the minimum CH_4 enhancement for plume width determination. The plume width was calculated as the *y* distance where the CH_4 enhancement is 0.1 ppm (A A3). However, this study acknowledges that current mobile surveys using highly sensitive instruments may capture leaks at low detection thresholds of 5 to 10 ppb; and the 100 ppb is set to account for the low-resolution instruments. Also, this study applies to survey methods that apply ROWs screening that survey near the centerline of ROWs and close to pipelines. The percentage change in mean plume width estimates were calculated as [(Experiment*-Experiment 1)/Experiment 1 *100].

3.5 Determining leak survey speed for detection

The approximate surveying speed is calculated based on the plume width (above) and the instrument's frequency to understand leak detection at survey speeds better. The calculated surveying speed assumes that CH_4 detection by the instrument is instantaneous, i.e., it does not account for the delay in air exchange within the cell as a factor of the instrument's response time, which would smooth out plumes making peaks lower (i.e., harder to distinguish from background) but longer in time (i.e., easier to detect by making them persist longer). Referencing driving surveys that are conducted between 4 and 13 m s^{-1} (Eapi et al., 2014; von Fischer et al., 2017; Weller et al., 2019), the calculated survey speeds are compared to the minimum driving speed of 4 m s^{-1}, and used to determine if the plume can be detected using a 1 Hz frequency instrument.

3.6 Uncertainty analysis

The main causes of uncertainty in this study are the surface expression size for a non-homogenous surface area emission, effects of subsurface conditions on surface emission, background concentration determination (C_b), atmospheric averaging, and binning. In this study, uncertainties from C_b determination (± 0.01 ppm) (A A2.1); and 15-minute atmospheric averaging and 4° binning (± 0.07 ° s^{-1}) (A A2.3) were considered negligible. The baseline experiment, Experiment

1, was used to evaluate uncertainty due to surface presentation size and effects of subsurface conditions (A A2.4). WindTrax 2.0 software (http://www.thunderbeachscientific.com/) was used to investigate the Gaussian assumption for an area source using backward Lagrangian stochastic dispersion modeling and determine the uncertainty due to surface expression size and subsurface conditions. Riddick et al. (2021) reported maximum surface expression radius of 4.5 m hence, simulations were done between 0.5 and 5 m to reflect the heterogenous areal surface emission for a subsurface leak, with highest concentration at the leak center (A A2.4). As WindTrax assumes a homogenous ground source areal emission, free of obstructions, the difference between the simulated plume widths for different surface expressions and Experiment 1 mean plume width estimate, was assumed to account for effects of subsurface factors and surface presentation of the leak. The relative uncertainty in plume width due to surface expression and subsurface factors is [-42/+14] % (A A2.4). To emphasize the effect of leak variation on NG detection, mean plume width estimates have been discussed below in neutral conditions, PGSC D. Plume width results for non-neutral conditions are provided in the Appendix (A A3.2).

3.7 Case study

3.7.1 Generalized linear model (GLM)

A generalized linear model (GLM) with a Gaussian family using Companion to Applied Regression statistical package in R was used to generate relationships between the variables height AGL, gas composition (density), leak rate, and leak depth using mean plume width estimates. The GLM model creates a linear relationship between the response (plume width) and predictors: height (m), gas density (g/L), leak rate (slpm), and leak depth (m). The study uses the plume widths results calculated from Experiments 1 to 6 to calculate the variables' correlation. Experiment 7 results were excluded from the analysis as a leak depth of 1.8 m is not typical in the flowline/gathering system (COGCC, 2021).

3.7.2 Estimating plume widths from leaks in gathering lines in five major production regions in the US

Previous studies are used to generate gas compositions for the five major producing regions in the US as classified by Kennedy (2015): Fayetteville Shale, Arkoma Basin (Speight, 2020); Haynesville Shale, North Louisiana Salt Basin (Speight, 2020); Barnett Shale, Fort Worth Basin (Ethridge et al., 2015); Marcellus Shale, Appalachian Basin (Laughrey, 2022); and the Permian (Howard et al., 2015) (A A4.2). The generated GLM equation (3.7.1) is used to estimate mean plume widths for a simulated pipeline leak, 10 slpm at 0.9 m leak depth, for a flowline/gathering line transporting NG from the five major US basins.

4 RESULTS

4.1 Effect of gas composition

The plume width generally decreased with the increase in gas density of the NG mixture (Figure 4). The percentage change in mean plume width estimates for Experiment 2, 70% CH_4 30% C_2H_6 (0.83 g/L), compared to Experiment 1, 85% CH_4 15% air (0.74 g/L), were -12%, -36%, +61%, and -34% at 0.5, 2, 5 and 7 m AGL, respectively. Comparing Experiment 3, 70% CH_4 10% C_2H_6 10% C_3H_8 10% C_4H_{10} (1.0 g/L), to Experiment 1, the mean plume width estimates changed by -56% at 0.5 m AGL. The plume for Experiment 3 was indistinguishable from the background at 2, 5, and 7 m AGL. The plume for Experiment 3 at 0.5 m AGL had a maximum fitted enhancement of 0.7 ppm compared to 2.8 ppm in Experiment 2 and was indistinguishable from the background at 2, 5, and 7 m AGL (A A3.1). This indicated that gas density reduced the above-ground CH_4 plume width and enhancement. The calculated surveying speed was above minimum practical driving survey speed of 4 m s^{-1} (Eapi et al., 2014; von Fischer et al., 2017; Weller et al., 2019), at 0.5 to 7 m AGL in Experiments 1 and 2 and at 0.5 m AGL in Experiment 3 (Figure 4). These results indicate that Experiments 1 and 2 can be detected by a driving survey or a UAV at 0.5 to 7 m surveying heights. In comparison, Experiment 3 can only be detected by a driving survey at 0.5 m AGL. A repeat of Experiment 3 prolonging the leak from 24 hours to 72 hours did not increase the above-ground plume width (A A3.3). This indicates that leak duration may not affect above-ground plume width and hence, detection of dense NG leaks.

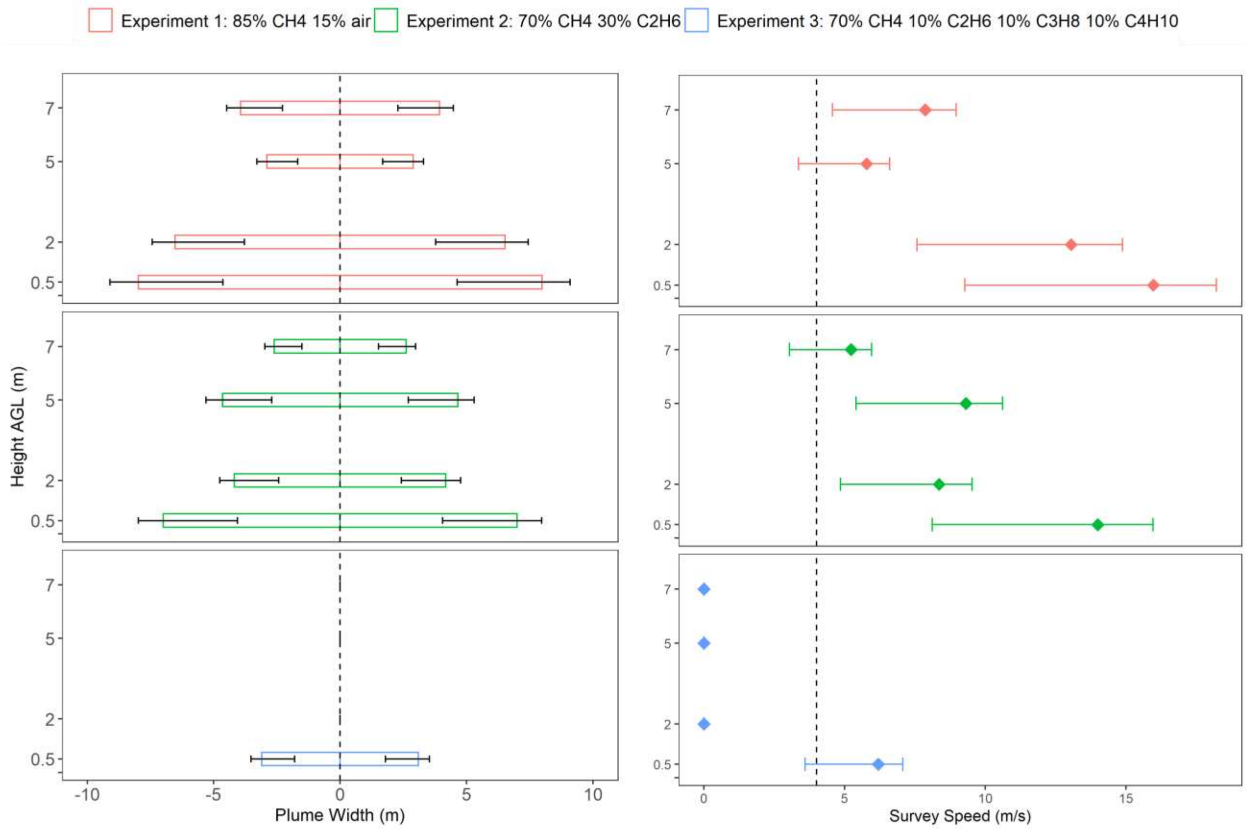

Figure 4 Plume width estimates and maximum surveying speeds for detection for different gas compositions at 0.5 to 7 m AGL, 95% confidence interval. The error bars represent the relative uncertainty in plume width estimation [-42/+14]%. The absence of a plume in Experiment 3 at 2, 5, and 7 m AGL was due to CH_4 enhancements being below 0.1 ppm. The dotted line on the figure to the right indicates the minimum practical surveying speed of 4 m s^{-1} using a 1 Hz frequency instrument.

4.2 Effect of leak rate

The plume width generally decreased with the decrease in leak rate (Figure 5). The percentage change in mean plume width estimates for Experiment 4, 4.25 slpm (167 g CH_4 h^{-1}), compared to Experiment 1, 85% CH_4 15% air (335 g CH_4 h^{-1}), were -26%, -86%, -100% and -93% at 0.5, 2, 5 and 7 m AGL, respectively. The plume for Experiment 5, 0.85 slpm (33 g CH_4 h^{-1}), was indistinguishable from the background at 0.5, 2, 5, and 7 m AGL. The calculated surveying speed for Experiment 4 was above minimum practical driving survey speed of 4 m s^{-1} at 0.5 m AGL (Figure 5). This indicates that Experiment 4 can be detected by a driving survey at 0.5 m AGL, while above-ground surveys may not detect Experiment 5's leak.

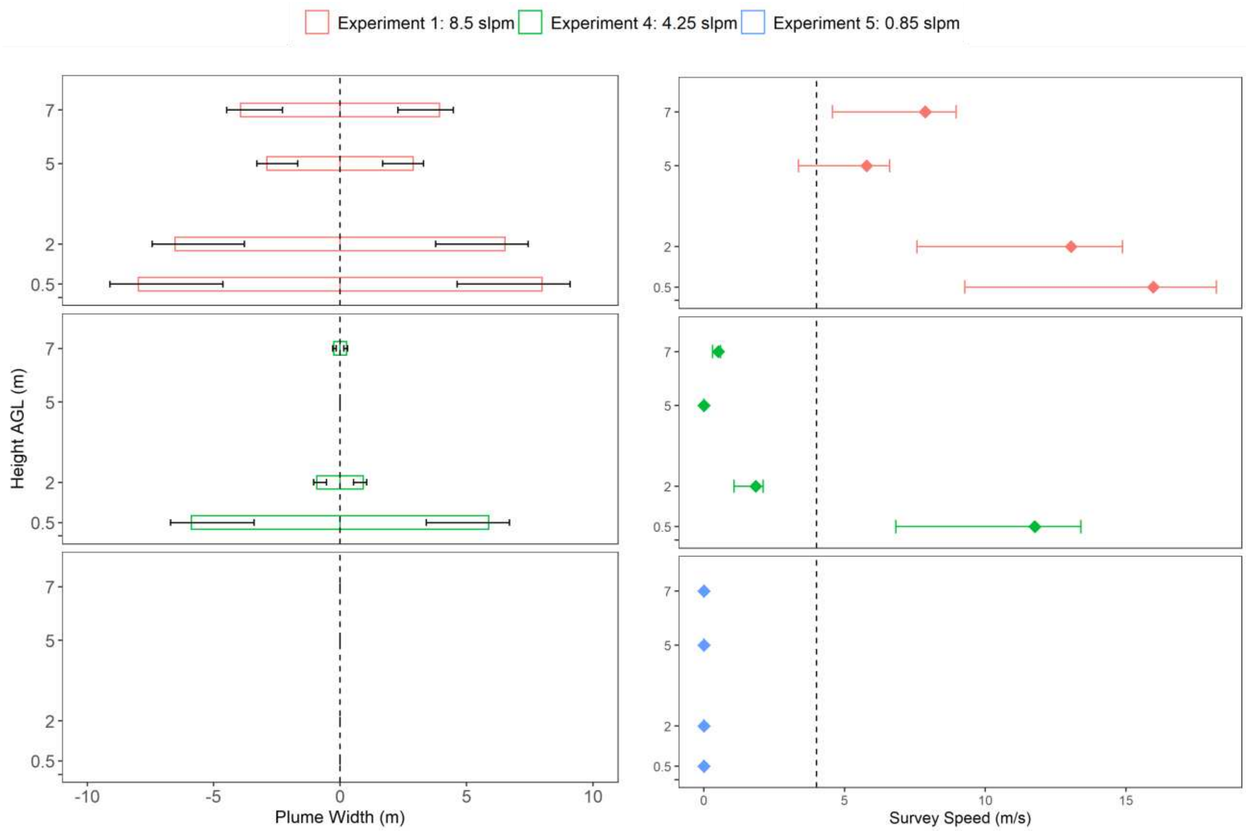

Figure 5 Plume width estimates and maximum surveying speeds for detection for different leak rates at 0.5 to 7 m AGL, 95% confidence interval. The error bars represent the relative uncertainty in plume width estimation [-42/+14]%. The absence of a plume in Experiment 4 at 5 m AGL, and Experiment 5 at 0.5 to 7 m AGL was due to CH_4 enhancements being below 0.1 ppm. The dotted line on the figure to the right indicates the minimum practical surveying speed of 4 m s^{-1} using a 1 Hz frequency instrument.

4.3 Effect of leak depth

The above-ground CH_4 plume width increased with depth between 0.6 and 0.9 m, but the above surface plume was undetectable above the background for leaks 1.8 m deep (Figure 6). The percentage change in mean plume width estimates for Experiment 6, 0.6 m leak depth, compared to Experiment 1, 0.9 m leak depth, were -58% and -99% at 0.5 and 2 m AGL, respectively. The plume for Experiment 6 and Experiment 7, 1.8 m leak depth, were indistinguishable from the background at 5 to 7 m, and 0.5 to 7 m AGL, respectively. For Experiment 6, the calculated surveying speed was above 4 m s^{-1} at 0.5 m AGL (Figure 6). This indicates that the leak from

Experiment 6 can be detected by a driving survey at 0.5 m surveying height, while above-ground surveying methods may not detect Experiment 7's leak.

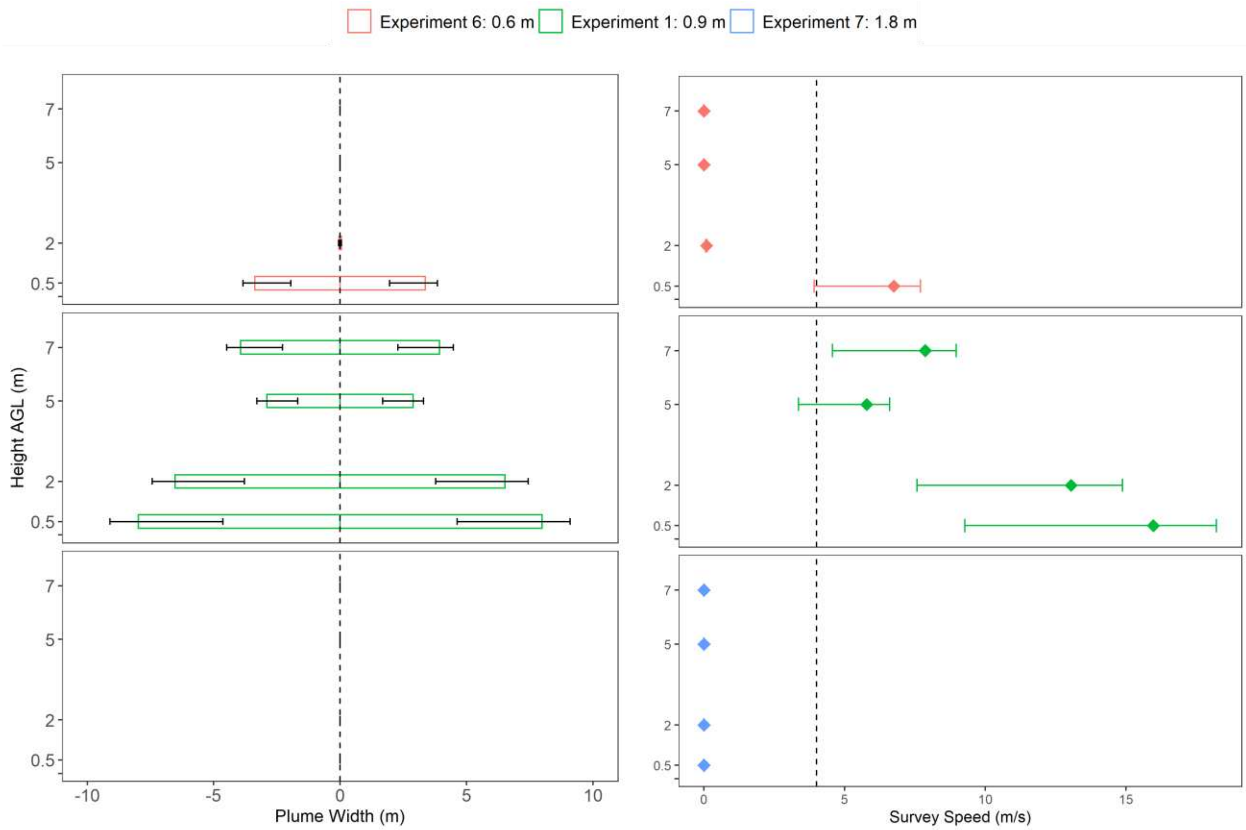

Figure 6 Plume width estimates and maximum surveying speeds for detection for different leak depths at 0.5 to 7 m AGL, 95% confidence interval. The error bars represent the relative uncertainty in plume width estimation [-42/+14]%. The absence of a plume in Experiment 6 at 2 to 7 m AGL, and Experiment 7 at 0.5 to 7 m AGL was due to CH_4 enhancements being below 0.1 ppm. The dotted line on the figure to the right indicates the minimum practical surveying speed of 4 m s^{-1} using a 1 Hz frequency instrument.

4.4 Case study

4.4.1 Generalized linear model (GLM)

Table 2 A GLM equation for calculating plume width from height (*z, m*), NG density (*ρ*, g/L), leak rate (*r*, slpm), and leak depth (*d*, m).

	Estimate	Standard Error	t-value	Pr(>|t|)
z	-0.92	0.22	-4.18	0.0005
ρ	-34.8	7.14	-4.87	0.0001
r	1.29	0.20	6.54	0.0000
d	31.1	5.87	5.30	0.0000
(Intercept)	-0.80	5.74	-0.14	0.8902

* The R^2 for the GLM modeled plume widths compared to calculated widths is 0.83 (Section A4.1).

The GLM results indicate that height, gas density, leak rate, and leak depth have significant effect on plume width ($p < 0.01$). Height, and NG density have a negative effect on plume width, meaning their increase will cause a decrease in plume width. Leak rate and depth have a positive effect on plume width; their increase will cause an increase in plume width.

4.4.2 Estimating plume widths from leaks in gathering lines in five major production regions in the US

Of the five major producing basins investigated in this study, NG from the Fayetteville Shale has the least density, 0.66 g/L, while the Permian has the highest, 1.01 g/L. (A A4.2). Using a minimum practical surveying speed of 4 m s^{-1} and a 1 Hz frequency instrument (ABB, 2023), the GLM results indicate that a leak from a gathering line transporting NG from the Permian may only be detected at 0.5 AGL (Figure 7). For the Marcellus, Barnett, Haynesville, and Fayetteville shale, gas leaks can be detected by a survey at 0.5, 2, 5, and 7 m AGL (Figure 7).

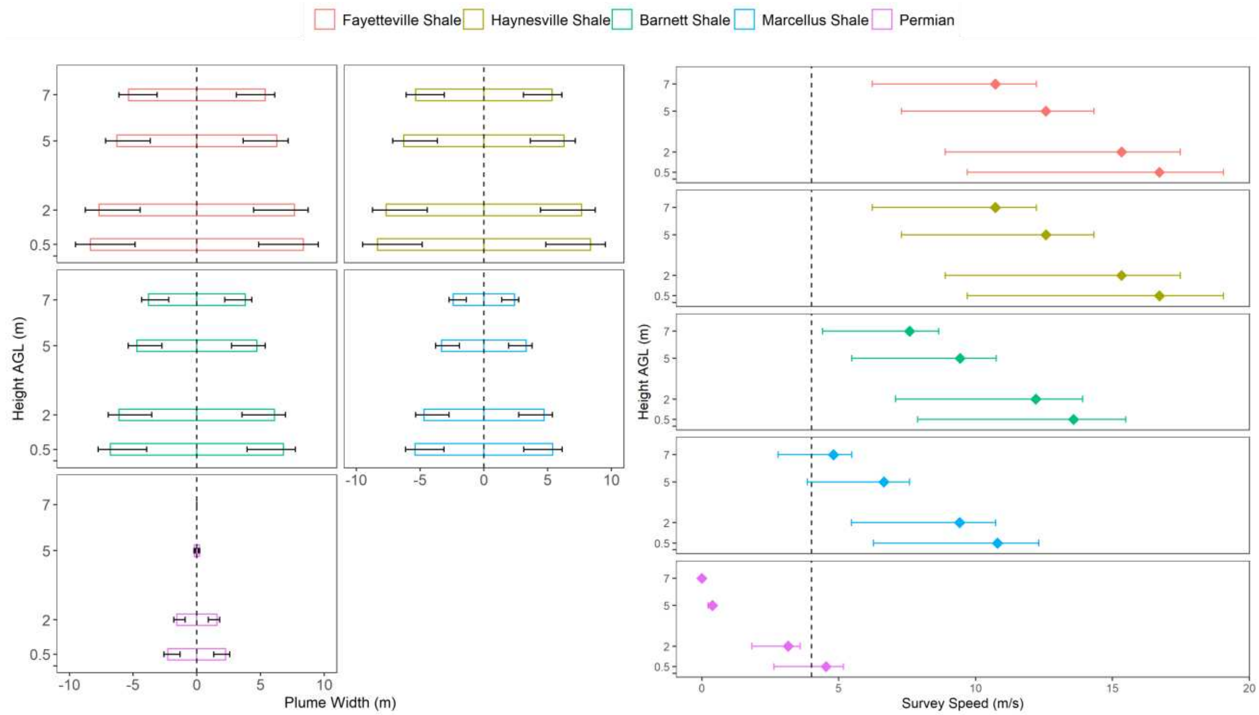

Figure 7 Modelled above-ground plume widths and maximum above-ground surveying speeds for a simulated 10 slpm leak, 0.9 m leak depth, for the five largest producing basins in the US. The error bars represent the relative uncertainty in plume width estimation [-42/+14]%. The dotted line on the figure to the right indicates the minimum practical surveying speed of 4 m s^{-1} using a 1 Hz frequency instrument.

5 DISCUSSION

5.1 Effect of gas composition

The study's results indicate that for the same total leak rate, increased gas density resulting from adding 20% of heavier hydrocarbons (C_3H_8 and C_4H_{10}) to the NG mixture reduces the above-ground plume width, CH_4 enhancement, and detection at different surveying heights. This suggests a decrease in surface emission for dense NG leaks. This study could not ascertain whether reduced plume width and CH_4 enhancement for heavy gases was due to slow NG dispersion above the surface due to gas density i.e., velocities at which NG is entrained in air above-ground depends on turbulence, and density difference relative to air; and/or CH_4 oxidation by methanotrophic bacteria. Gas density may slow dispersion until the point of dilution where the density of dispersed gas becomes close to that of surrounding air (Blackmore et al., 1982). This could cause the plume to be trapped close to the surface resulting in a narrow plume above-ground. Also, CH_4 oxidation has been reported in areas with high CH_4 activities like METEC with oxidation rates including 115 g CH_4 h^{-1} in a nitrogen-fertilized paddy soil (Vaksmaa et al., 2017), 385 g CH_4 h^{-1} in a landfill (Cébron et al., 2007), and 410 g CH_4 h^{-1} in alkaline soil (Han et al., 2009). As methanotrophic bacteria only require a source of carbon and moisture for survival (Hanson & Hanson, 1996), current research has not addressed the driving factor for CH_4 oxidation i.e., type of soil, presence of organic matter, or presence of carbon and moisture.

5.2 Effect of leak rate

Results indicate a decrease in above-ground CH_4 plume width with decreased leak rate. The decrease in leak rate reduces the number of molecules migrating from the leak point to the surface and the surface expression of the gas. While the atmospheric dispersion of gas may be the same at all leak rates, the enhancements are necessarily reduced, therefore dropping below the 0.1 ppm threshold nearer the center line of the plume downwind of the source. Relating the effect of gas composition to leak rate, this study established that adding 20% of C_3H_8 and C_4H_{10} to the NG mixture results in a plume width equivalent to decreasing the total release rate by 64%. This indicates how presence of heavy gases in the NG mixture significantly affects the above-ground plume width, and hence, leak detection.

5.3 Effect of leak depth

The effect of leak depth on the above-ground plume is not linear. Leak depth affects the surface expression of the gas. At 0.6 m depth, the gas travels a short distance before escaping into the atmosphere. The narrow surface expression of the gas results in the dispersion of the above-ground plume close to the surface. At 0.9 m, the surface expression of the gas is wider; a plume is present at 0.5 to 7 m AGL. At 1.8 m depth, the surface expression is much wider than the 0.6 and 0.9 m leak depths. Due to increased gas migration distance from the leak point to the surface, a large surface-air interface with lower gas flux per unit area is formed. Methane concentrations may drop below the enhancement threshold.

In field conditions, the Colorado Oil and Gas Conservation Commission COGCC (2021) rulemaking stipulates that subsurface flowlines must have a minimum cover of 3 feet (0.9 m) on cropland (COGCC, 2021). However, in areas where underground structure, geologic, or other uncontrollable conditions prevent a flowline installation at the minimum 3 feet cover, the pipeline may be installed with less than minimum cover, or above-ground (COGCC, 2021). This study's results of 0.9 m leak depth represent plume widths for flowlines buried at the minimum cover of 0.9 m. However, this study's results show that flowlines buried at less than minimum cover of 0.9 m may be detectable at heights very close to the surface, as plume width decreases with decrease in burial depth. This means that pipelines laid in complex regions at lower 0.9 m depth may be harder to detect than those in cropland regions.

5.4 Case study

5.4.1 Generalized linear model (GLM)

The GLM results show that diluting the CH_4 percentage in the NG mixture by adding heavier hydrocarbons reduces the in-atmosphere, above-ground plume width and concentrations due to increased NG density. Comparing the effect of NG density to leak rate and leak depth, the effect of NG density, $\Delta\rho$, on plume width is equivalent to -0.04Δr (effect of increased leak rate) and -0.89Δd (effect of increased leak depth) (A A4.3). This means that leak sizes reported in areas with high percentages of heavier hydrocarbons in the NG mixture may be underestimated, and smaller leaks missed.

5.4.2 Estimating plume widths from leaks in gathering lines in five major production regions in the US

Plume width results for the five major US basins indicate that leak detection by above-ground survey methods should be basin and height dependent. As practical surveying heights for driving surveys are 0.5 to 5 m AGL, a 10-slpm leak in Fayetteville Shale at 0.9 m leak depth can be detected while driving between 11 and 17 m s^{-1}. However, a similar leak in the Permian can be detected only while driving between 0.4 and 5 m s^{-1}; an on-road driving speed of 0.4 m s^{-1} is impractical, although it may be possible but expensive for off-road ROWs. Previous driving survey studies have indicated that most driving surveys are between 4 and 13 m s^{-1} (Eapi et al., 2014; von Fischer et al., 2017; Weller et al., 2019), resulting in an average driving speed of approximately 9 m s^{-1}. This indicates that a typical survey speed (9 m s^{-1}) may detect a leak in Fayetteville Shale but not in the Permian.

Further, it is typical for leak surveyors to apply leak detection thresholds (minimum enhancement for detection) based on the background concentration of an area, if known, or apply experiences from other areas to set detection thresholds in the current surveying area. Gas gathering lines carrying gas with heavy hydrocarbon components often contain hydrocarbon liquids and soluble aromatic hydrocarbons, e.g., BTEX (benzene, toluene, ethylbenzene, xylene). If a survey captures most emissions in Fayetteville shale, a similar approach applied in the Permian will likely result in missed detections or underestimating the size of detected leaks. Erroneously reporting few or smaller leaks from heavy gas basins may lead to increased safety risks, increased greenhouse emissions, and detrimental effects due to co-emitted liquid contaminants that can cause soil and water contamination. Previous studies investigating spills from oil and gas pipelines reported groundwater contamination due to high mutagenicity threatening human health (Rice et al., 1995), causing birth defects, and cancer (Landon & Belitz, 2012). As a result, it is vital to apply leak detection protocols that are practical and workable to flowlines and gathering lines to find and repair pipeline leaks.

6 CONCLUSION AND RECOMMENDATIONS

This study established that gas composition, leak rate, and depth affect the above-ground plume width and subsurface pipelines' leak detection. Leak detection can be improved if survey protocols are tailored to the contents and depth of the surveyed pipeline, especially for flowlines and gathering lines in the oil and gas upstream sector. The study established that the effect of adding heavy hydrocarbons to the NG mixture on plume width is equivalent to the effect of increased leak rate and depth on plume width multiplied by -0.04 and -0.89, respectively. This shows that reported leaks in areas with heavier hydrocarbons could currently be missed or underestimated. Further, leaks from pipelines laid in covers meeting the COGCC minimum depth requirement of 0.9 m could be easier to detect compared to those buried less than the minimum depth. This study shows that understanding the effect of leak characteristics on above-ground plume can significantly improve detection. This study recommends that leak survey protocols for flowlines and gathering lines should be different from distribution pipelines and tailored to the compositions of the transported NG to report emissions accurately.

This study plans follow-up experiments to understand the driving factor for reduced CH_4 plume width and enhancement for NG mixture with heavier hydrocarbons. The follow-up experiments aim to investigate the effect of heavier hydrocarbons on advection, diffusion, CH_4 oxidation, buoyancy, and atmospheric gas dispersion.

REFERENCES

ABB. (2021). *LGR-ICOS™ GLA132-GGA Greenhouse gas analyzer—Ultraportable*. https://library.e.abb.com/public/82d15ff8e70f40289f90ac571c6346f3/ABB%20GLA132-GGA_DS-EN%20Rev.%20C.pdf?x-sign=KYdHIL2OqBaIs02vO2JKmKaS6wWAWxxPgDZd76BV2zeQxA1liPvcHbz1PSkgXtjH

ABB. (2023). *LGR-ICOS- Portable analyzers GLA131 M-GGA-918*. Measurement Products. https://new.abb.com/products/measurement-products/analytical/laser-gas-analyzers/laser-analyzers/lgr-icos-portable-analyzers/lgr-icos-microportable-analyzers-gla131-series/lgr-icos-portable-analyzers-gla131-gga

Akande, S., Adetunla, A., Olanrewaju, T., & Adeoye, A. (2021). UAV and Its Approach in Oil and Gas Pipeline Leakage Detection. *Journal of Robotics*, *2021*, e1300740. https://doi.org/10.1155/2021/1300740

Bahlmann, L. M., Smits, K. M., Heck, K., Coltman, E., Helmig, R., & Neuweiler, I. (2020). Gas Component Transport Across the Soil-Atmosphere Interface for Gases of Different Density: Experiments and Modeling. *Water Resources Research*, *56*(9). https://doi.org/10.1029/2020WR027600

Barchyn, T. E., Hugenholtz, C. H., Myshak, S., & Bauer, J. (2018). A UAV-based system for detecting natural gas leaks. *Journal of Unmanned Vehicle Systems*, *6*(1), 18–30. https://doi.org/10.1139/juvs-2017-0018

Blackmore, D. R., Herman, M. N., & Woodward, J. L. (1982). Heavy gas dispersion models. *Journal of Hazardous Materials*, *6*(1–2), 107–128. https://doi.org/10.1016/0304-3894(82)80036-8

Breedt, H. J., Craig, K. J., & Jothiprakasam, V. D. (2018). Monin-Obukhov similarity theory and its application to wind flow modelling over complex terrain. *Journal of Wind Engineering and Industrial Aerodynamics*, *182*, 308–321. https://doi.org/10.1016/j.jweia.2018.09.026

Bretschneider, T. R., & Shetti, K. (2014). *UAV-BASED GAS PIPELINE LEAK DETECTION*.

Castenschiold, J. H. F., Gehrlein, J. B., Bech-Hansen, M., Kallehauge, R. M., Pertoldi, C., & Bruhn, D. (2022). Monitoring Dropping Densities with Unmanned Aerial Vehicles (UAV): An Effective Tool to Assess Distribution Patterns in Field Utilization by Foraging Geese. *Symmetry*, *14*(10), 2175. https://doi.org/10.3390/sym14102175

Caulton, D. R., Li, Q., Bou-Zeid, E., Fitts, J. P., Golston, L. M., Pan, D., Lu, J., Lane, H. M., Buchholz, B., Guo, X., McSpiritt, J., Wendt, L., & Zondlo, M. A. (2018). Quantifying uncertainties from mobile-laboratory-derived emissions of well pads using inverse Gaussian methods. *Atmospheric Chemistry and Physics*, *18*(20), 15145–15168. https://doi.org/10.5194/acp-18-15145-2018

Cébron, A., Bodrossy, L., Chen, Y., Singer, A. C., Thompson, I. P., Prosser, J. I., & Murrell, J. C. (2007). Identity of active methanotrophs in landfill cover soil as revealed by DNA-stable isotope probing: Methanotrophs in landfill soil. *FEMS Microbiology Ecology*, *62*(1), 12–23. https://doi.org/10.1111/j.1574-6941.2007.00368.x

Chen, J., Dietrich, F., Maazallahi, H., Forstmaier, A., Winkler, D., Hofmann, M. E. G., Denier van der Gon, H., & Röckmann, T. (2020). Methane emissions from the Munich Oktoberfest. *Atmospheric Chemistry and Physics*, *20*(6), 3683–3696. https://doi.org/10.5194/acp-20-3683-2020

COGCC. (2021). *Complete Rules (100—1200 Series).pdf*. https://cogcc.state.co.us/documents/reg/Rules/LATEST/Complete%20Rules%20(100%20-%201200%20Series).pdf

Cooper, J., Dubey, L., & Hawkes, A. (2022). Methane detection and quantification in the upstream oil and gas sector: The role of satellites in emissions detection, reconciling and reporting. *Environmental Science: Atmospheres*, *2*(1), 9–23. https://doi.org/10.1039/D1EA00046B

Discover Advanced Mobile Leak Detection (AMLD). (2023). *Heath Consultants*. https://heathus.com/products/discover-advanced-mobile-leak-detection-amld/

Duren, R. M., Thorpe, A. K., Foster, K. T., Rafiq, T., Hopkins, F. M., Yadav, V., Bue, B. D., Thompson, D. R., Conley, S., Colombi, N. K., Frankenberg, C., McCubbin, I. B., Eastwood, M. L., Falk, M., Herner, J. D., Croes, B. E., Green, R. O., & Miller, C. E. (2019). California's methane super-emitters. *Nature*, *575*(7781), 180–184. https://doi.org/10.1038/s41586-019-1720-3

Eapi, G. R., Sabnis, M. S., & Sattler, M. L. (2014). Mobile measurement of methane and hydrogen sulfide at natural gas production site fence lines in the Texas Barnett Shale. *Journal of the Air & Waste Management Association*, *64*(8), 927–944. https://doi.org/10.1080/10962247.2014.907098

EIA. (2022). *Use of natural gas—U.S. Energy Information Administration (EIA)*. EIA. https://www.eia.gov/energyexplained/natural-gas/use-of-natural-gas.php

EIA. (2023a). *Natural Gas Monthly (NGM)—Energy Information Administration—February 2023 With Data for December 2022*. https://www.eia.gov/naturalgas/monthly/

EIA. (2023b). *U.S. natural gas production grew by 4% in 2022*. https://www.eia.gov/todayinenergy/detail.php?id=56000

EPA. (2023). *Inventory of U.S. Greenhouse Gas Emissions and Sinks: 1990-2021* [Reports and Assessments]. https://www.epa.gov/ghgemissions/inventory-us-greenhouse-gas-emissions-and-sinks-1990-2021

Ethridge, S., Bredfeldt, T., Sheedy, K., Shirley, S., Lopez, G., & Honeycutt, M. (2015). The Barnett Shale: From problem formulation to risk management. *Journal of Unconventional Oil and Gas Resources*, *11*, 95–110. https://doi.org/10.1016/j.juogr.2015.06.001

Falta, R. W., Javandel, I., Pruess, K., & Witherspoon, P. A. (1989). Density-driven flow of gas in the unsaturated zone due to the evaporation of volatile organic compounds. *Water Resources Research*, *25*(10), 2159–2169. https://doi.org/10.1029/WR025i010p02159

Flesch, T. K., Wilson, J. D., Harper, L. A., Crenna, B. P., & Sharpe, R. R. (2004). Deducing Ground-to-Air Emissions from Observed Trace Gas Concentrations: A Field Trial. *Journal of Applied Meteorology and Climatology*, *43*(3), 487–502. https://doi.org/10.1175/1520-0450(2004)043<0487:DGEFOT>2.0.CO;2

Foster-Wittig, T. A., Thoma, E. D., & Albertson, J. D. (2015). Estimation of point source fugitive emission rates from a single sensor time series: A conditionally-sampled Gaussian plume reconstruction. *Atmospheric Environment*, *115*, 101–109. https://doi.org/10.1016/j.atmosenv.2015.05.042

Fox, D. T., Hayman, A., & Moorhouse, B. (2022). *Leak detection methods for natural gas gathering, transmission, and distribution pipelines*. 40.

Gao, B., Mitton, M. K., Bell, C., Zimmerle, D., Deepagoda, T. K. K. C., Hecobian, A., & Smits, K. M. (2021). Study of methane migration in the shallow subsurface from a gas pipe leak. *Elementa: Science of the Anthropocene*, *9*(1), 00008. https://doi.org/10.1525/elementa.2021.00008

Gas Technology Institute. (2022). *Validation of Remote Sensing and Leak Detection Technologies Under Realistic and Differing Conditions*. Operations Technology Development. https://primis.phmsa.dot.gov/matrix/FilGet.rdm?fil=16505

Government of Canada, C. E. R. (2022, July 13). *CER – Natural Gas Pipeline Transportation System*. https://www.cer-rec.gc.ca/en/data-analysis/facilities-we-regulate/canadas-pipeline-system/2021/natural-gas-pipeline-transportation-system.html

Gryning, S.-E., Batchvarova, E., Brümmer, B., Jørgensen, H., & Larsen, S. (2007). On the extension of the wind profile over homogeneous terrain beyond the surface boundary layer. *Boundary-Layer Meteorology*, *124*(2), 251–268. https://doi.org/10.1007/s10546-007-9166-9

Han, B., Chen, Y., Abell, G., Jiang, H., Bodrossy, L., Zhao, J., Murrell, J. C., & Xing, X.-H. (2009). Diversity and activity of methanotrophs in alkaline soil from a Chinese coal mine. *FEMS Microbiology Ecology*, *70*(2), 196–207. https://doi.org/10.1111/j.1574-6941.2009.00707.x

Hanson, R. S., & Hanson, T. E. (1996). Methanotrophic bacteria. *Microbiological Reviews*, *60*(2), 439–471. https://doi.org/10.1128/mr.60.2.439-471.1996

HEATH. (2022). Gas Leak Detection | Natural Gas | Detecto Pak-Infrared. *Heath Consultants*. https://heathus.com/products/detecto-pak-infrared/

Howard, T., Ferrara, T. W., & Townsend-Small, A. (2015). Sensor transition failure in the high flow sampler: Implications for methane emission inventories of natural gas infrastructure. *Journal of the Air & Waste Management Association*, *65*(7), 856–862. https://doi.org/10.1080/10962247.2015.1025925

IEA. (2021). *Methane and climate change – Methane Tracker 2021 – Analysis*. IEA. https://www.iea.org/reports/methane-tracker-2021/methane-and-climate-change

Jackson, R. B., Down, A., Phillips, N. G., Ackley, R. C., Cook, C. W., Plata, D. L., & Zhao, K. (2014). Natural Gas Pipeline Leaks Across Washington, DC. *Environmental Science & Technology*, *48*(3), 2051–2058. https://doi.org/10.1021/es404474x

Jayarathne, N. J. R. R., Smits, K. M., Riddick, S. N., Zimmerle, D. J., Cho, Y., Schwartz, M., Cheptonui, F., Cameron, K., & Ronney, P. (2022). *Supplementary Information for "Understanding Mid-to Large Underground Leaks from Buried Pipelines as Affected by Soil and Atmospheric Conditions – Field Scale Experimental Study"* [Data set]. Texas Data Repository. https://doi.org/10.18738/T8/MRX54H

Jayarathne, N. J., Smits, K. M., Riddick, S. N., Zimmerle, D. J., Cho, Y., Schwartz, M., Cheptonui, F., Cameron, K., & Ronney, P. (2022). *Understanding Mid-to Large Underground Leaks from Buried Pipelines as Affected by Soil and Atmospheric Conditions – Field Scale Experimental Study*. https://energy.colostate.edu/wp-content/uploads/sites/28/2022/12/PRCI-REX2022-020_Jayarathne.pdf

Kahl, J. D. W., & Chapman, H. L. (2018). Atmospheric stability characterization using the Pasquill method: A critical evaluation. *Atmospheric Environment*, *187*, 196–209. https://doi.org/10.1016/j.atmosenv.2018.05.058

Kennedy, C. (2015). *These are the 10 largest oil and gas fields in the US*. Business Insider. https://www.businessinsider.com/these-are-the-10-largest-oil-and-gas-fields-in-the-us-2015-4

Landon, M. K., & Belitz, K. (2012). Geogenic Sources of Benzene in Aquifers Used for Public Supply, California. *Environmental Science & Technology*, *46*(16), 8689–8697. https://doi.org/10.1021/es302024c

Laughrey, C. D. (2022). Produced Gas and Condensate Geochemistry of the Marcellus Formation in the Appalachian Basin: Insights into Petroleum Maturity, Migration, and Alteration in an Unconventional Shale Reservoir. *Minerals*, *12*(10), 1222. https://doi.org/10.3390/min12101222

LGR. (2014). *Ultra-Portable Greenhouse Gas Analyzer User Manual-Model 915-0011*. https://www.ecotech.com/wp-content/uploads/2015/03/UltraPortable-GGA-User-Manual-Rev-1.01.pdf

Mendoza, C. A., & Frind, E. O. (1990). Advective-dispersive transport of dense organic vapors in the unsaturated zone: 2. Sensitivity analysis. *Water Resources Research*, *26*(3), 388–398. https://doi.org/10.1029/WR026i003p00388

METEC Facility. (2021). Energy Institute. https://energy.colostate.edu/metec/facility/

Mitton, M. (2018). *Subsurface Methane Migration from Natural Gas Distribution Pipelines as Affected by Soil Heterogeneity: Field Scale Experimental and Numerical Study* [M.S., Colorado School of Mines]. https://www.proquest.com/docview/2129711130/abstract/5C6D4464931B4771PQ/1

Murrell, J. C. (2010). The Aerobic Methane Oxidizing Bacteria (Methanotrophs). In K. N. Timmis (Ed.), *Handbook of Hydrocarbon and Lipid Microbiology* (pp. 1953–1966). Springer. https://doi.org/10.1007/978-3-540-77587-4_143

National Research Council (US) Committee on Toxicology. (1984). METHANE. In *Emergency and Continuous Exposure Limits for Selected Airborne Contaminants: Volume 1*. National Academies Press (US). https://www.ncbi.nlm.nih.gov/books/NBK208285/

Nugent, A., & DeCou, D. (2019). *Chapter 5: Atmospheric Stability*. http://pressbooks-dev.oer.hawaii.edu/atmo/chapter/chapter-5-atmospheric-stability/

Phillips, N. G., Ackley, R., Crosson, E. R., Down, A., Hutyra, L. R., Brondfield, M., Karr, J. D., Zhao, K., & Jackson, R. B. (2013). Mapping urban pipeline leaks: Methane leaks across Boston. *Environmental Pollution*, *173*, 1–4. https://doi.org/10.1016/j.envpol.2012.11.003

PHMSA. (2022). *U.S. Department of Transportation Pipeline and Hazardous Materials Safety Administration Office of Pipeline Safety*. https://portal.phmsa.dot.gov/analytics/saw.dll?Portalpages&PortalPath=%2Fshared%2FPDM%20Public%20Website%2F_portal%2FSC%20Incident%20Trend&Page=All%20Reported

Rice, D. W., Grose, R. D., Michaelsen, J. C., Dooher, B. P., MacQueen, D. H., Cullen, S. J., Kastenberg, W. E., Everett, L. G., & Marino, M. A. (1995). *California Leaking Underground Fuel Tank (LUFT) Historical Case Analyses*.

Riddick, S. N., Bell, C. S., Duggan, A., Vaughn, T. L., Smits, K. M., Cho, Y., Bennett, K. E., & Zimmerle, D. J. (2021). Modeling temporal variability in the surface expression above a methane leak: The ESCAPE model. *Journal of Natural Gas Science and Engineering*, *96*, 104275. https://doi.org/10.1016/j.jngse.2021.104275

Robbins, C. A., Grauberger, B. M., Garland, S. D., Carlson, K. H., Lin, S., Bandhauer, T. M., & Tong, T. (2020). On-site treatment capacity of membrane distillation powered by waste heat or natural gas for unconventional oil and gas wastewater in the Denver-Julesburg

Basin. *Environment International*, *145*, 106142. https://doi.org/10.1016/j.envint.2020.106142

Scanlon, B. R., Nicot, J. P., & Massmann, J. W. (2001). *Soil Gas Movement in Unsaturated Systems*. Soil physics companion, 389, 297-341. https://citeseerx.ist.psu.edu/document?repid=rep1&type=pdf&doi=2cd231efc9f661190295acbc4670134ad01f5142

Speight, J. (2020). Processing gas from tight formations. In *Shale Oil and Gas Production Processes* (pp. 451–518). Elsevier. https://doi.org/10.1016/B978-0-12-813315-6.00008-7

Takahashi, A., Urano, Y., Tokuhashi, K., Hidekazu Nagai, Kaise, M., & Kondo, S. (1998). Fusing ignition of various metal wires for explosion limits measurement of methane/air mixture. *Journal of Loss Prevention in the Process Industries*, *11*(5), 353–360. https://doi.org/10.1016/S0950-4230(98)00010-2

Tian, S. (2022). *STUDY OF THE IMPACT OF ATMOSPHERIC VARIABILITY ON SUBSURFACE METHANE EMISSIONS: APPLICATION TO LEAK DETECTION AND QUANTIFICATION FOR UNDERGROUND NATURAL GAS PIPELINE LEAKS* [Ph.D, The University of Texas]. https://rc.library.uta.edu/uta-ir/bitstream/handle/10106/31015/TIAN-DISSERTATION-2022.pdf?sequence=1&isAllowed=y

Ulrich, B. A., Mitton, M., Lachenmeyer, E., Hecobian, A., Zimmerle, D., & Smits, K. M. (2019). Natural Gas Emissions from Underground Pipelines and Implications for Leak Detection. *Environmental Science & Technology Letters*, *6*(7), 401–406. https://doi.org/10.1021/acs.estlett.9b00291

Vaksmaa, A., van Alen, T. A., Ettwig, K. F., Lupotto, E., Valè, G., Jetten, M. S. M., & Lüke, C. (2017). Stratification of Diversity and Activity of Methanogenic and Methanotrophic Microorganisms in a Nitrogen-Fertilized Italian Paddy Soil. *Frontiers in Microbiology*, *8*, 2127. https://doi.org/10.3389/fmicb.2017.02127

von Fischer, J. C., Cooley, D., Chamberlain, S., Gaylord, A., Griebenow, C. J., Hamburg, S. P., Salo, J., Schumacher, R., Theobald, D., & Ham, J. (2017). Rapid, Vehicle-Based Identification of Location and Magnitude of Urban Natural Gas Pipeline Leaks. *Environmental Science & Technology*, *51*(7), 4091–4099. https://doi.org/10.1021/acs.est.6b06095

Weller, Z. D., Hamburg, S. P., & von Fischer, J. C. (2020). A National Estimate of Methane Leakage from Pipeline Mains in Natural Gas Local Distribution Systems. *Environmental Science & Technology*, *54*(14), 8958–8967. https://doi.org/10.1021/acs.est.0c00437

Weller, Z. D., Roscioli, J. R., Daube, W. C., Lamb, B. K., Ferrara, T. W., Brewer, P. E., & von Fischer, J. C. (2018). Vehicle-Based Methane Surveys for Finding Natural Gas Leaks and Estimating Their Size: Validation and Uncertainty. *Environmental Science & Technology*, acs.est.8b03135. https://doi.org/10.1021/acs.est.8b03135

Weller, Z. D., Yang, D. K., & Fischer, J. C. von. (2019). An open source algorithm to detect natural gas leaks from mobile methane survey data. *PLOS ONE*, *14*(2), e0212287. https://doi.org/10.1371/journal.pone.0212287

Yang, S., Talbot, R. W., Frish, M. B., Golston, L. M., Aubut, N. F., Zondlo, M. A., Gretencord, C., & McSpiritt, J. (2018). Natural Gas Fugitive Leak Detection Using an Unmanned Aerial Vehicle: Measurement System Description and Mass Balance Approach. *Atmosphere*, *9*(10), Article 10. https://doi.org/10.3390/atmos9100383

Zimmerle, D. J., Williams, L. L., Vaughn, T. L., Quinn, C., Subramanian, R., Duggan, G. P., Willson, B., Opsomer, J. D., Marchese, A. J., Martinez, D. M., & Robinson, A. L. (2015). Methane Emissions from the Natural Gas Transmission and Storage System in the United States. *Environmental Science & Technology*, *49*(15), 9374–9383. https://doi.org/10.1021/acs.est.5b01669

APPENDIX

A1 Meteorological conditions defining Pasquill-Gifford stability classes

Pasquill stability classes are not measurable physical parameters, and its application is based on England's weather conditions where;

	Daytime insolation			Night-time conditions	
Surface wind speed (m/s)	Strong	Moderate	Slight	Thin overcast or > 4/8 low cloud	<= 4/8 cloudiness
< 2	A	A - B	B	E	F
2 - 3	A - B	B	C	E	F
3 - 5	B	B - C	C	D	E
5 - 6	C	C - D	D	D	D
> 6	C	D	D	D	D

Figure A1 Pasquill-Gifford atmospheric stability classes classification

a. Strong insolation corresponds to sunny midday in England's midsummer.
b. Slight insolation corresponds to sunny midday conditions in midwinter in England.
c. Night refers to the period from 1 hour before sunset to 1 hour after sunrise.
d. The neutral category D should also be assumed, irrespective of wind speed, for overcast conditions during day or night, and for any sky conditions during the hour preceding or following night.

(Kahl & Chapman, 2018)

A2 Uncertainty Analysis

Uncertainty analysis was done using results from the baseline experiment (Experiment 1, 335 g CH_4 h^{-1}, 0.9 m leak depth), PGSC D, 0.5 m AGL.

A2.1 Background concentration

Background concentration data was collected for 2.5 hours before gas release. Analysis of data indicated that the stability class during this duration was PGSC D. For each of the heights, background concentration was calculated as the average concentration. The average C_b was 1.96 ± 0.01 ppm (1 SD) at 0.5 and 2 m AGL, and 1.95 ±0.01 ppm (1 SD) at 5 and 7 m AGL, respectively.

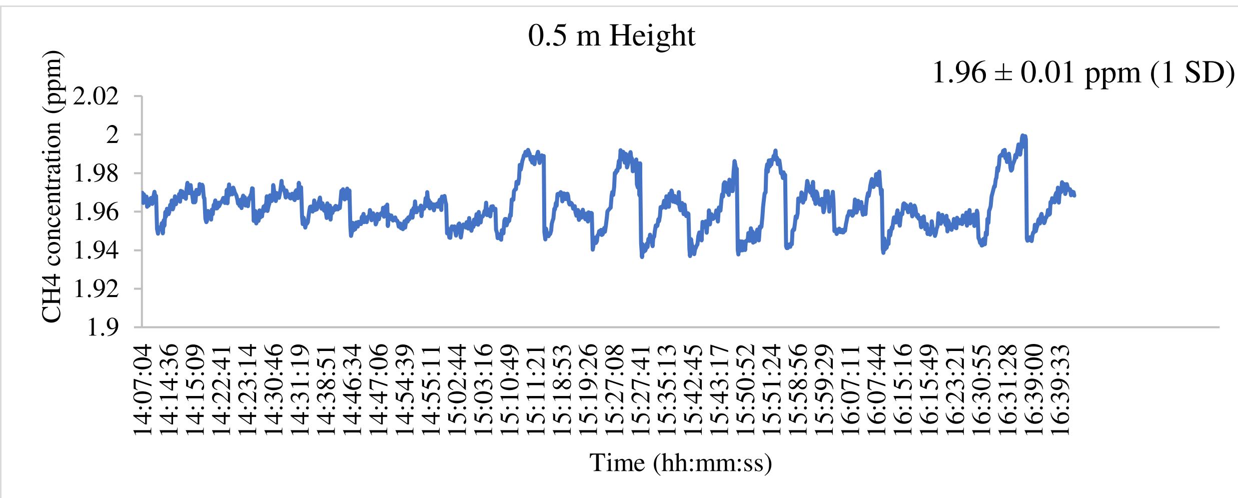

Figure A2 Background concentration at 0.5 m AGL

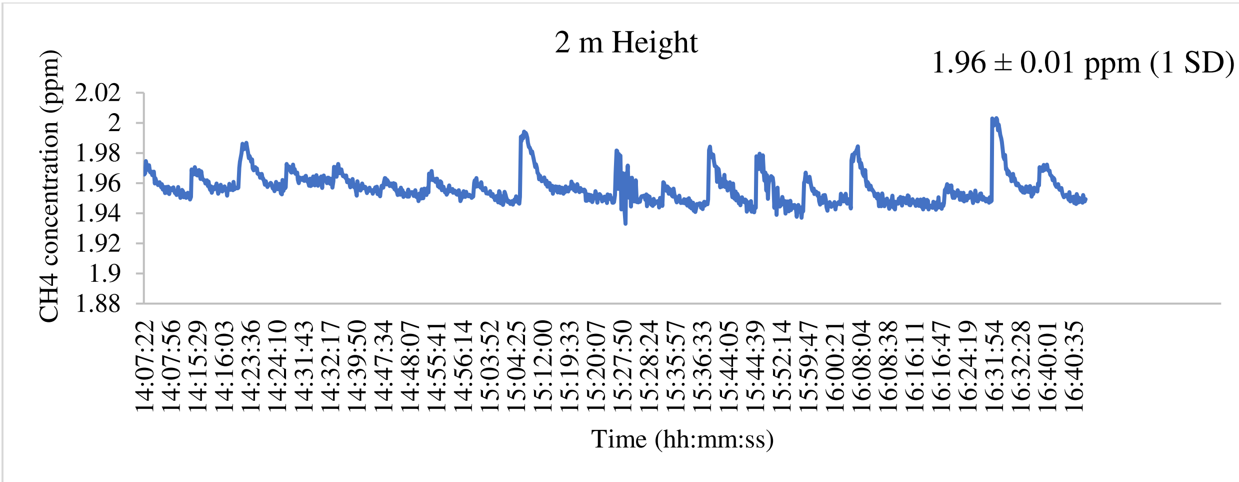

Figure A3 Background concentration at 2 m AGL

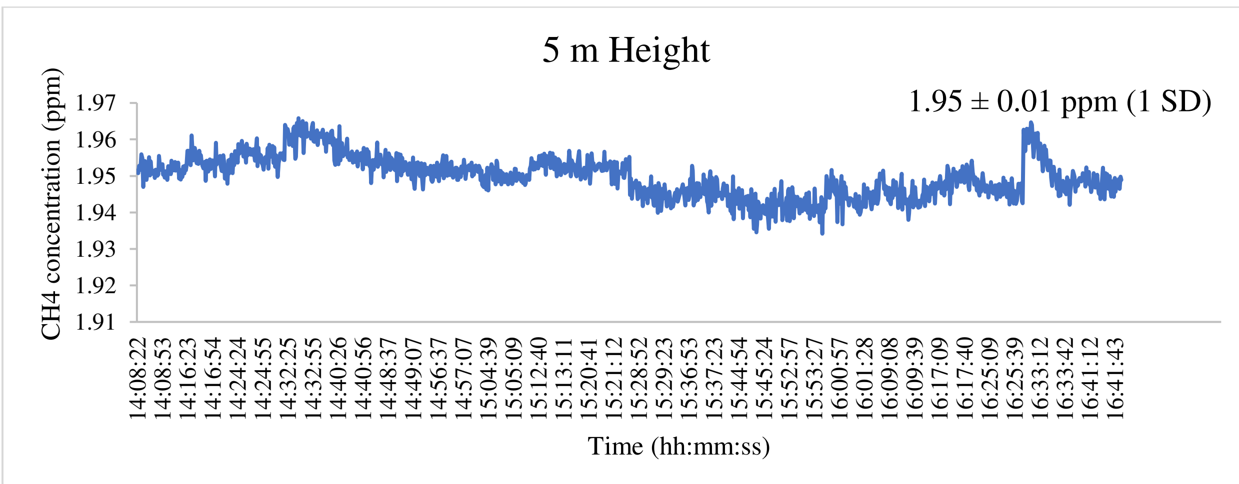

Figure A4 Background concentration at 5 m AGL

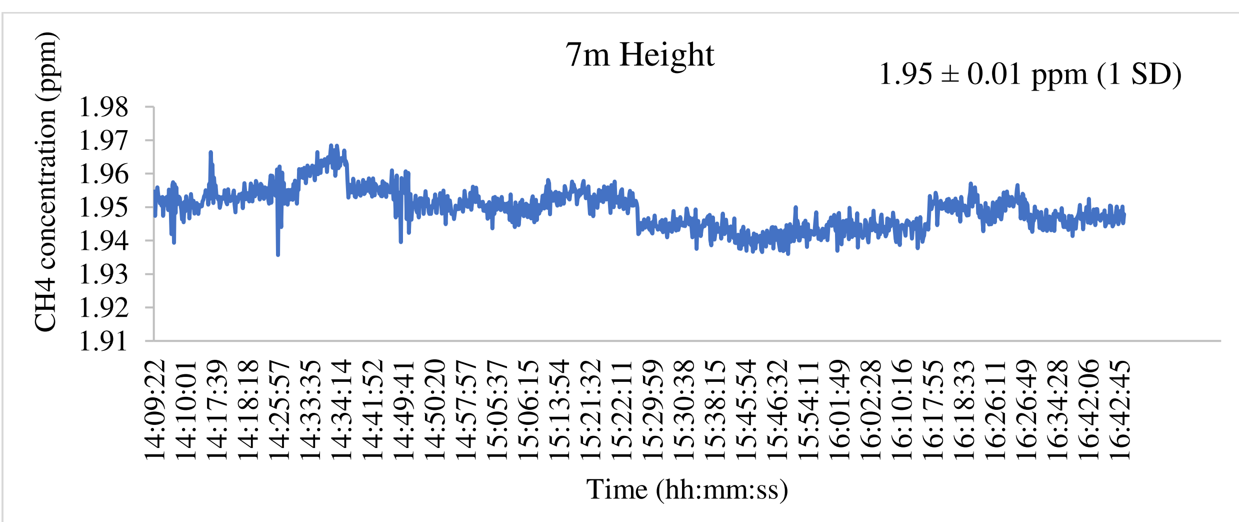

Figure A5 Background concentration at 7 m AGL

A2.2 Plume width calculation

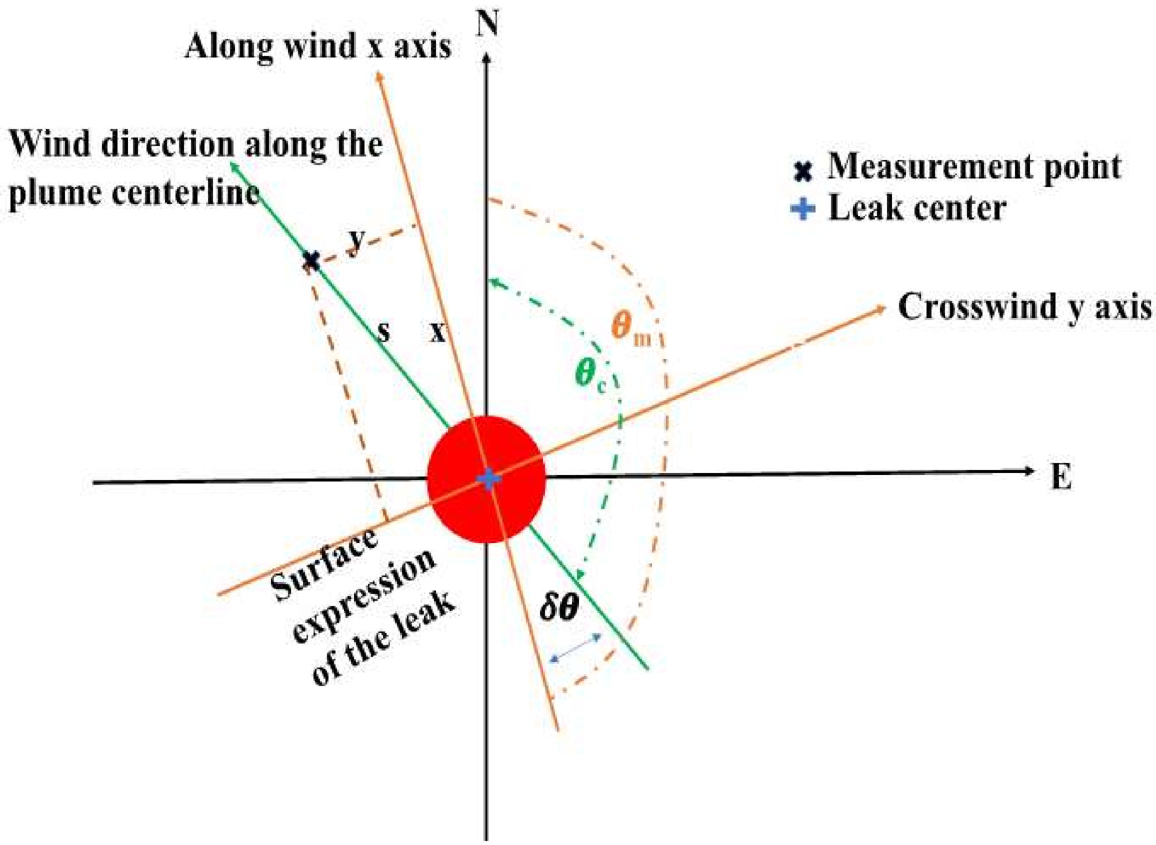

Figure A6 Calculation of crosswind y coordinates for each binned average CH_4 concentration. S : the distance from the leak center to the measurement point; θ_c : the wind direction of plume centerline at the measurement point; θ_m: the wind direction at the actual measurement time; $\delta\theta$ is $\theta_m - \theta_c$, the wind direction difference. $Y = s \cdot sin\ \delta\theta$

A2.3 Atmospheric stability and binning

4° was selected based on anemometer's *WD* accuracy ±2° (1 to 30 m/s). To evaluate the standard deviation in sampling for 15-minute atmospheric averaging:

σ sample $= \pm\frac{2°}{\sqrt{900s}} = \pm 0.07$

A2.4 Surface expression and subsurface conditions of the leak

The leaks in this study were subsurface point-source emissions, but the surface expression is an area source. To investigate if the surface expression of the leak would affect the above-ground plume width, WindTrax was used to simulate above-ground concentrations. WindTrax is a software tool that simulates short-range (within 1 km) atmospheric dispersion of the leak using backward Lagrangian stochastic model. 13 concentration sensors were positioned between 45°(N) and 225°(N) to replicate conditions when the mast (315°N) was downwind of the leak point, within 90°. The x and y locations of the concentration sensors were the along wind and crosswind distances relative to the mast location 5 m N 5 m W ($x = 7.07 \cos(315-\Theta)$; $y = 7.07 \sin(315-\Theta)$) used in the experiment. Meteorological conditions were the 15-minute average weather conditions from the baseline experiment, e.g., PGSC D, average wind speed (3.6 m/s), average temperature (11.21 °C), average pressure (84197.12 Pa), and wind direction (*WD* = 90°; the wind blowing directly to the central sensor). Input data to WindTrax were atmospheric stability PGSC, wind speed, *WD*, temperature, pressure, area of the emission, known leak rate per area, and background concentration. Concentrations were measured 0.5 m above-ground. The standard anemometer, pressure and temperature sensors were positioned 50 m N 20 m E (same location as METEC's meteorological station) at 6 m height. Area surface emissions were simulated for different area-source surface expressions, a Gaussian equation fitted to each of the area-source results, and plume width calculated. Limitations to simulating using WindTrax were that it assumes a surface, flat, homogenous area source, free of obstructions.

Table A1 Concentration sensors' position in WindTrax

Distance from central sensor (mast) to leak point	Sensor locations(Θ)	Angle between sensor and mast	X	Y
7.07	45	270	0.00	-7.07
	60	255	-1.83	-6.83
	75	240	-3.54	-6.12
	90	225	-5.00	-5.00
	105	210	-6.12	-3.54
	120	195	-6.83	-1.83
	135	180	-7.07	0.00
	150	165	-6.83	1.83
	165	150	-6.12	3.54
	180	135	-5.00	5.00
	195	120	-3.54	6.12
	210	105	-1.83	6.83
	225	90	0.00	7.07

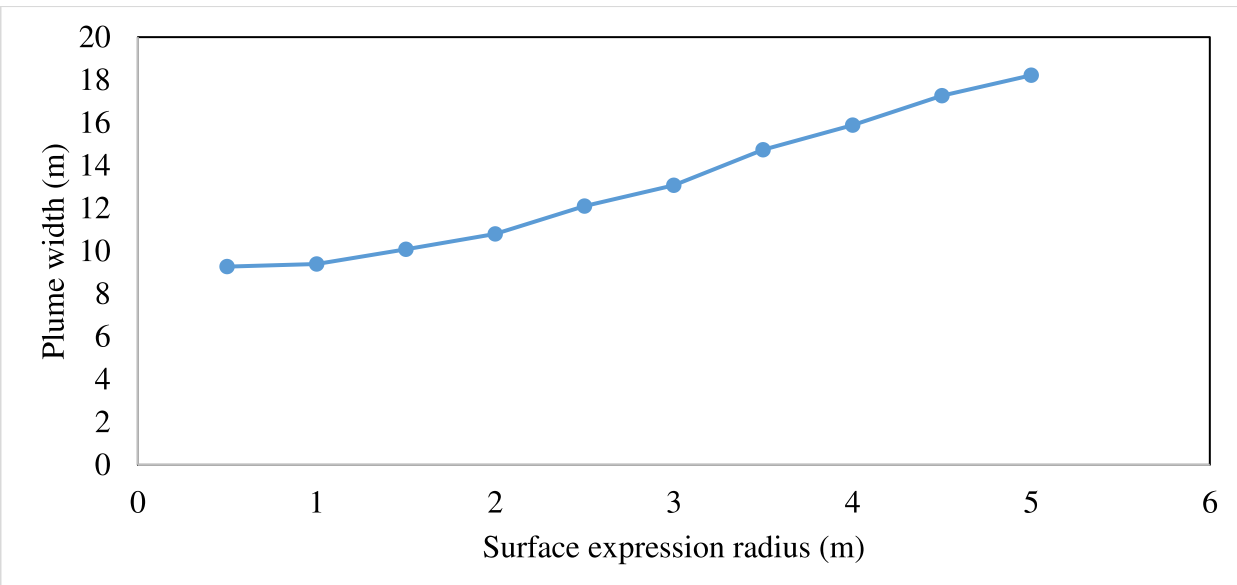

Figure A7 WindTrax simulation results

The plume widths for Experiment 1 were compared to WindTrax results. The uncertainty in plume width due to surface expression and subsurface effects is [-42/+14] %.

A3 Gaussian Model Fitting

Plots of the Gaussian fits are used to generate plume widths. The red line is the Gaussian fit, blue points are the data points, and the black horizontal line is the 0.1 threshold of concentrations above background (enhancement).

A3.1 Neutral conditions

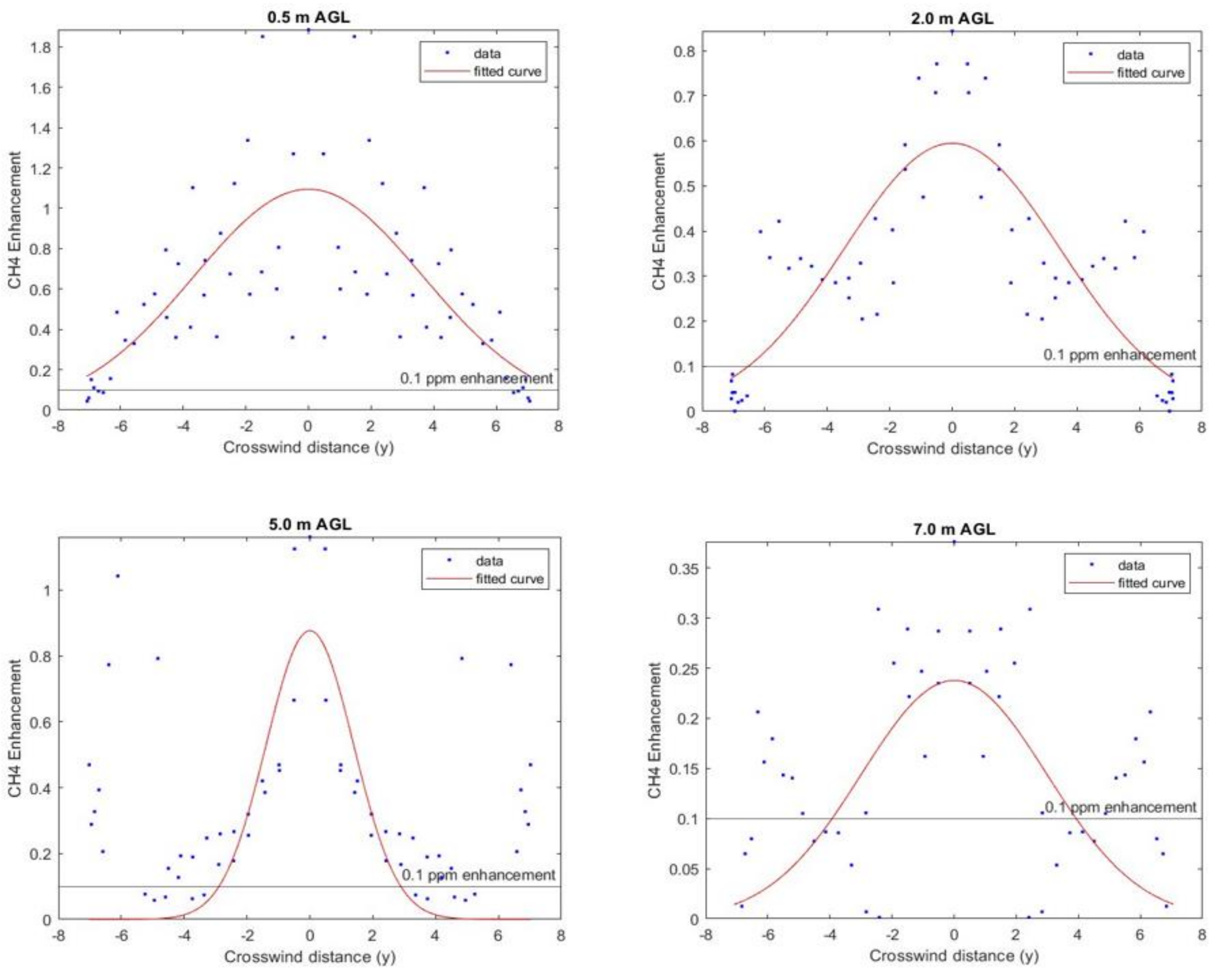

Figure A8 Plumes for Experiment 1, PGSC D

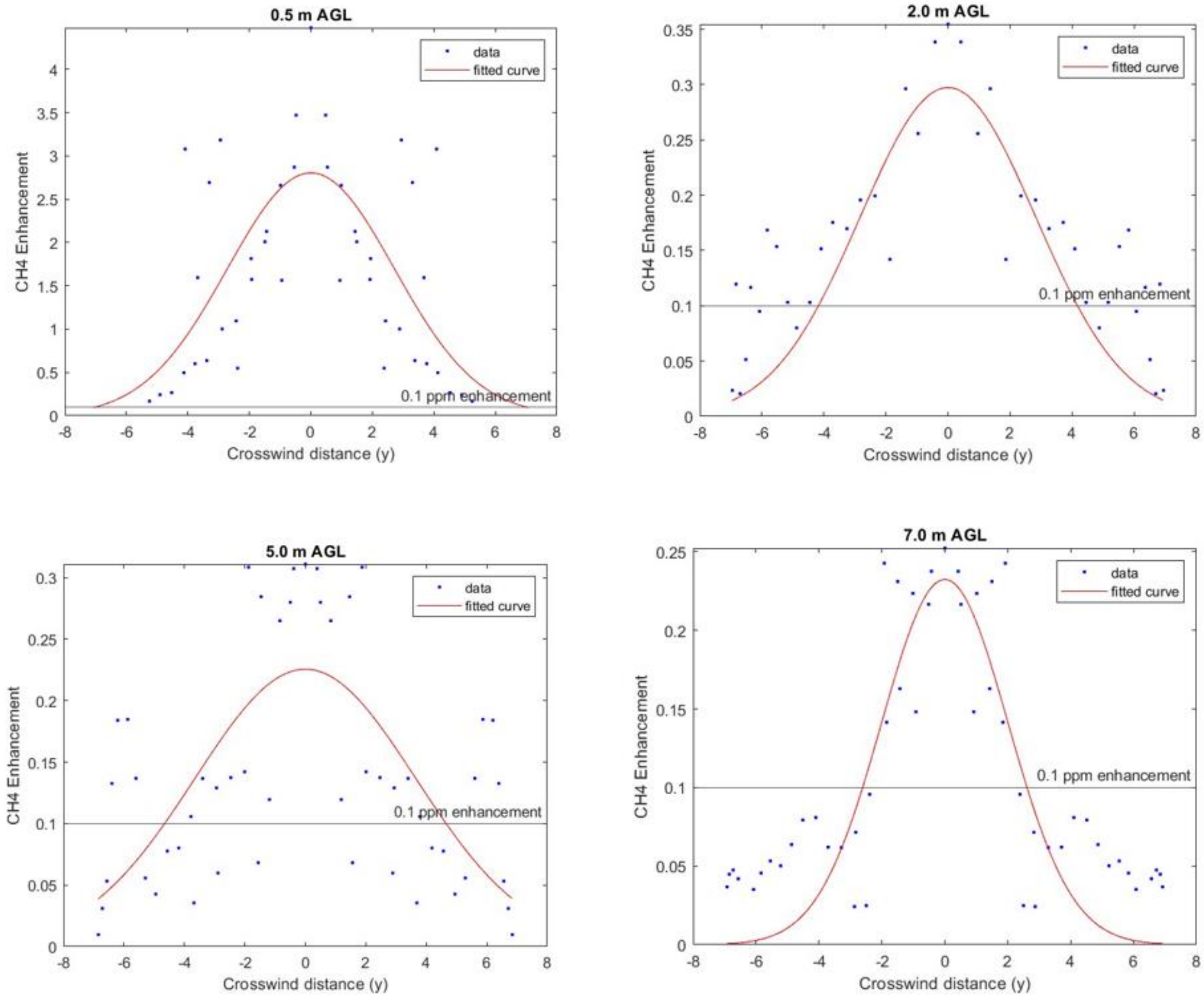

Figure A9 Plumes for Experiment 2, PGSC D

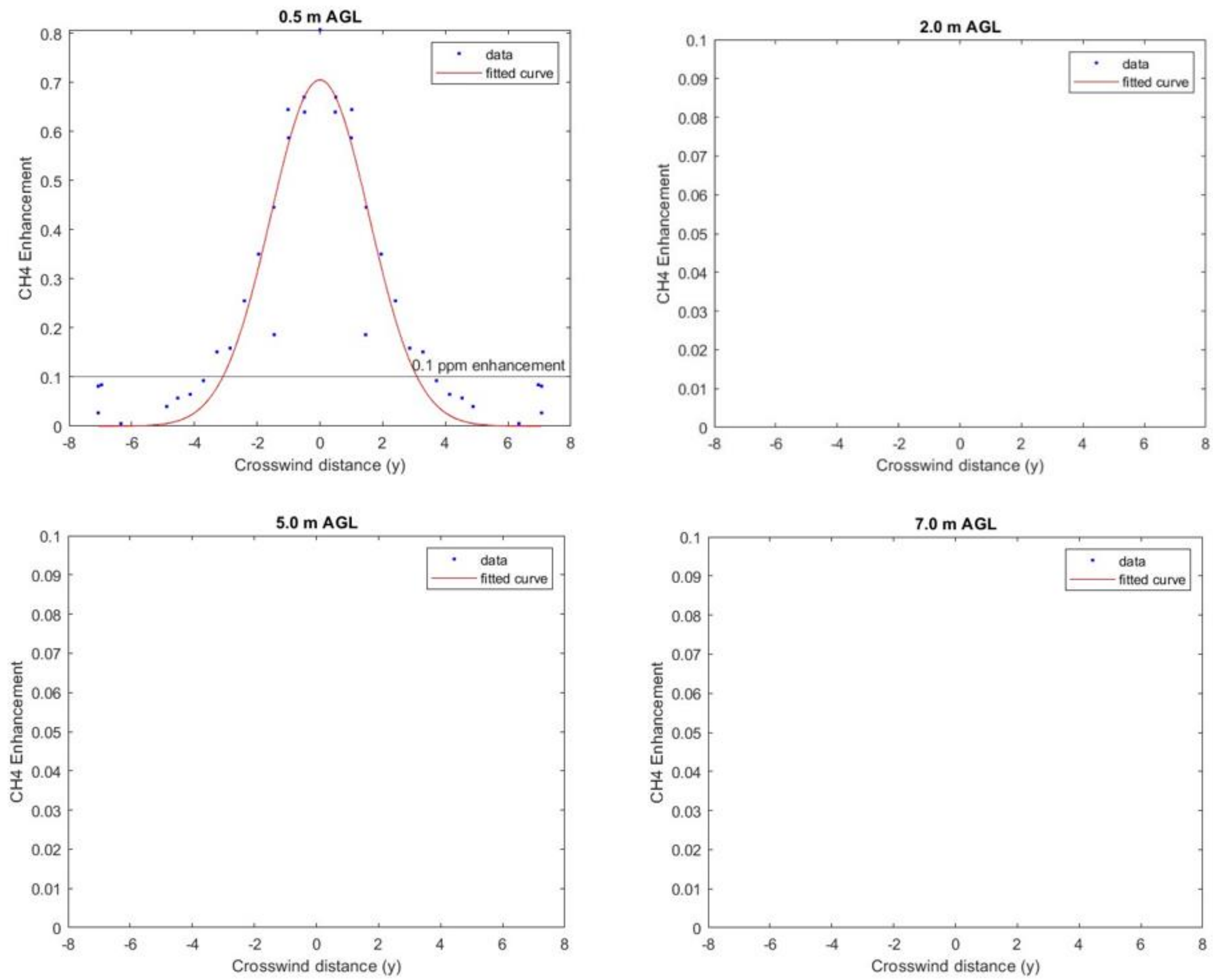

Figure A10 Plumes for Experiment 3, PGSC D

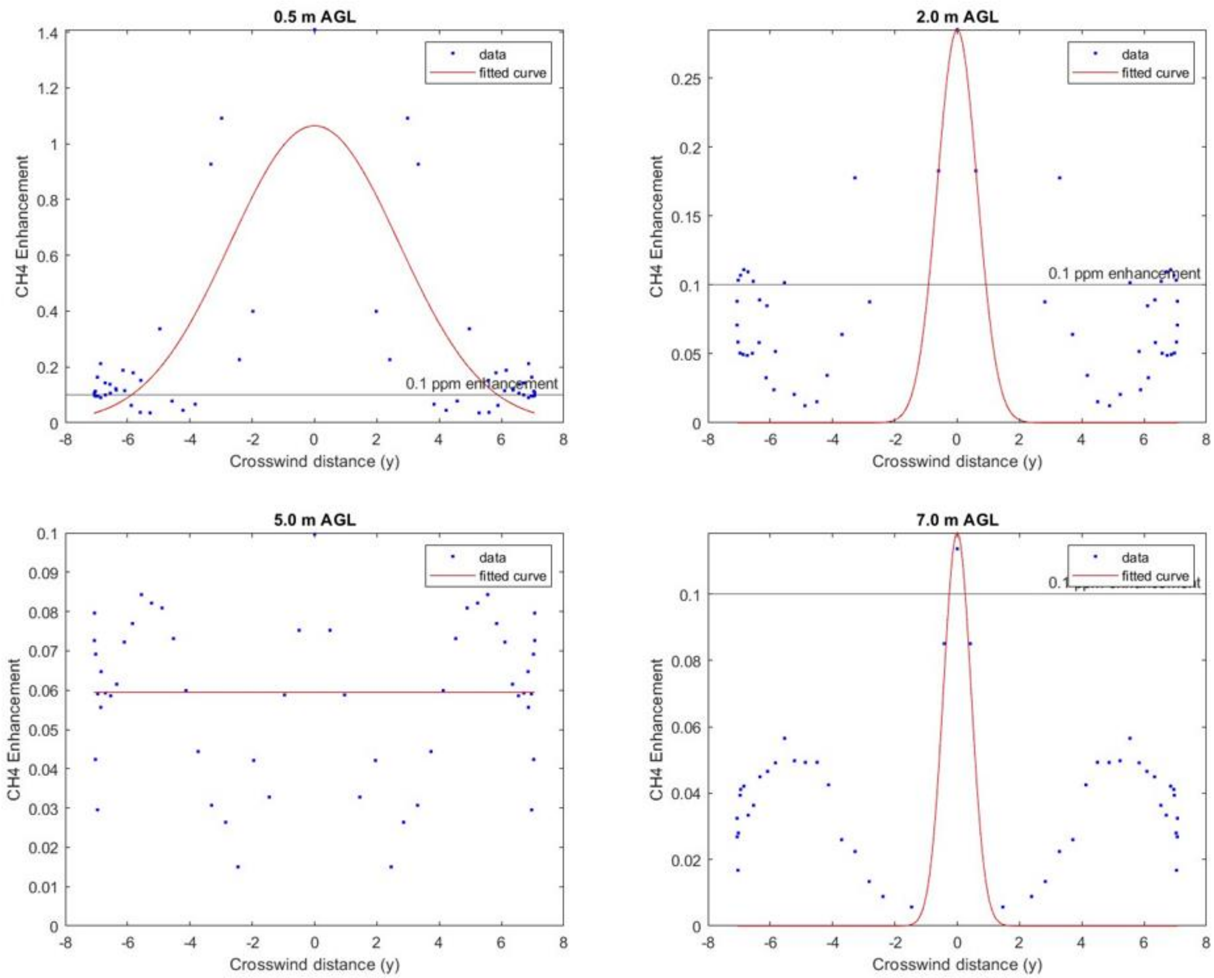

Figure A11 Plumes for Experiment 4, PGSC D

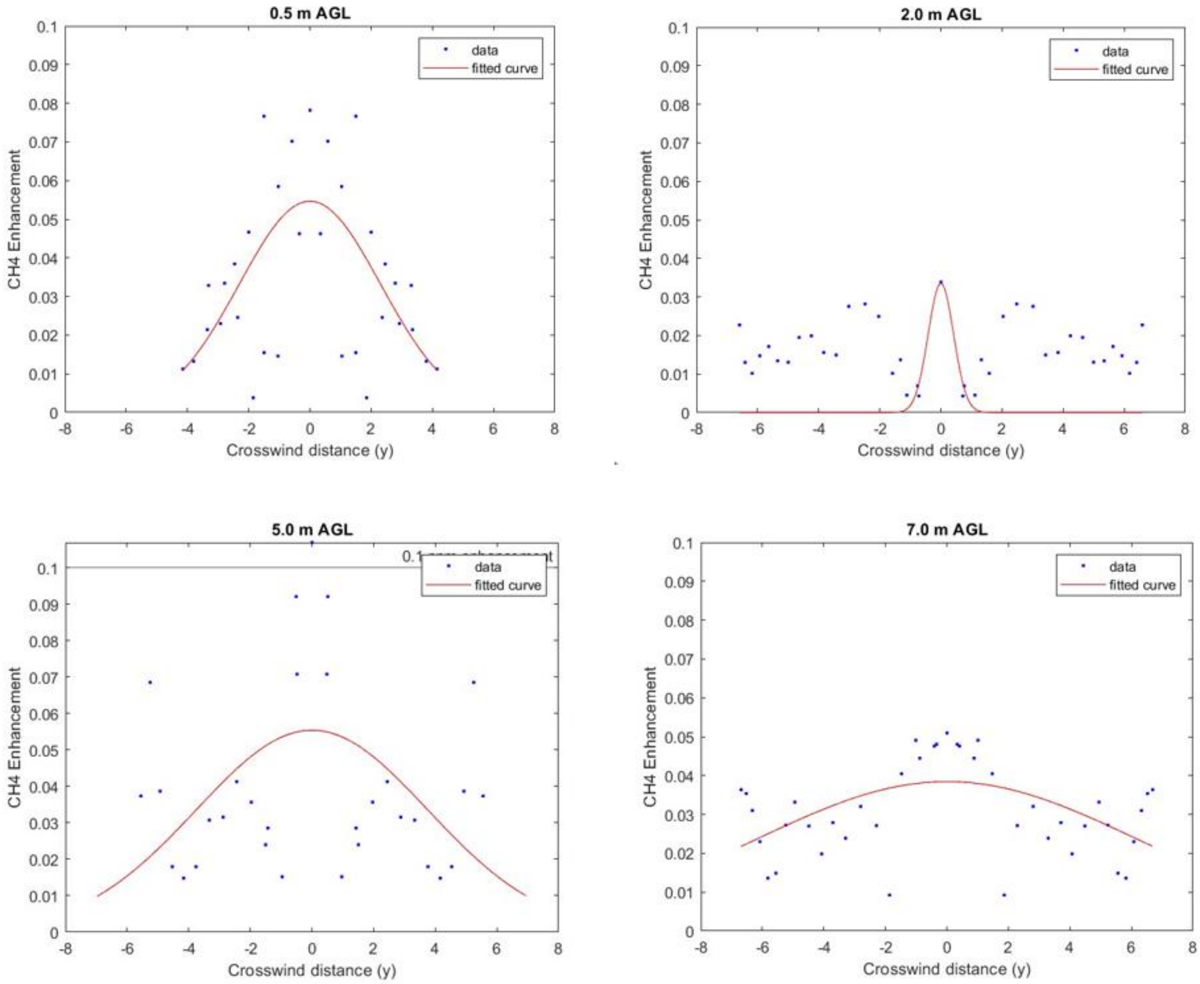

Figure A12 Plumes for Experiment 5, PGSC D

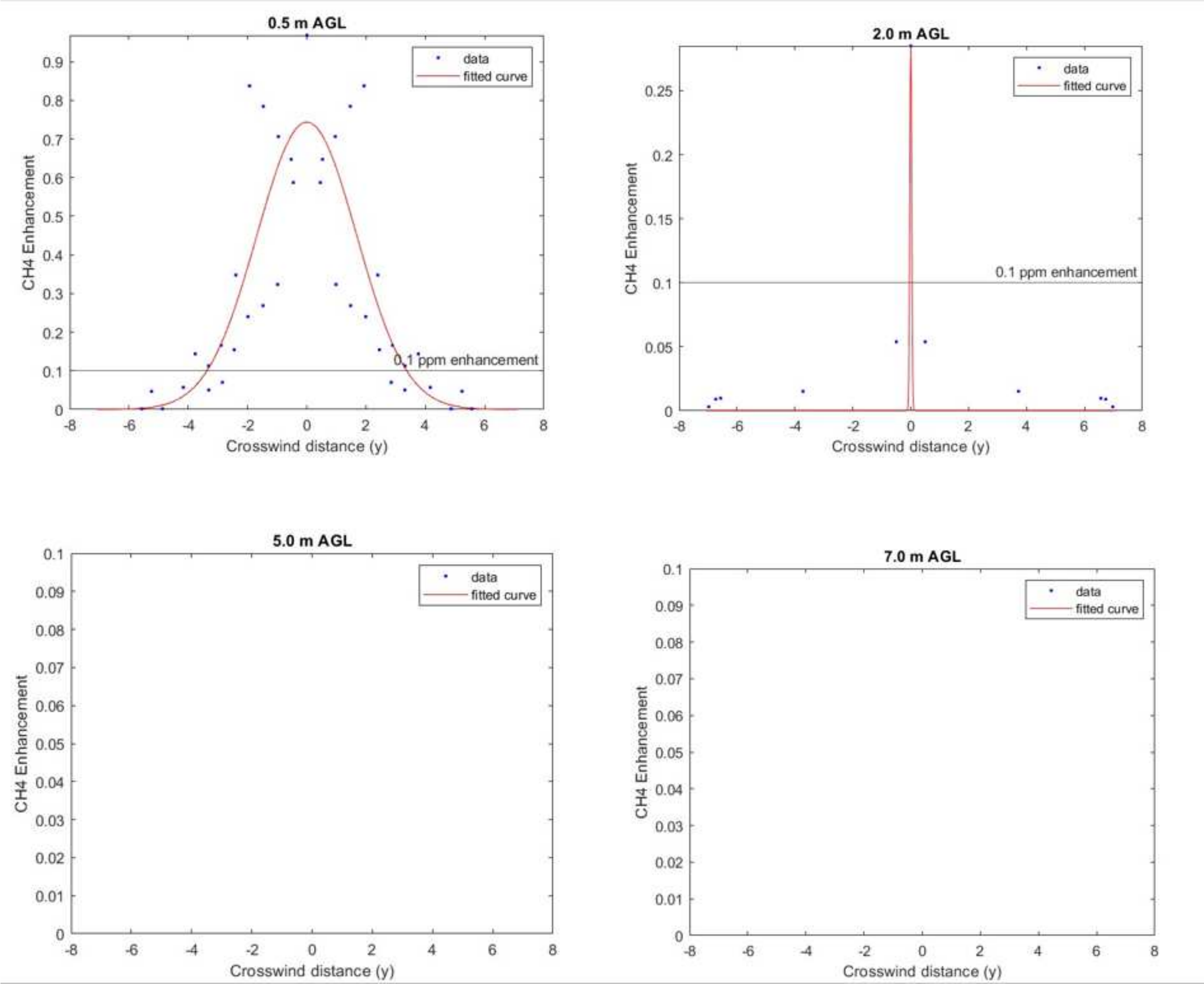

Figure A13 Plumes for Experiment 6, PGSC D

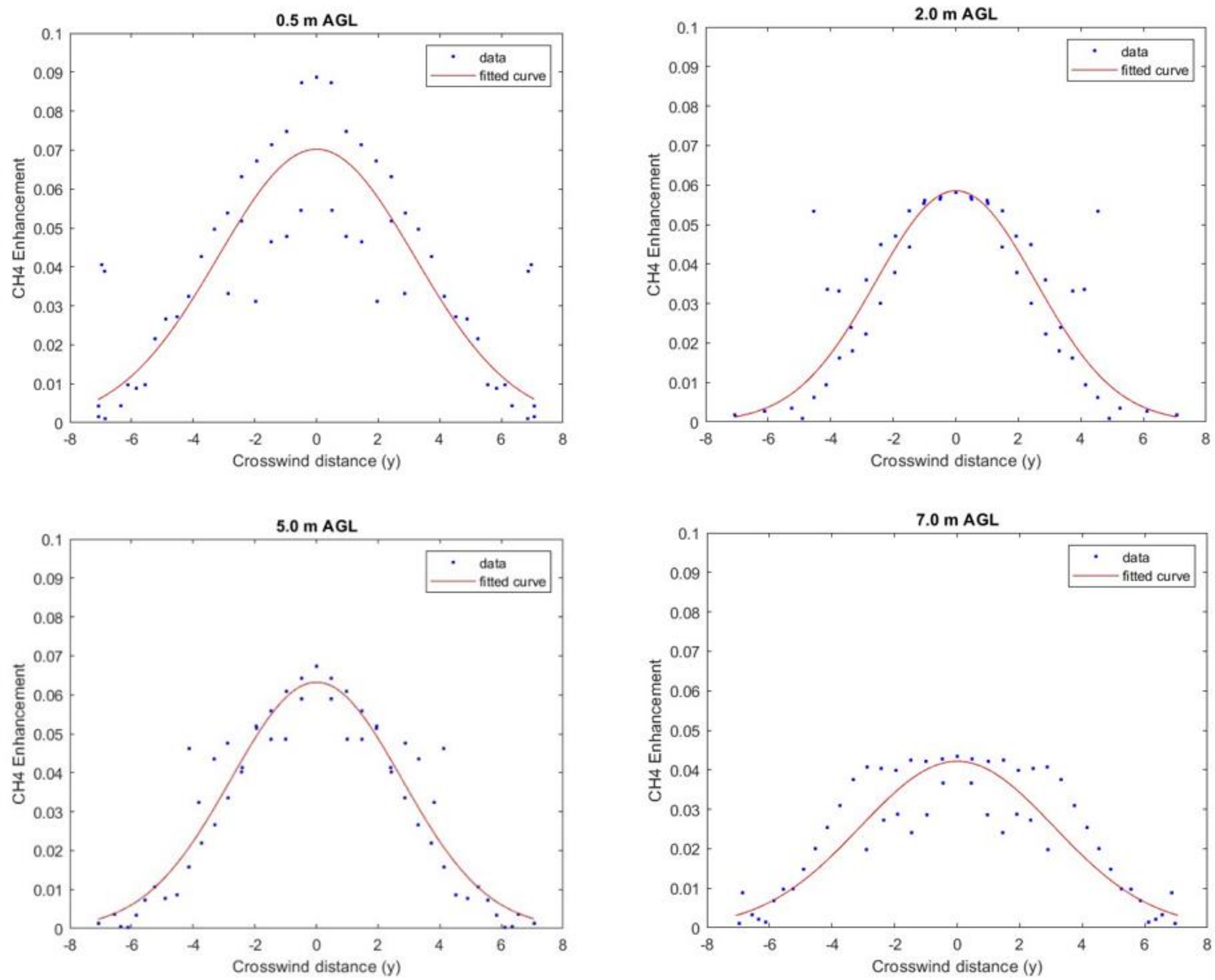

Figure A14 Plumes for Experiment 7, PGSC D

A3.2 Non-neutral conditions

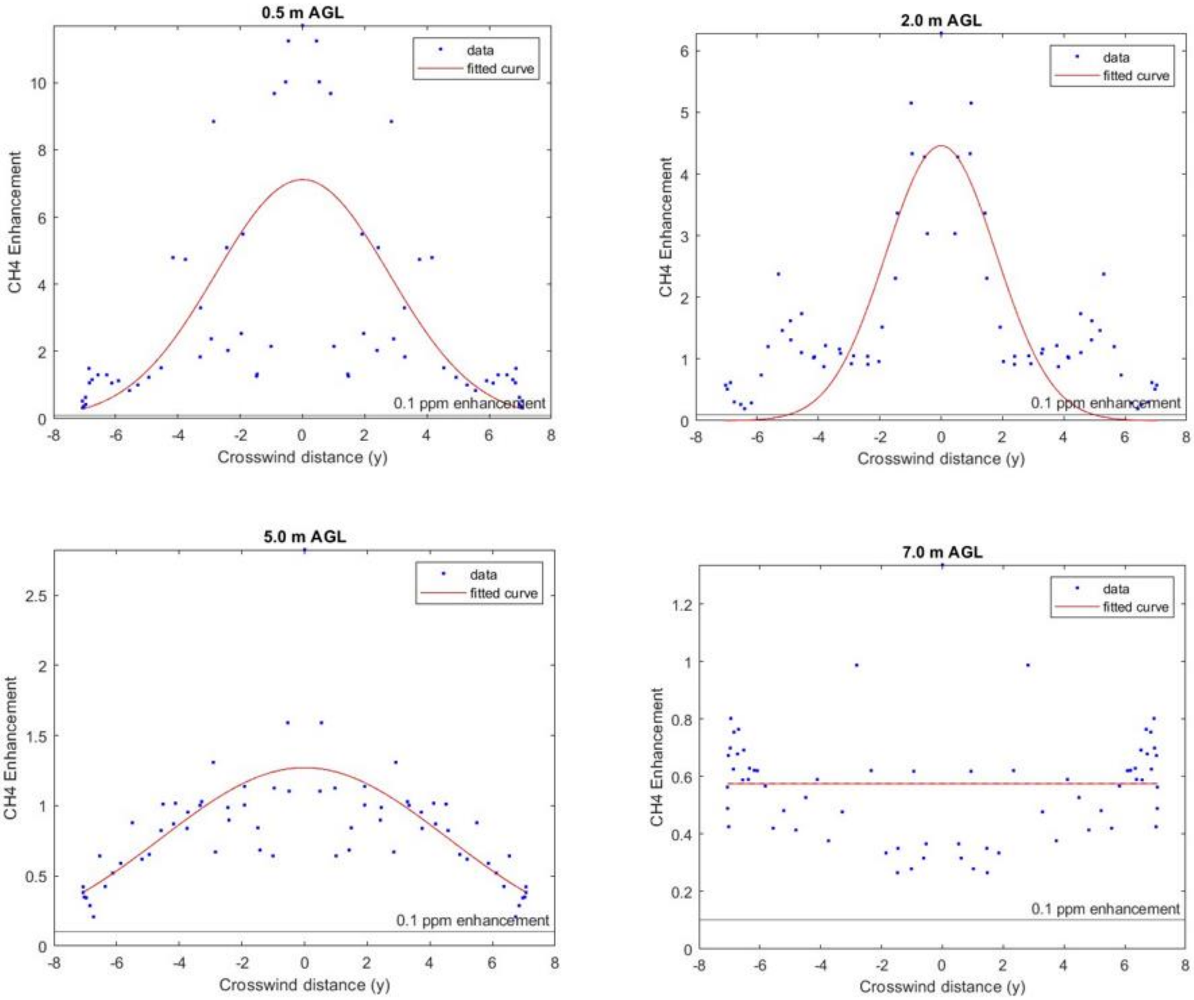

Figure A15 Plumes for Experiment 1, PGSC A

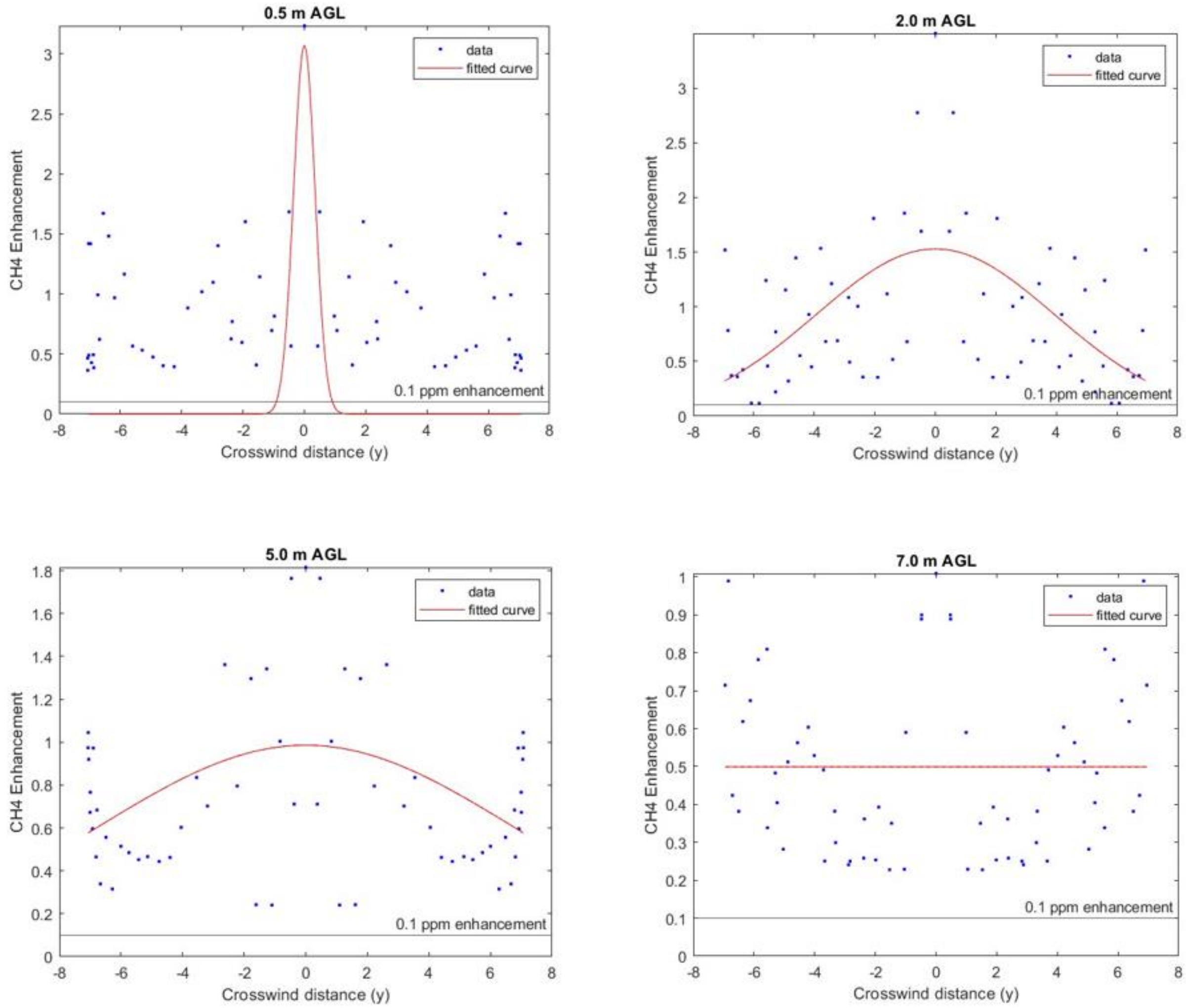

Figure A16 Plumes for Experiment 1, PGSC B-C

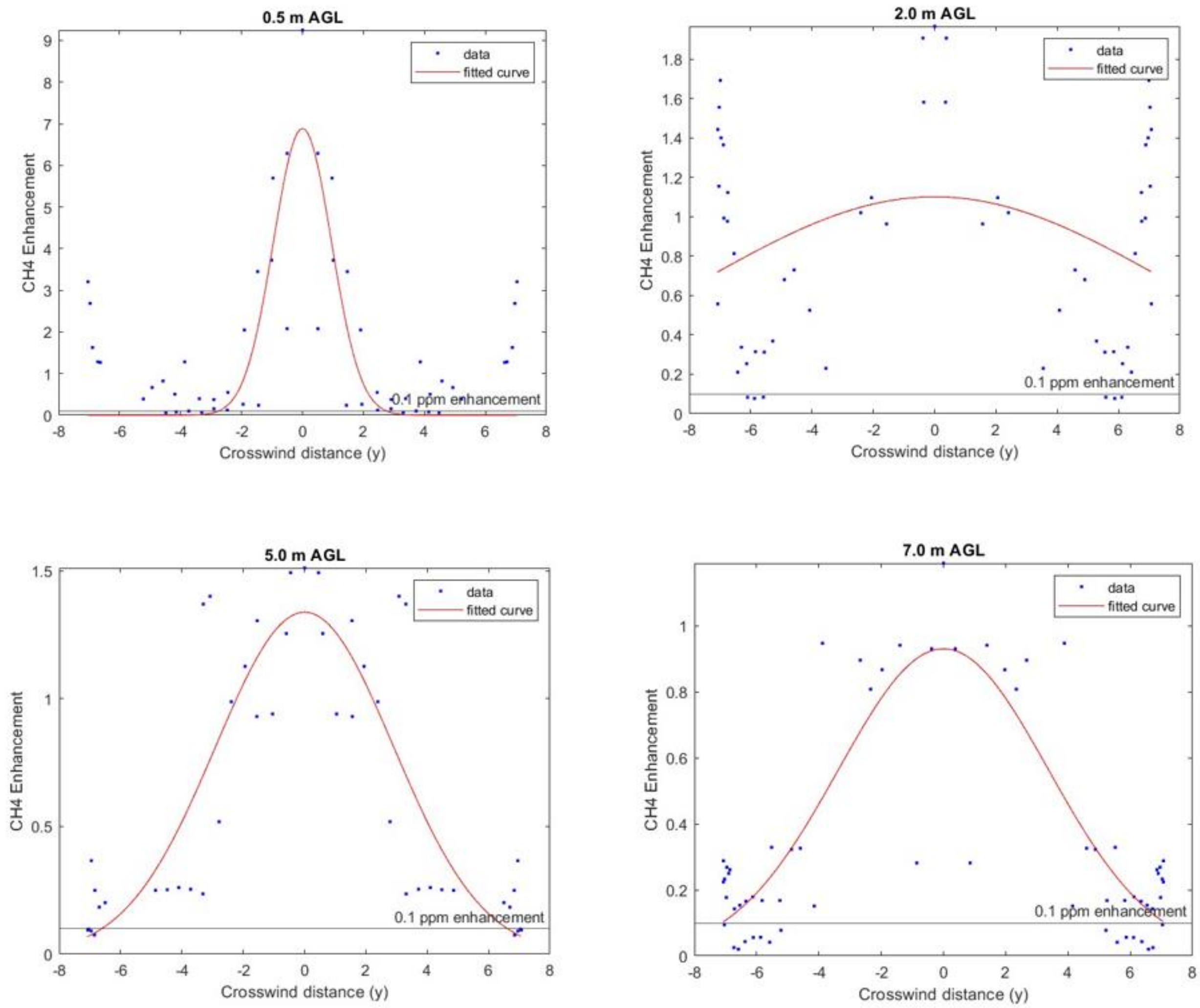

Figure A17 Plumes for Experiment 1, PGSC E-F

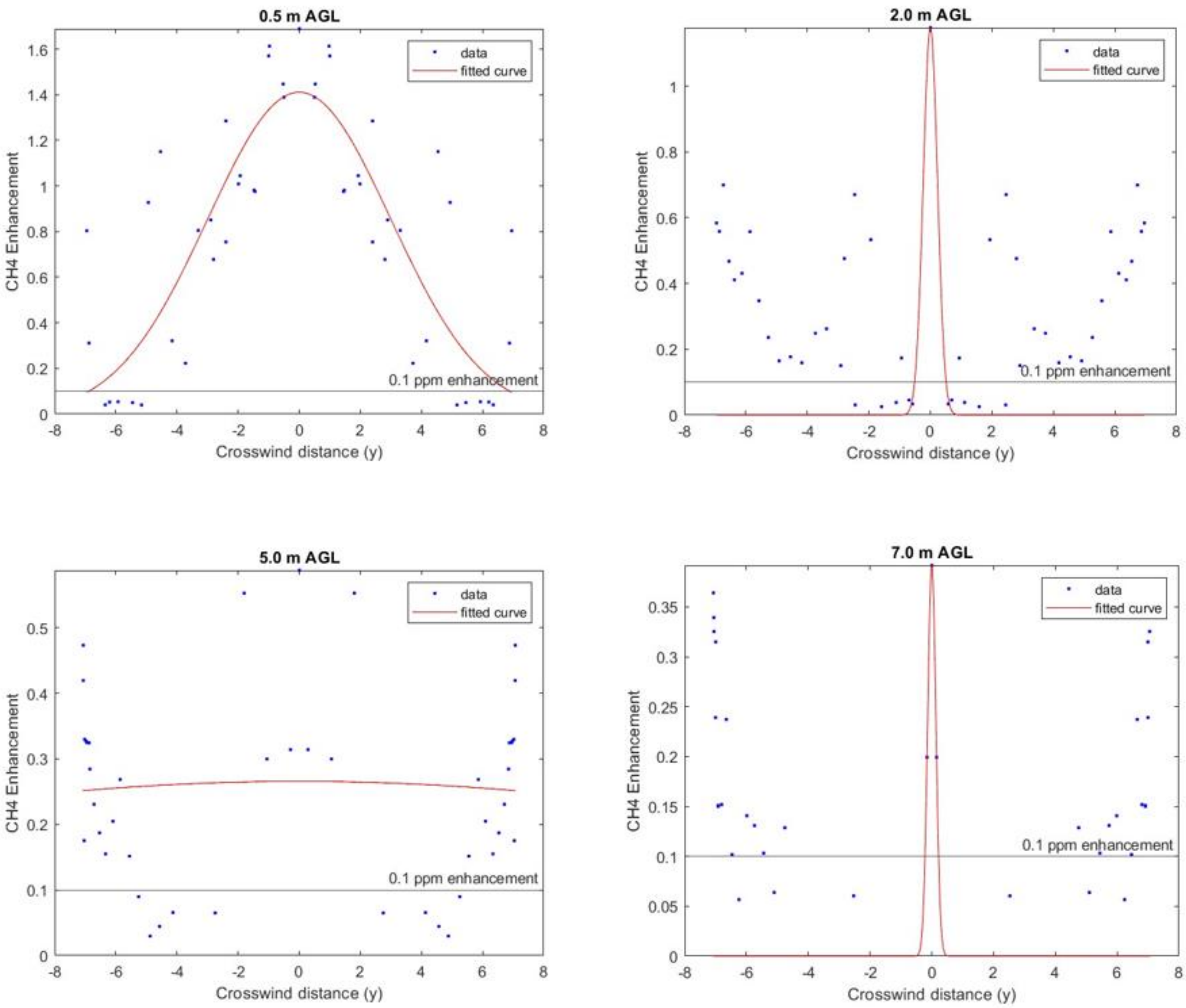

Figure A18 Plumes for Experiment 2, PGSC A

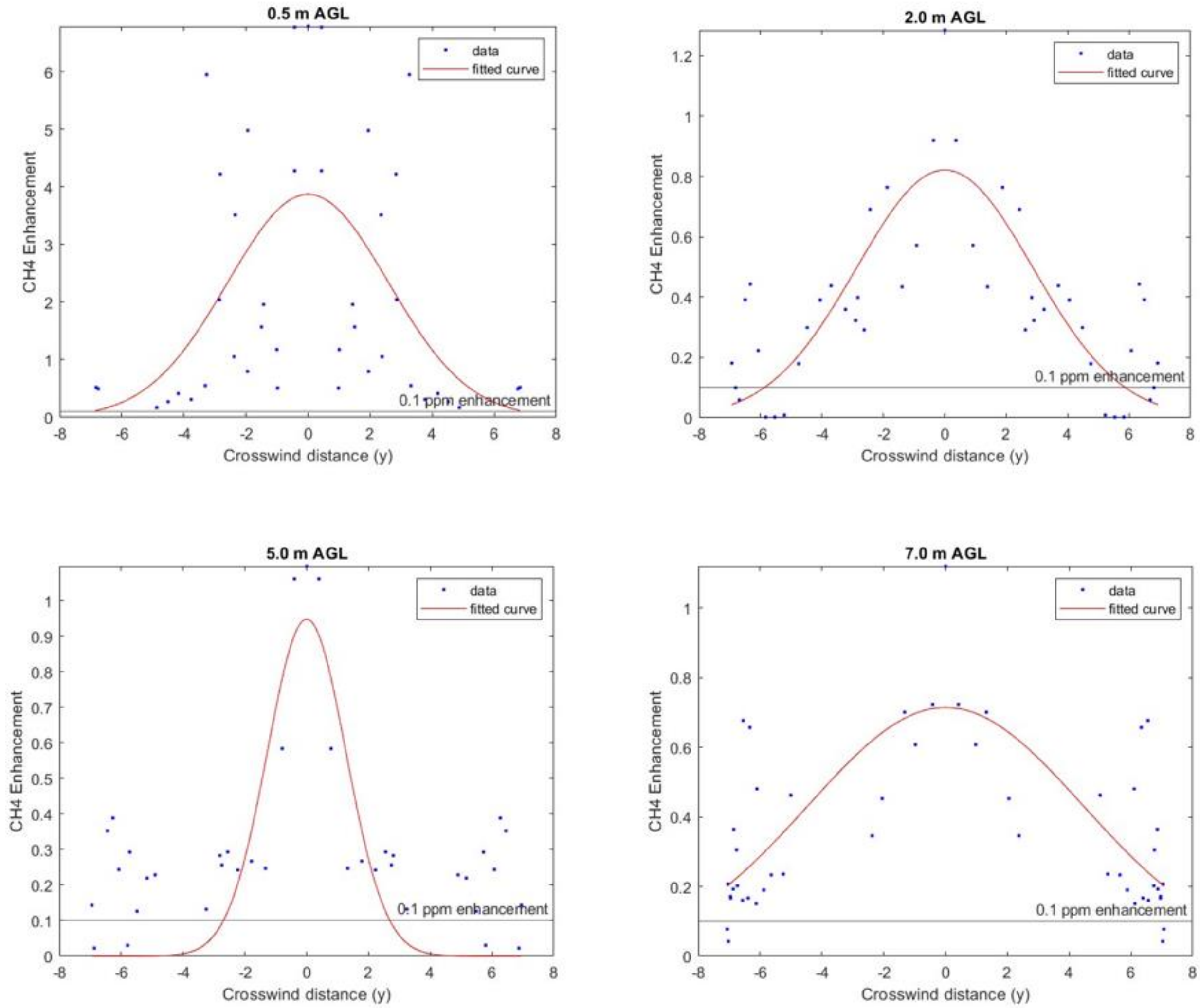

Figure A19 Plumes for Experiment 2, PGSC B-C

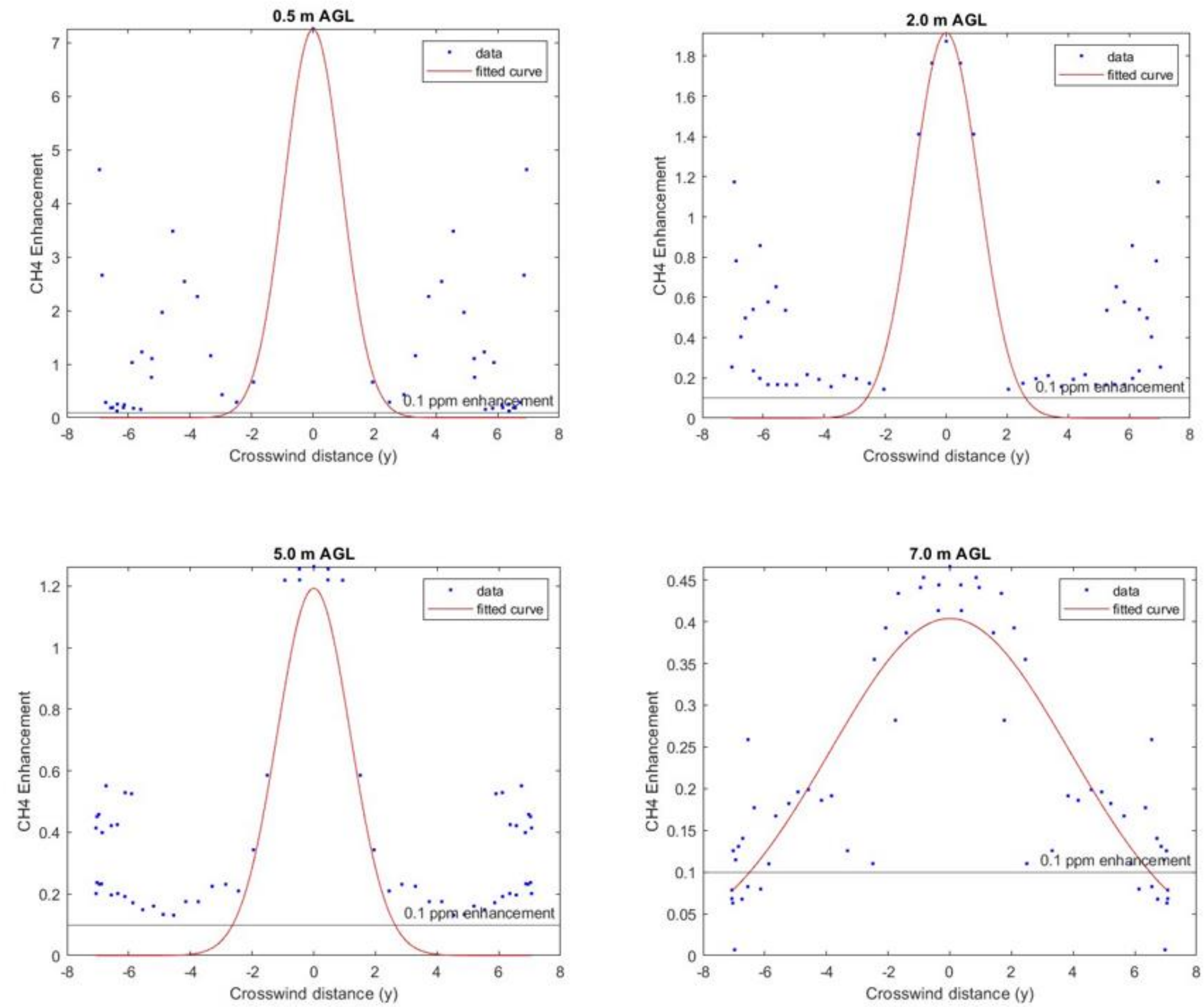

Figure A20 Plumes for Experiment 2, PGSC E-F

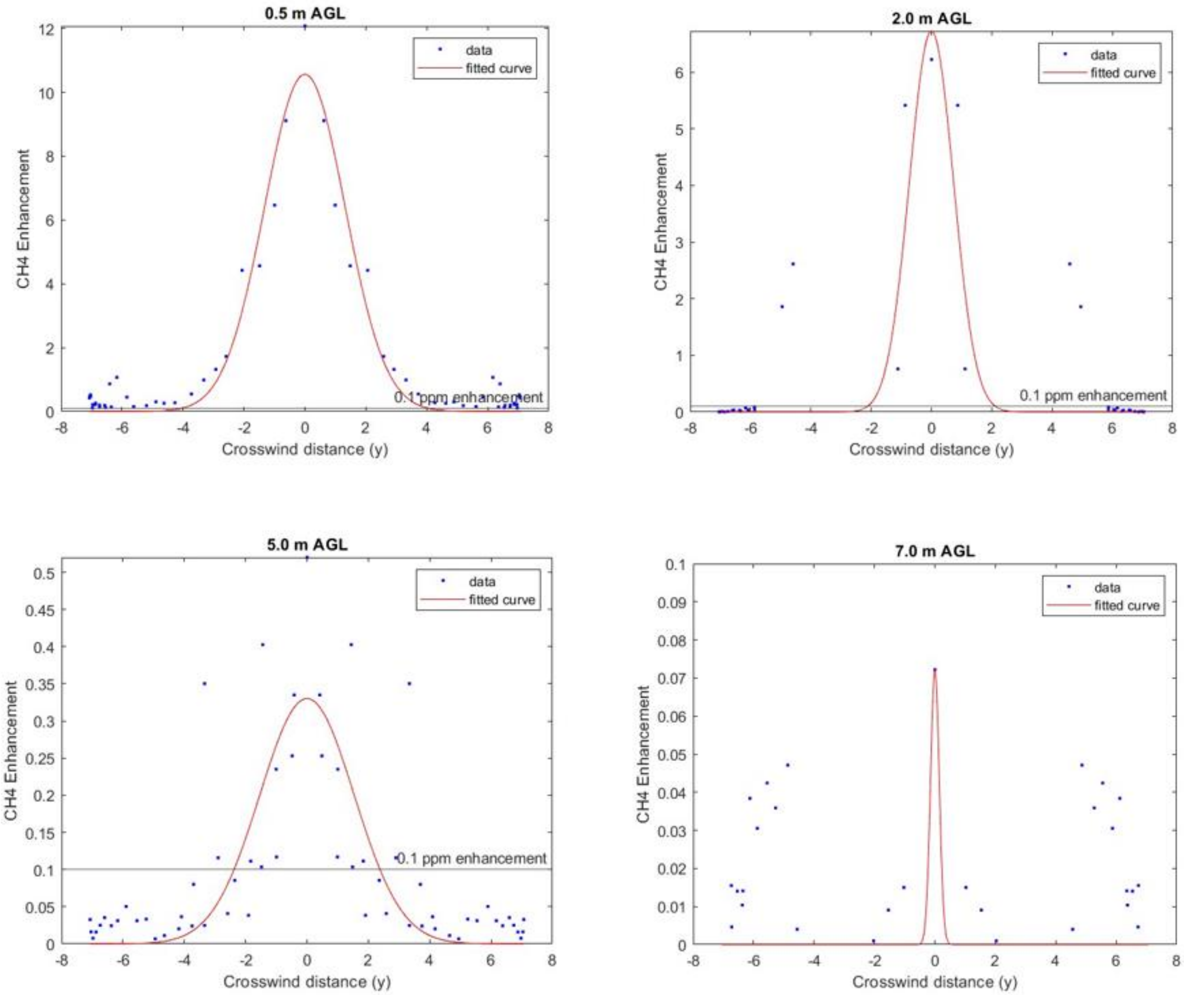

Figure A21 Plumes for Experiment 3, PGSC A

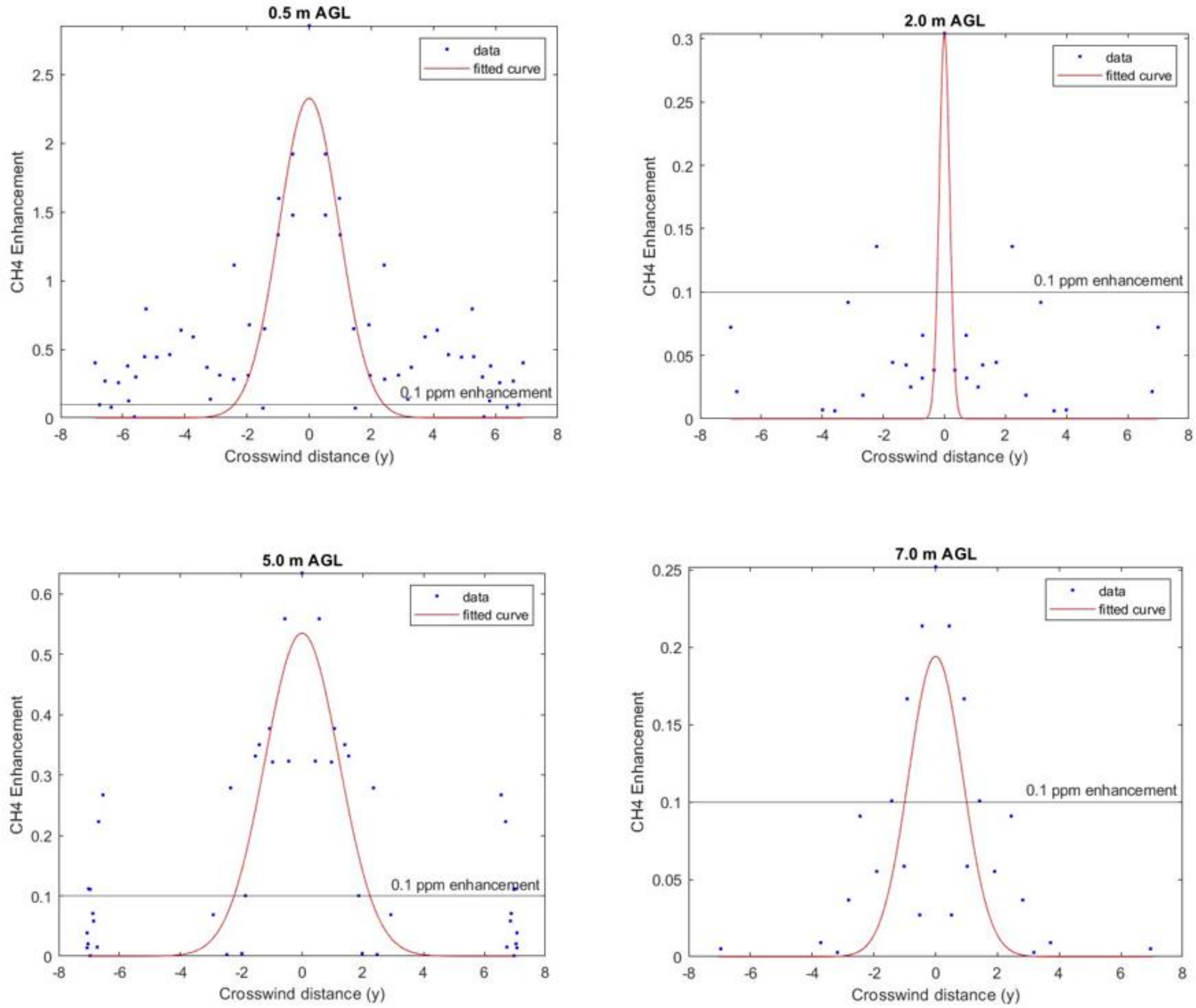

Figure A22 Plumes for Experiment 3, PGSC B-C

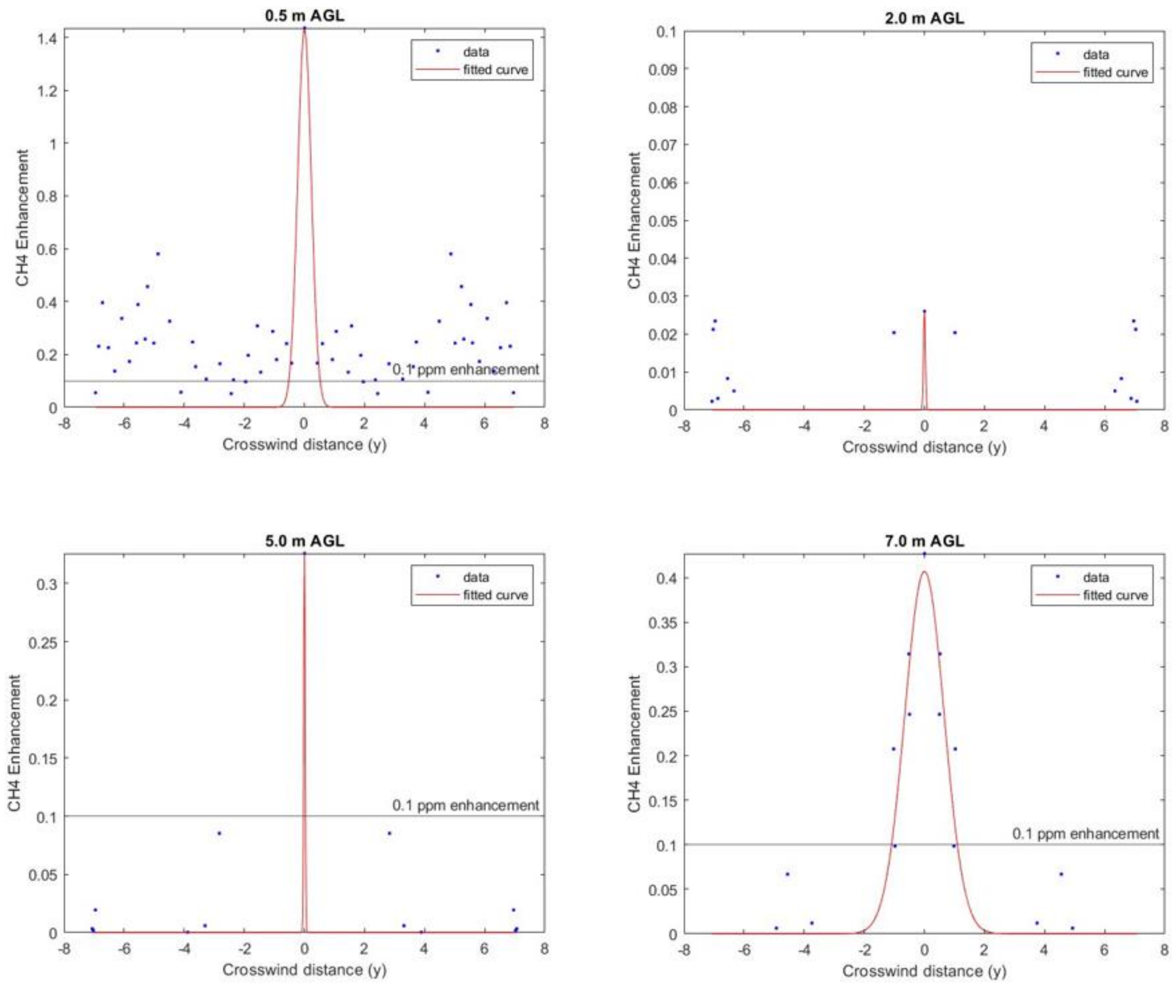

Figure A23 Plumes for Experiment 3, PGSC E-F

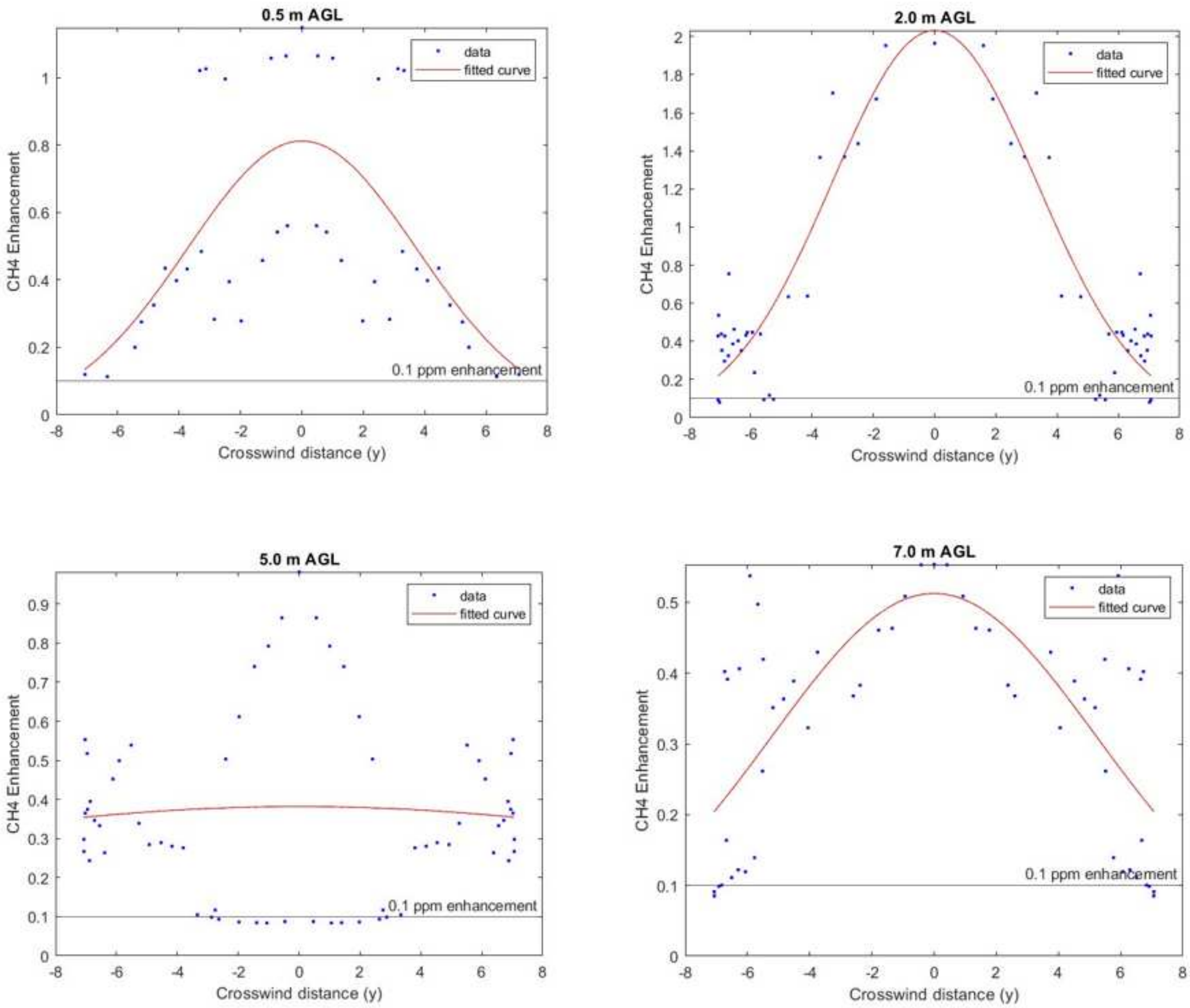

Figure A24 Plumes for Experiment 4, PGSC A

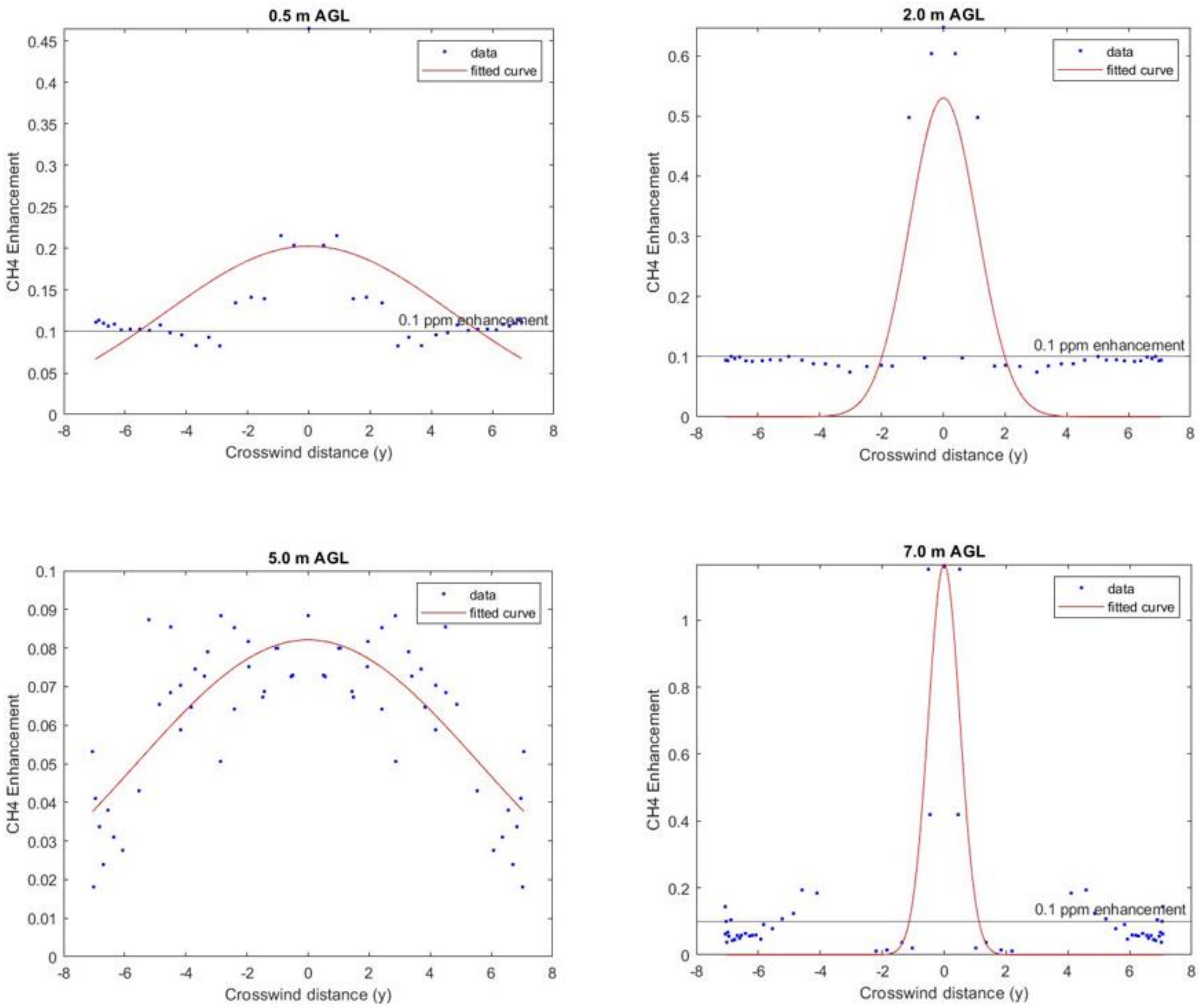

Figure A25 Plumes for Experiment 4, PGSC B-C

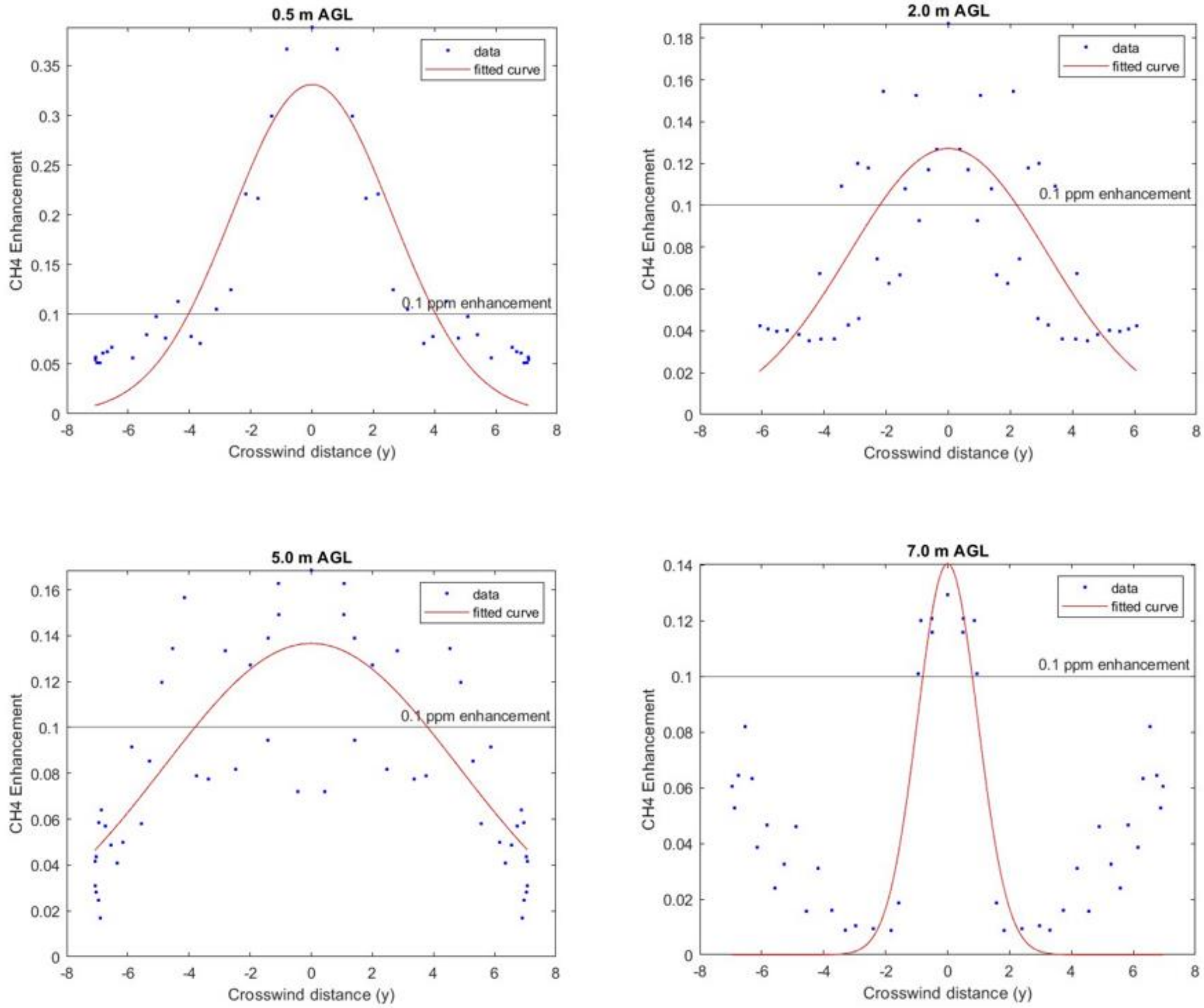

Figure A26 Plumes for Experiment 4, PGSC E-F

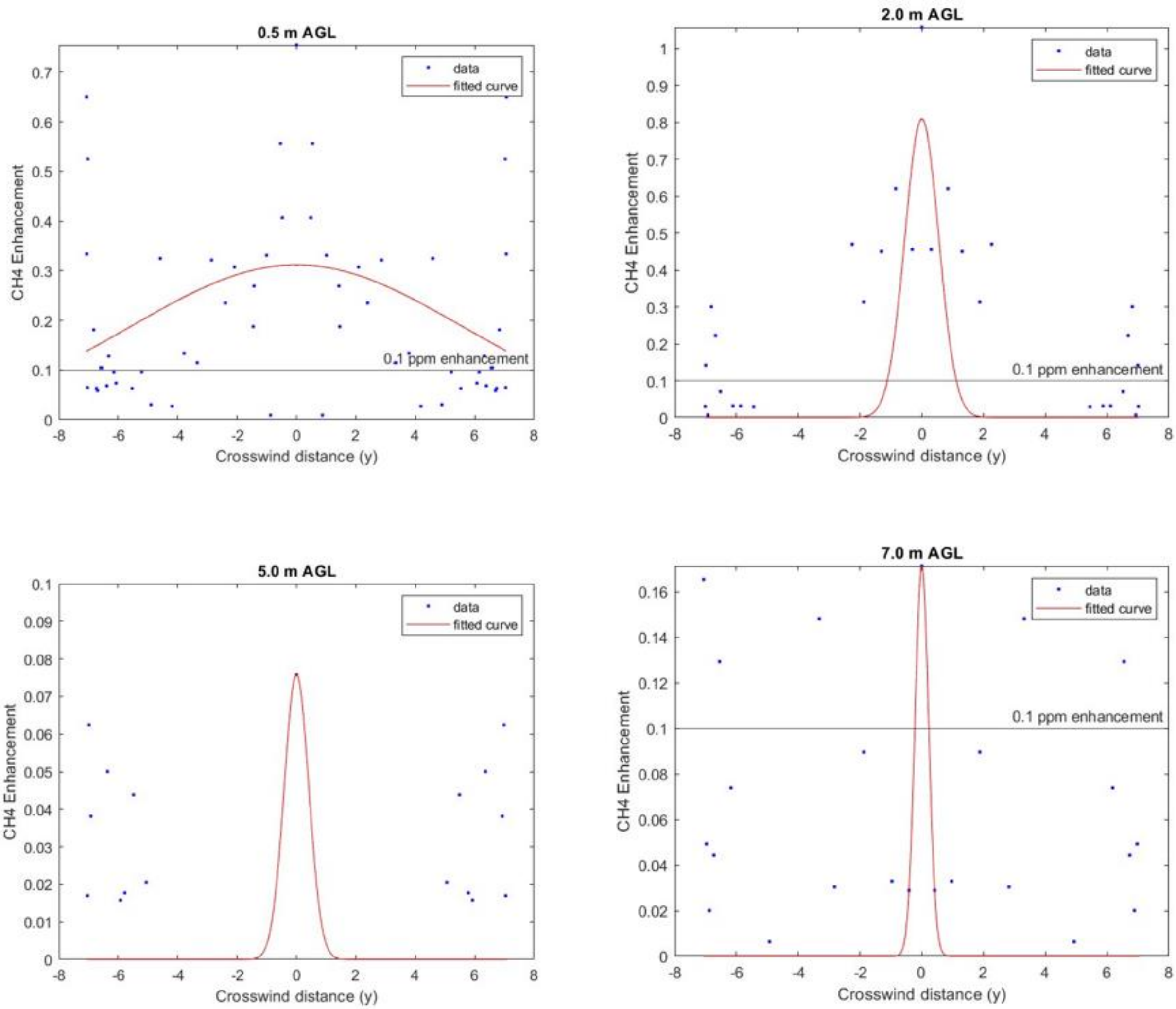

Figure A27 Plumes for Experiment 5, PGSC A

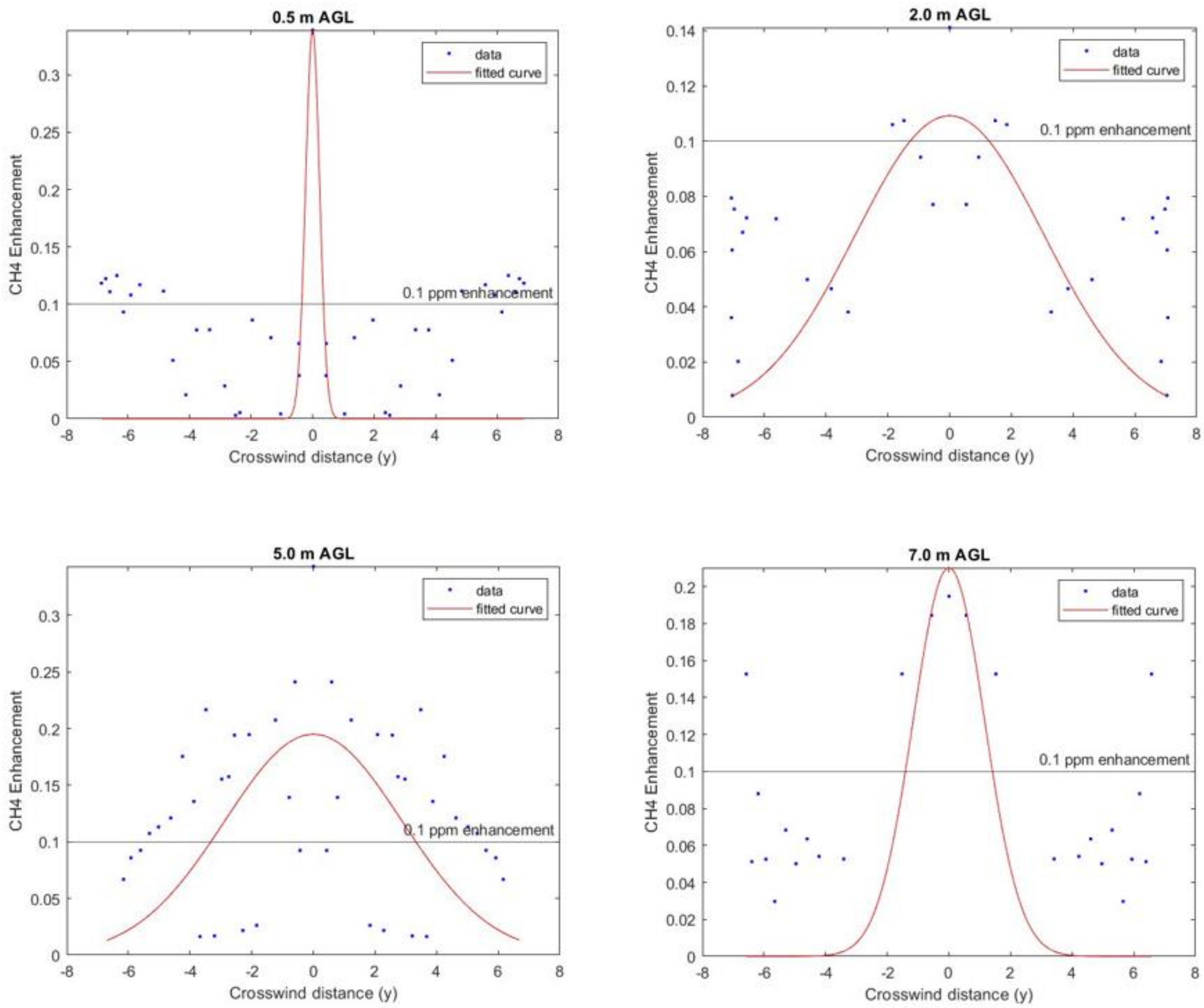

Figure A28 Plumes for Experiment 5, PGSC B-C

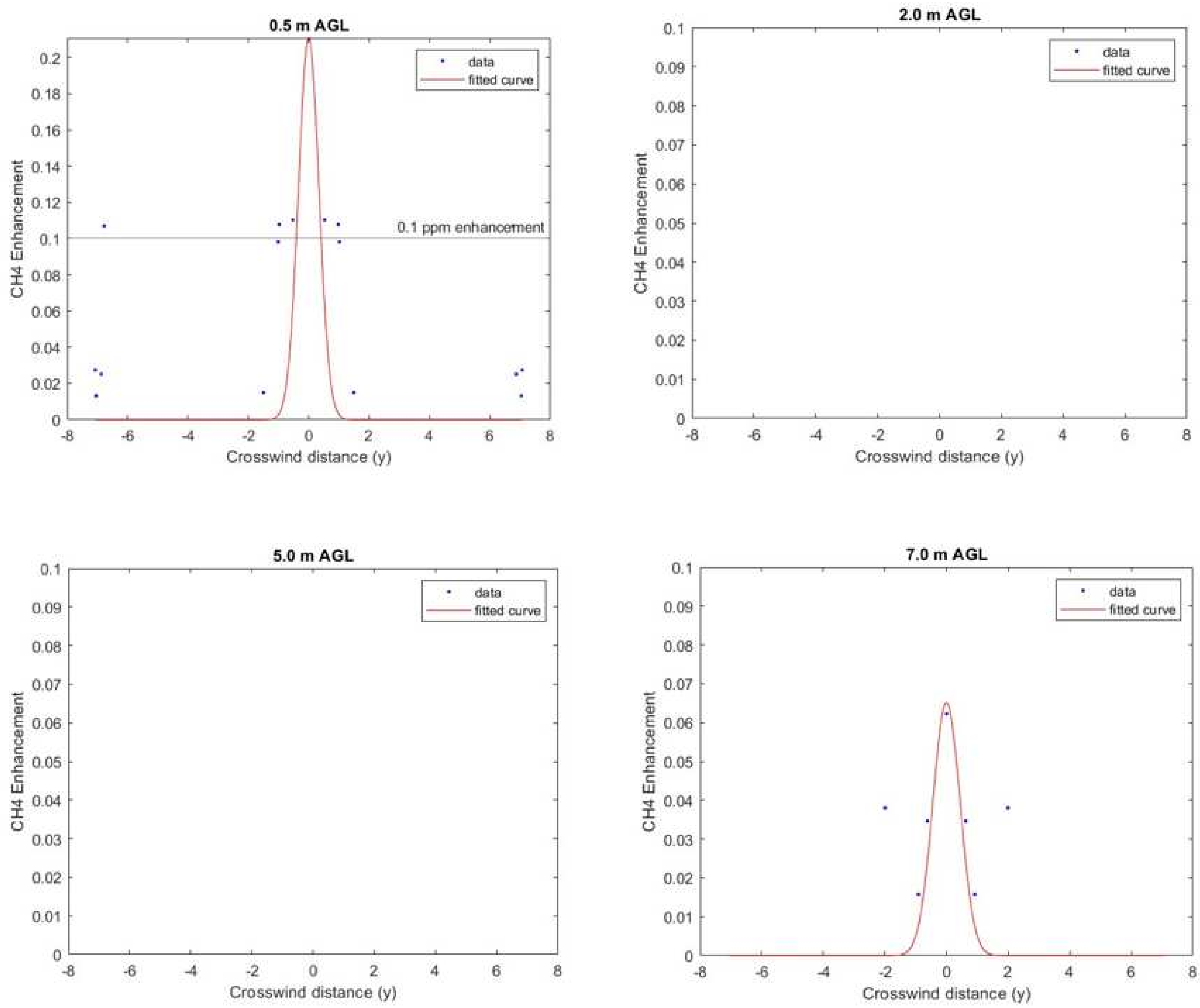

Figure A29 Plumes for Experiment 5, PGSC E-F

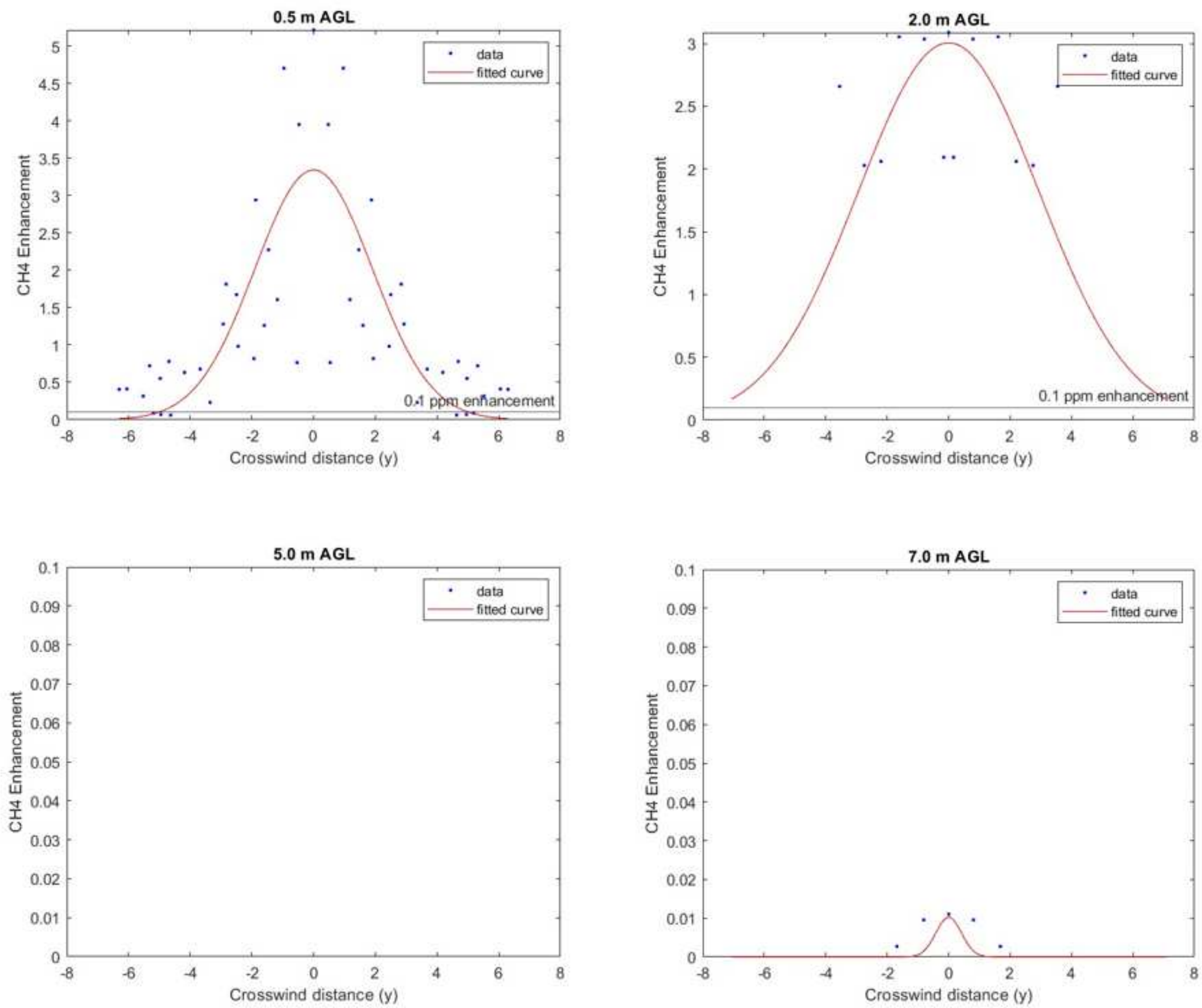

Figure A30 Plumes for Experiment 6, PGSC A

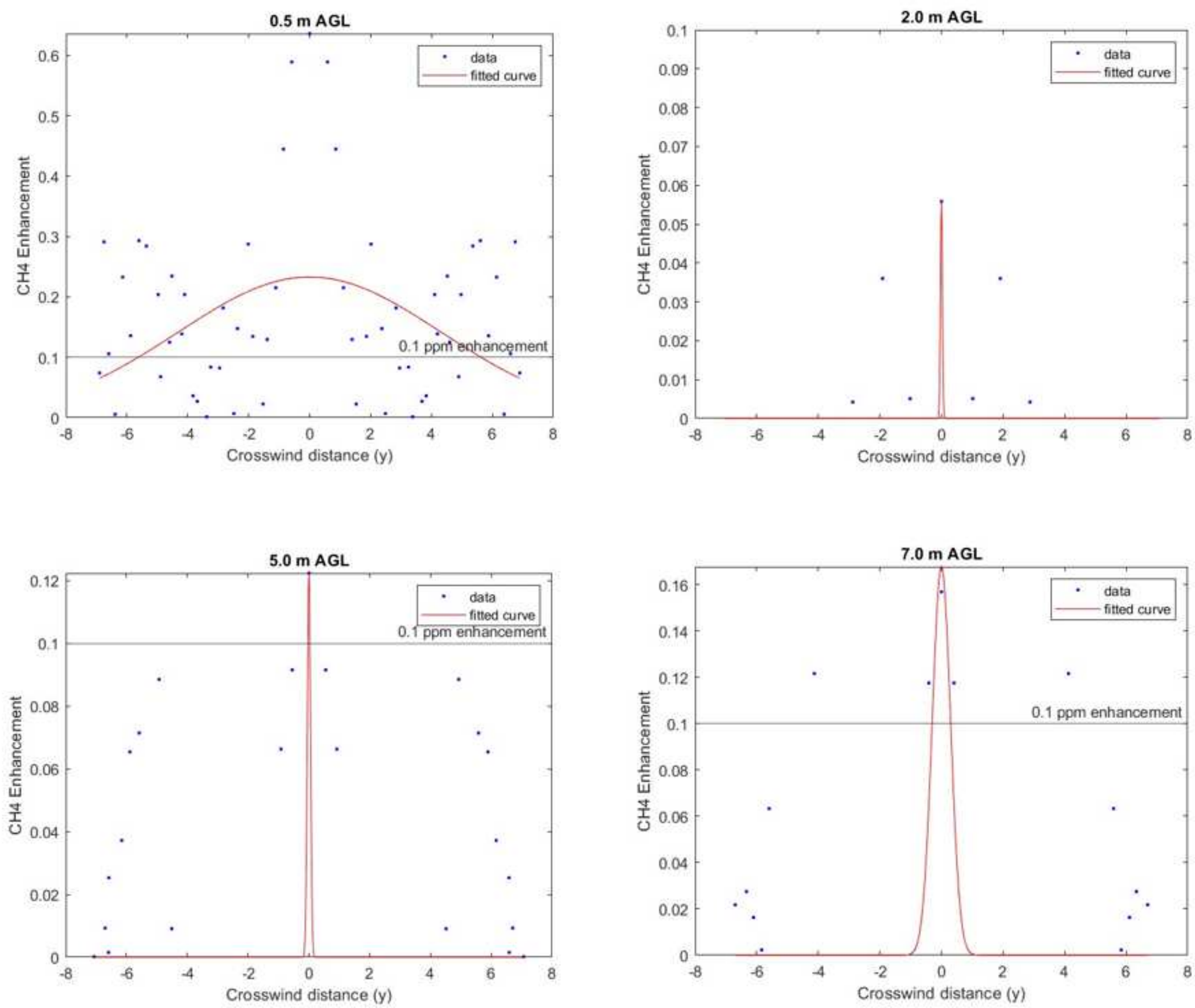

Figure A31 Plumes for Experiment 6, PGSC B-C

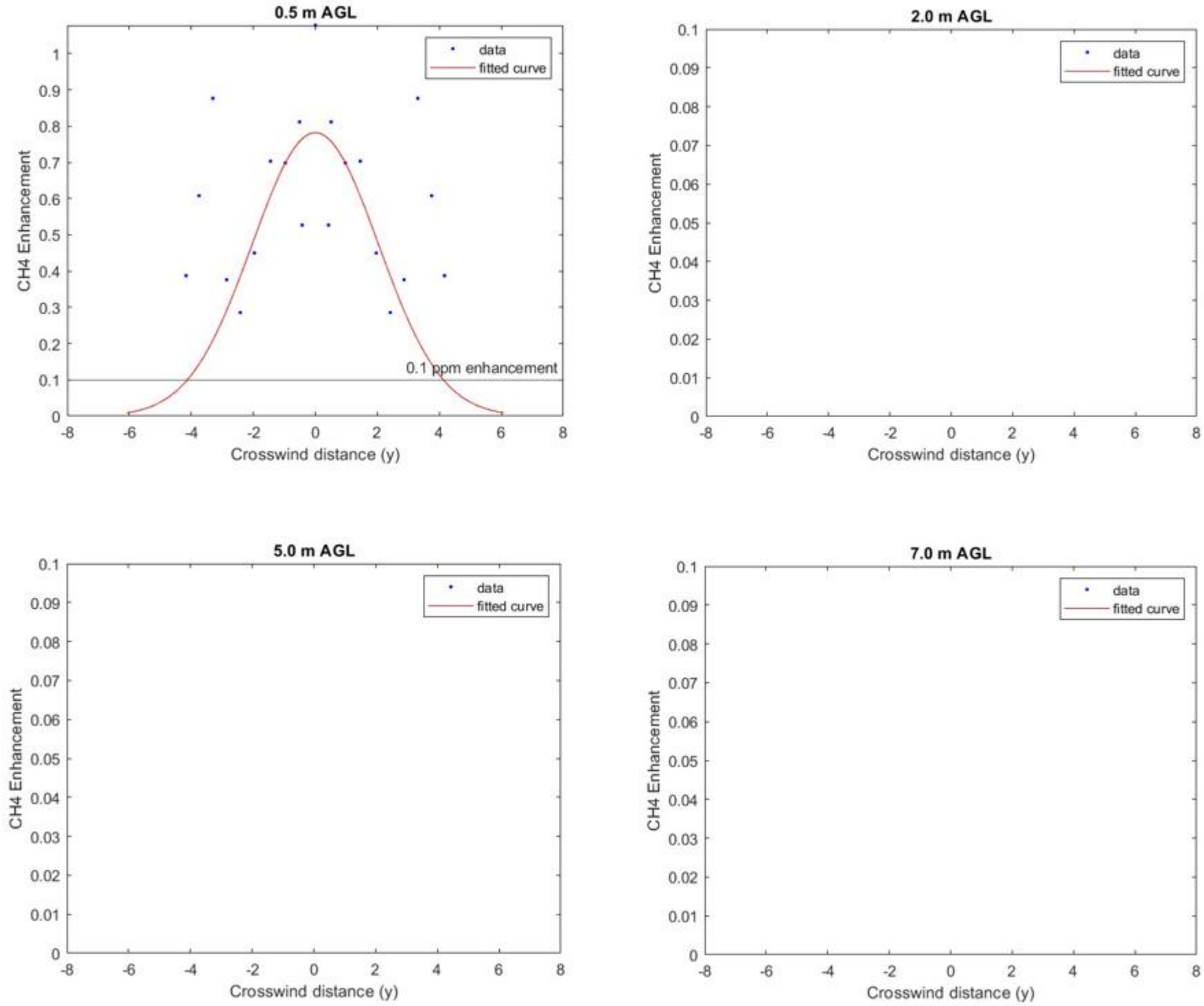

Figure A32 Plumes for Experiment 6, PGSC E-F

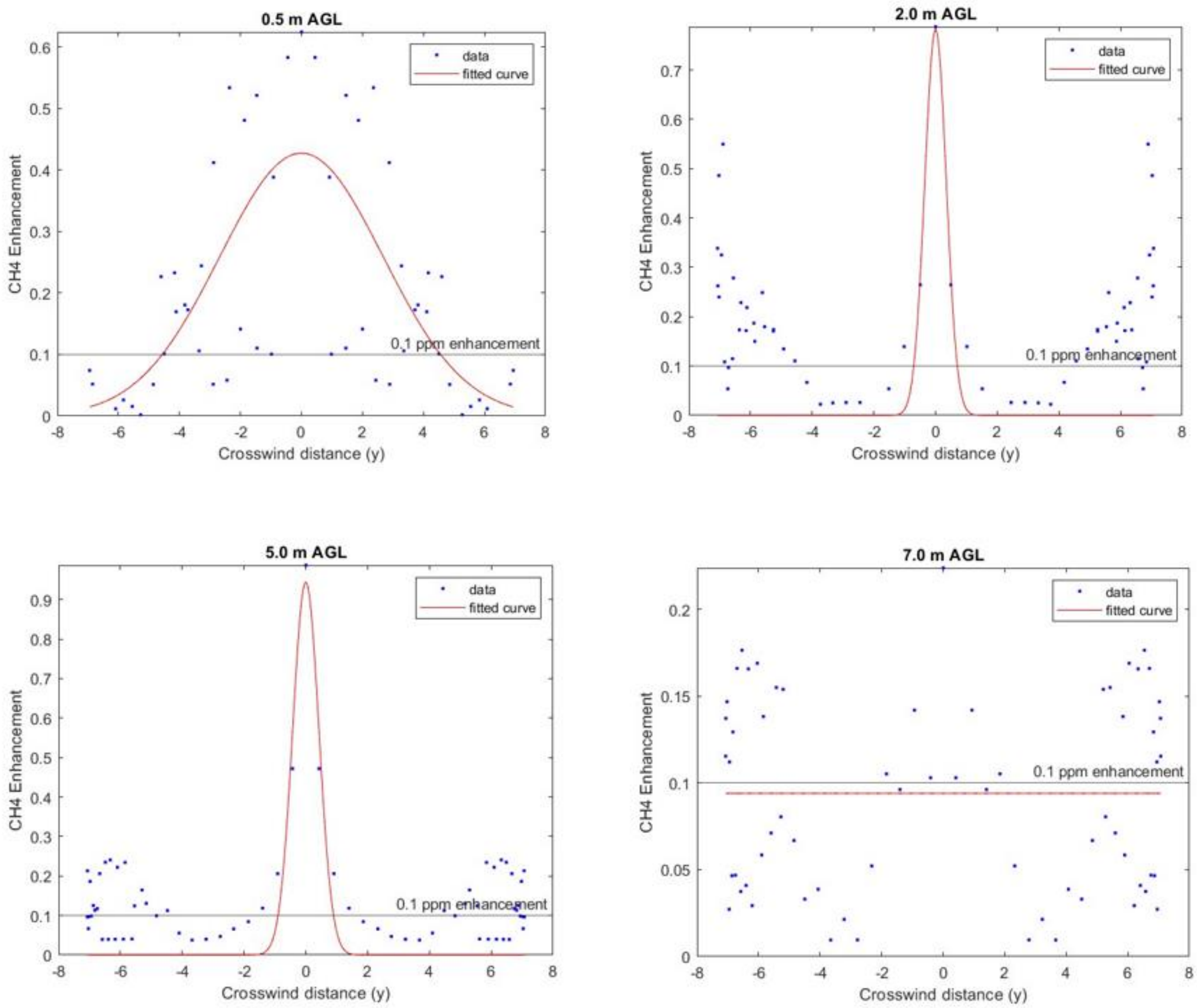

Figure A33 Plumes for Experiment 7, PGSC A

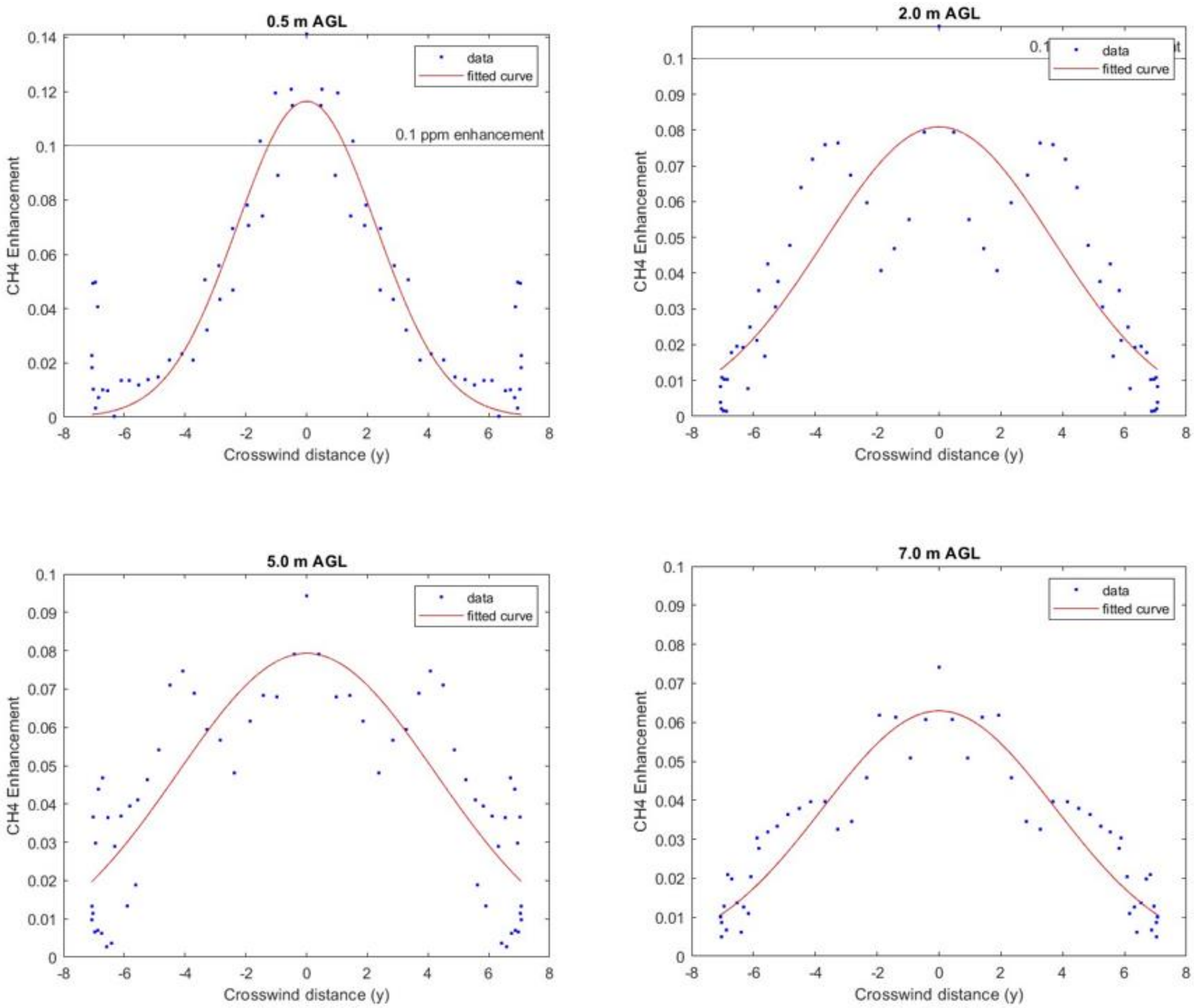

Figure A34 Plumes for Experiment 7, PGSC B-C

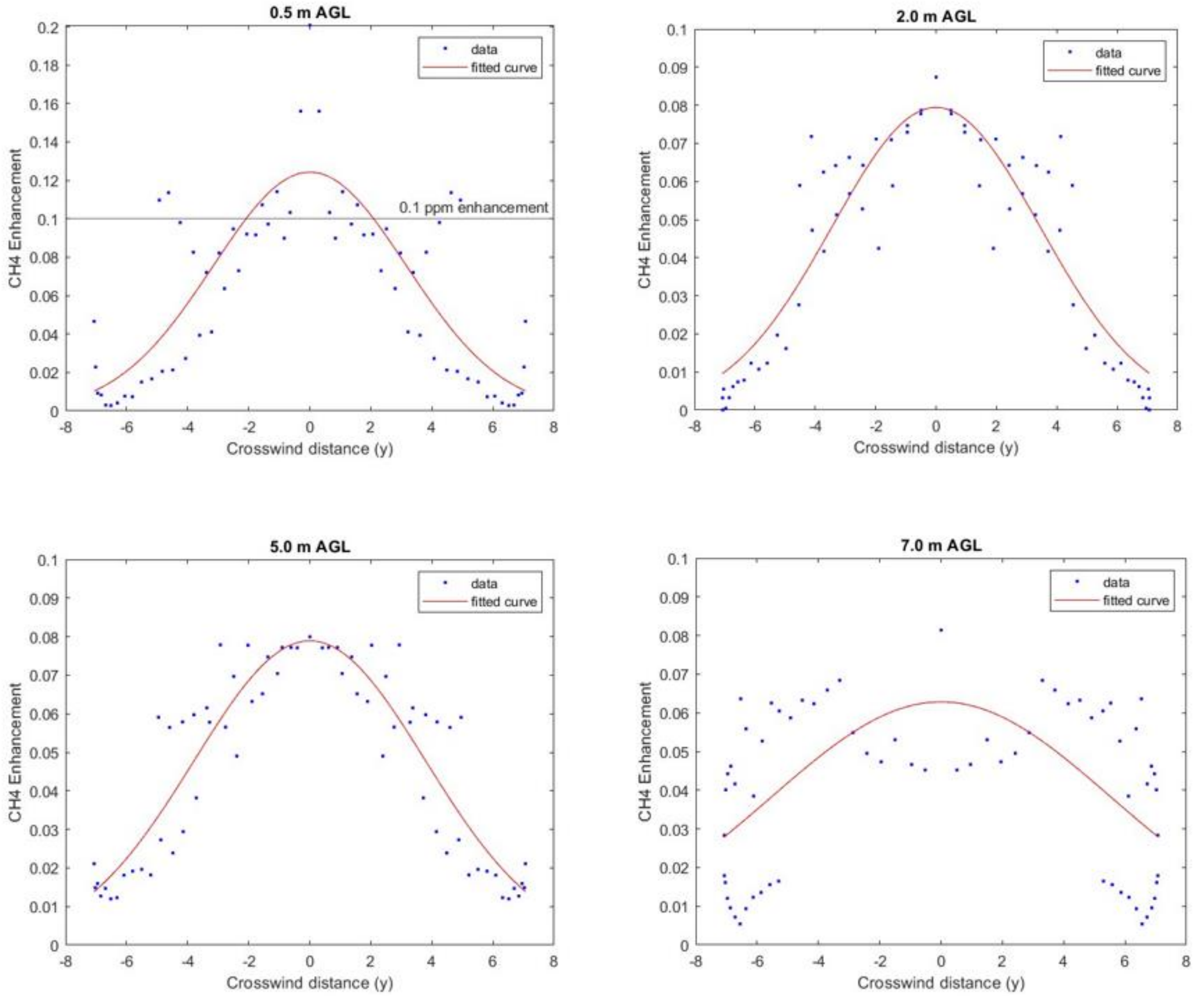

Figure A35 Plumes for Experiment 7, PGSC E-F

A3.3 Experiment 3-72 hours

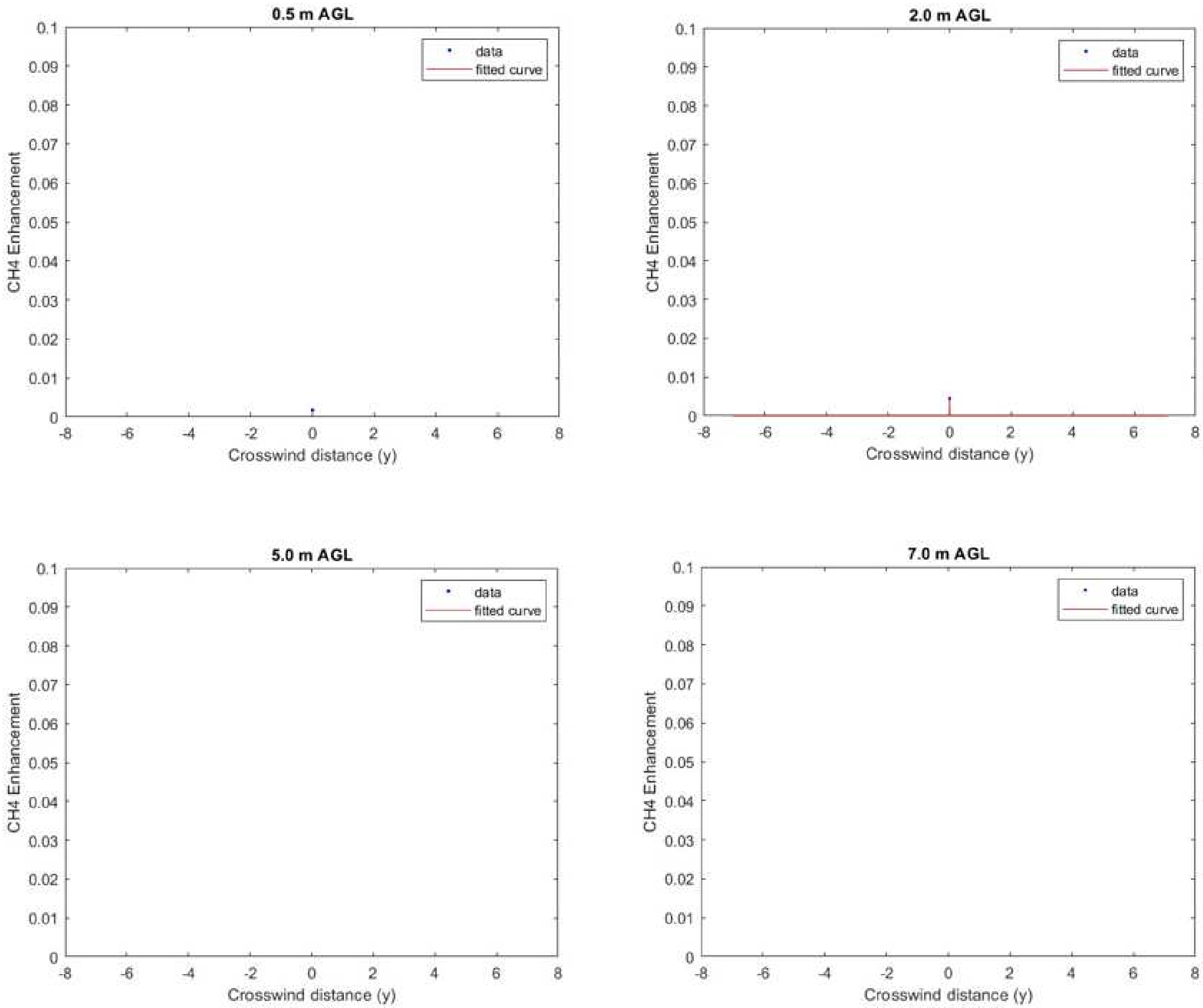

Figure A36 Plumes for Experiment 3-72 hours, PGSC D

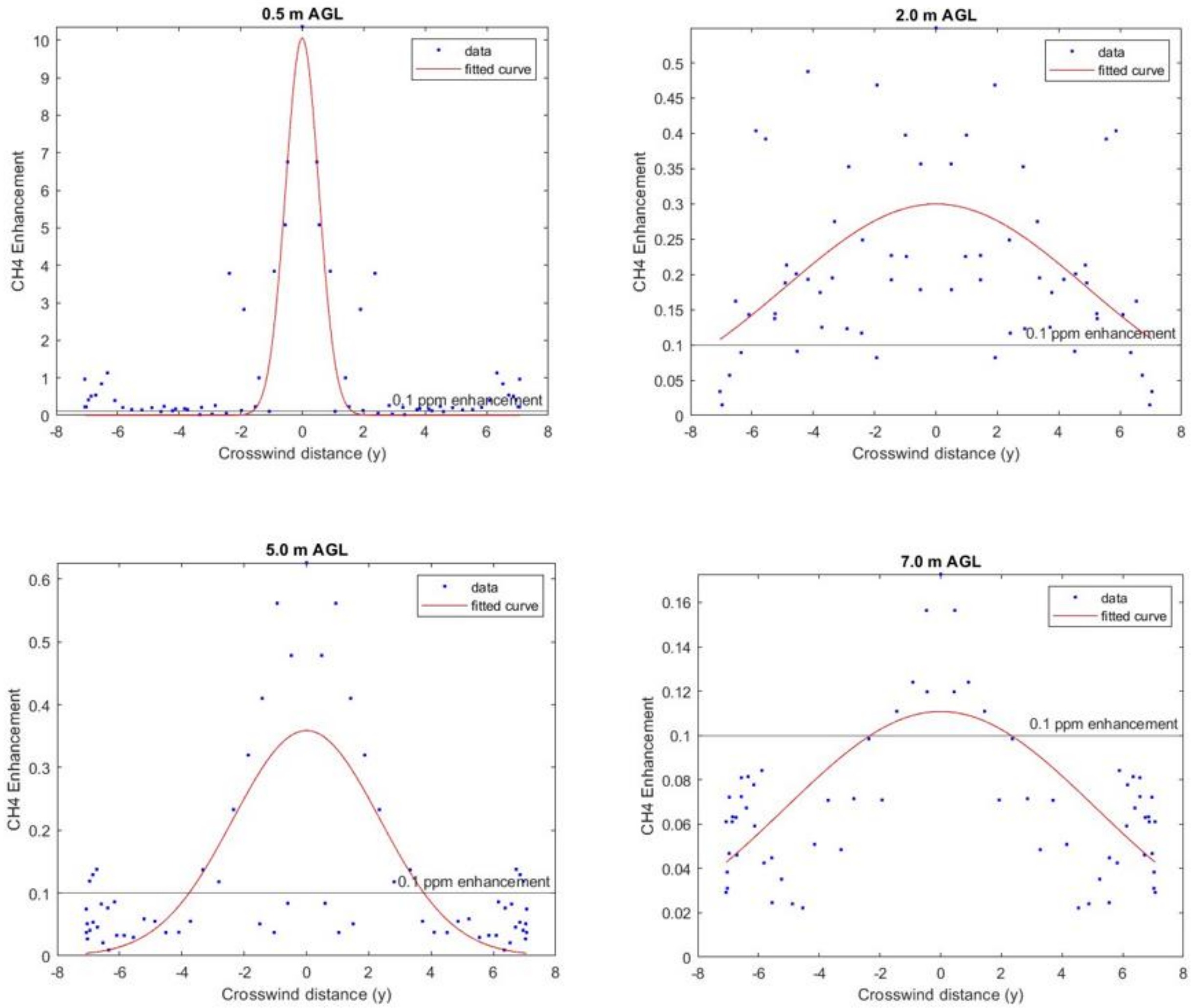

Figure A37 Plumes for Experiment 3-72 hours, PGSC A

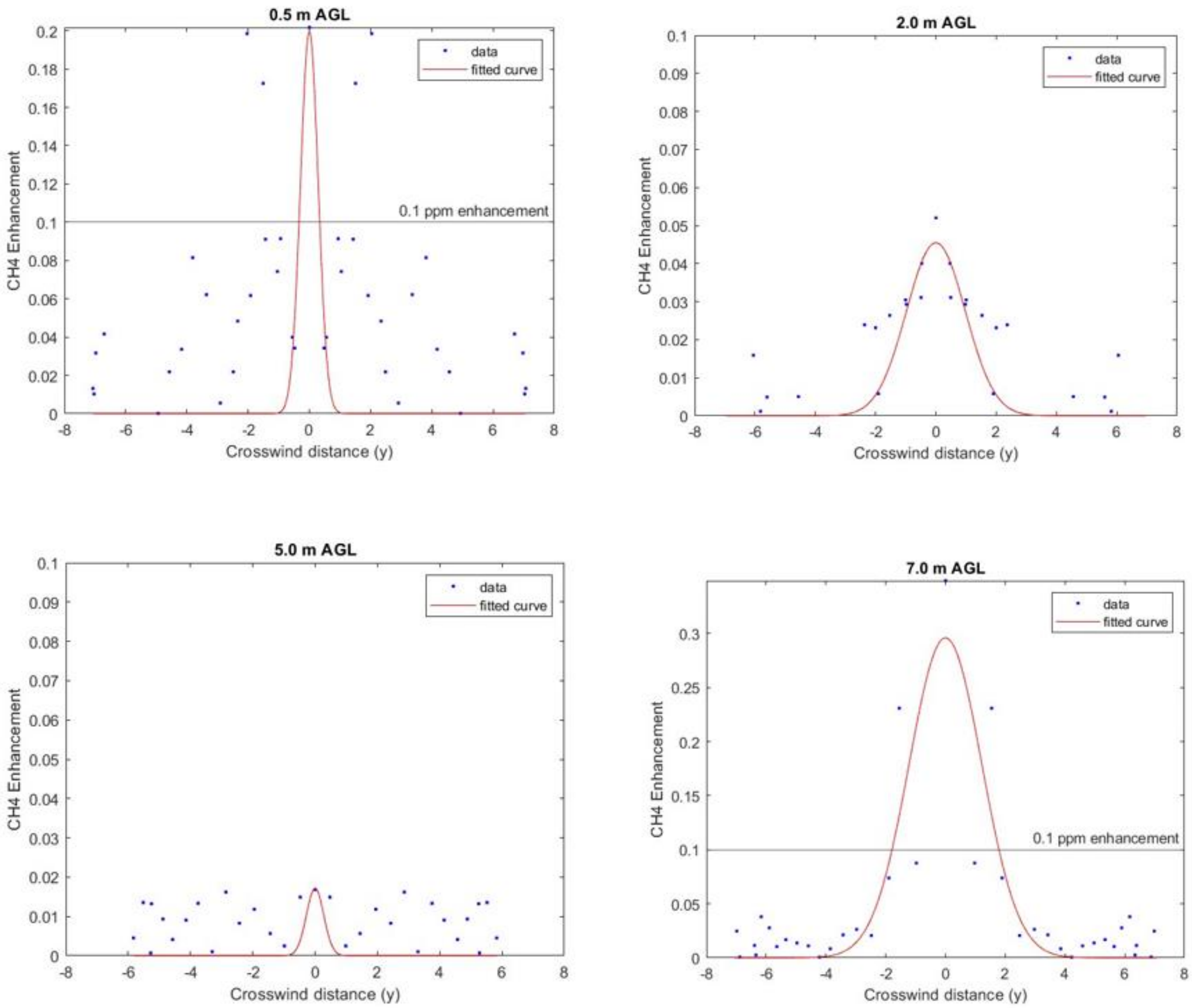

Figure A38 Plumes for Experiment 3-72 hours, PGSC B-C

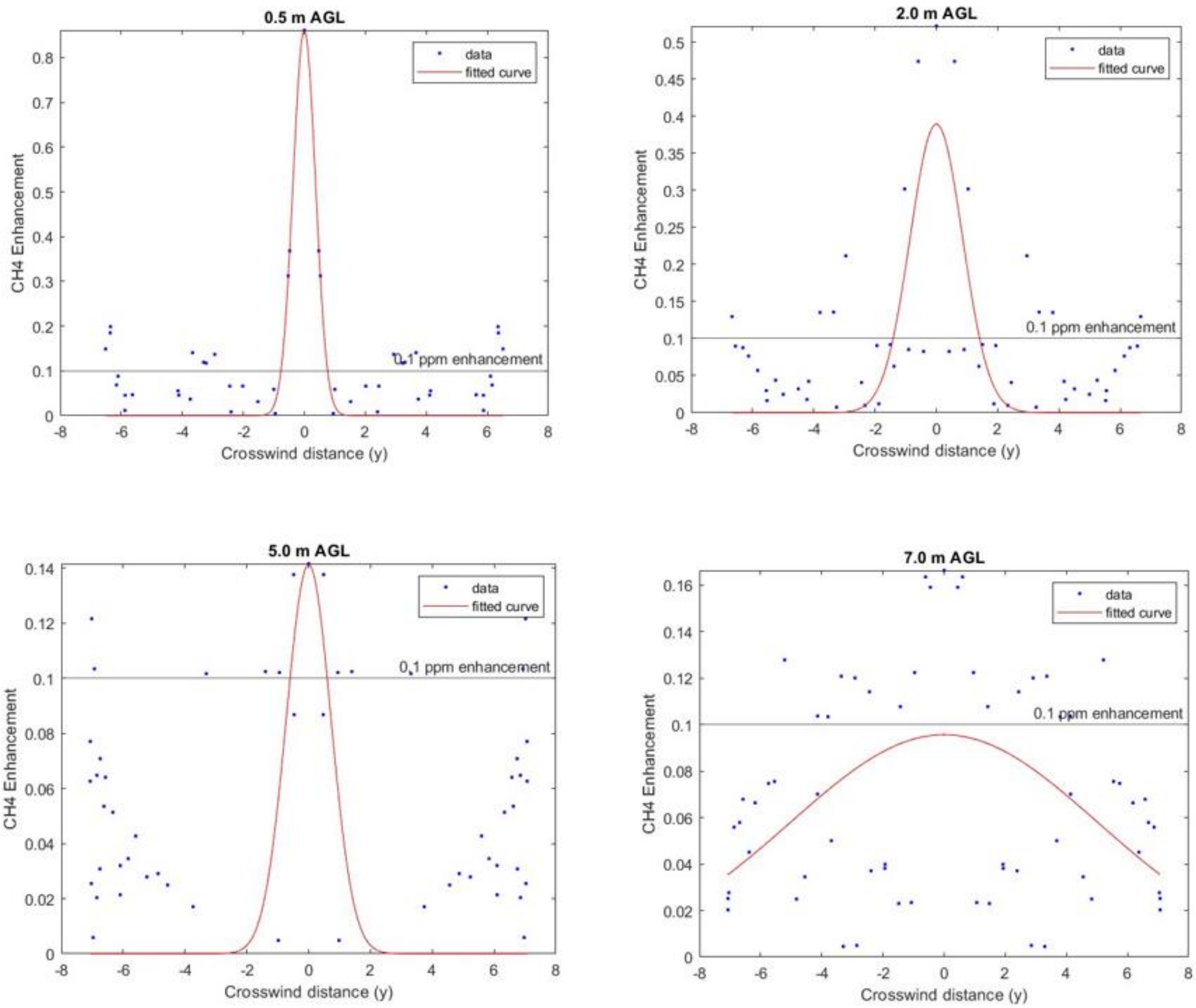

Figure A39 Plumes for Experiment 3-72 hours, PGSC E-F

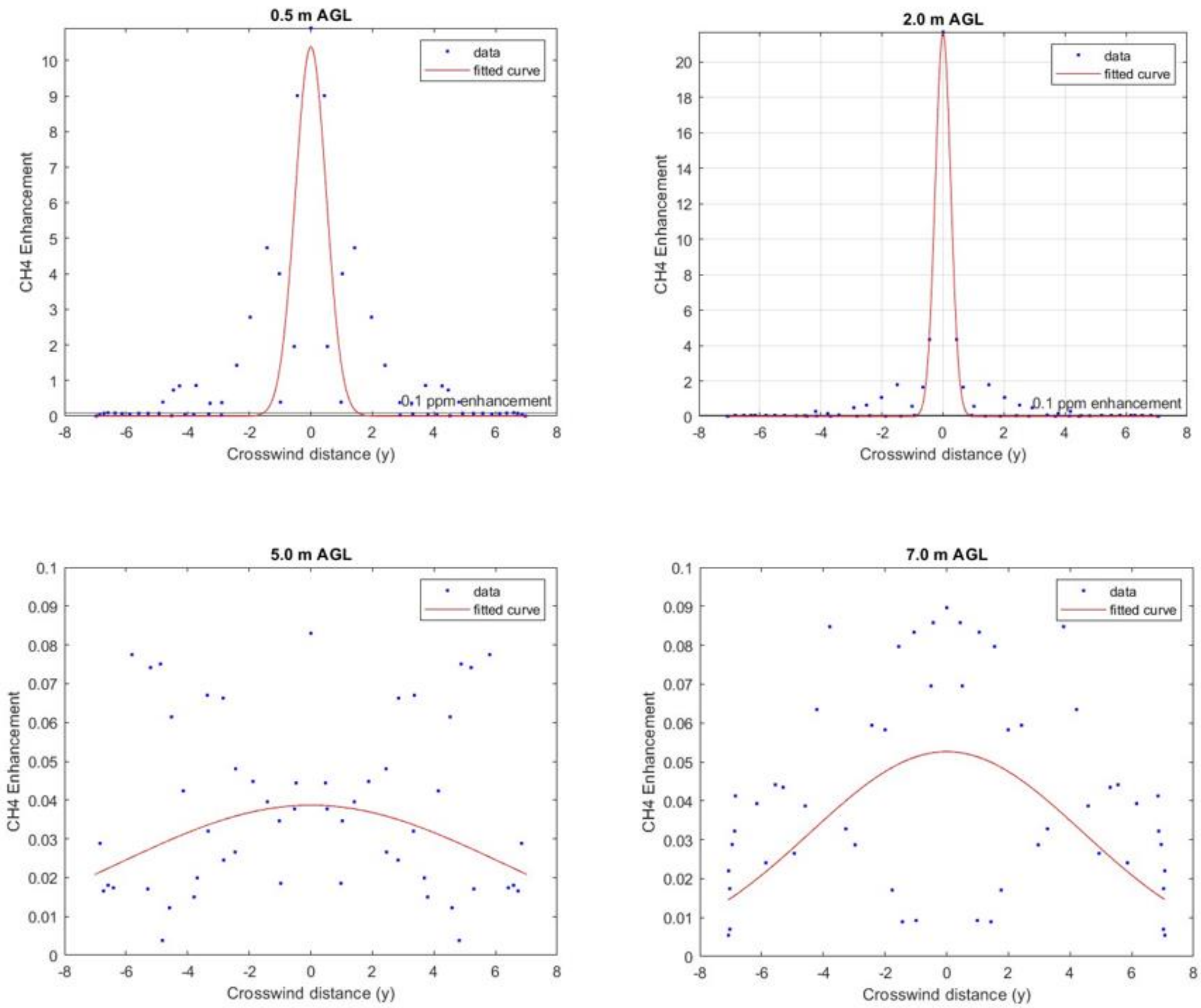

Figure A40 Plumes for Experiment 3-72 hours, PGSC G

A4 Generalized linear model (GLM)

A4.1 General linear model equation

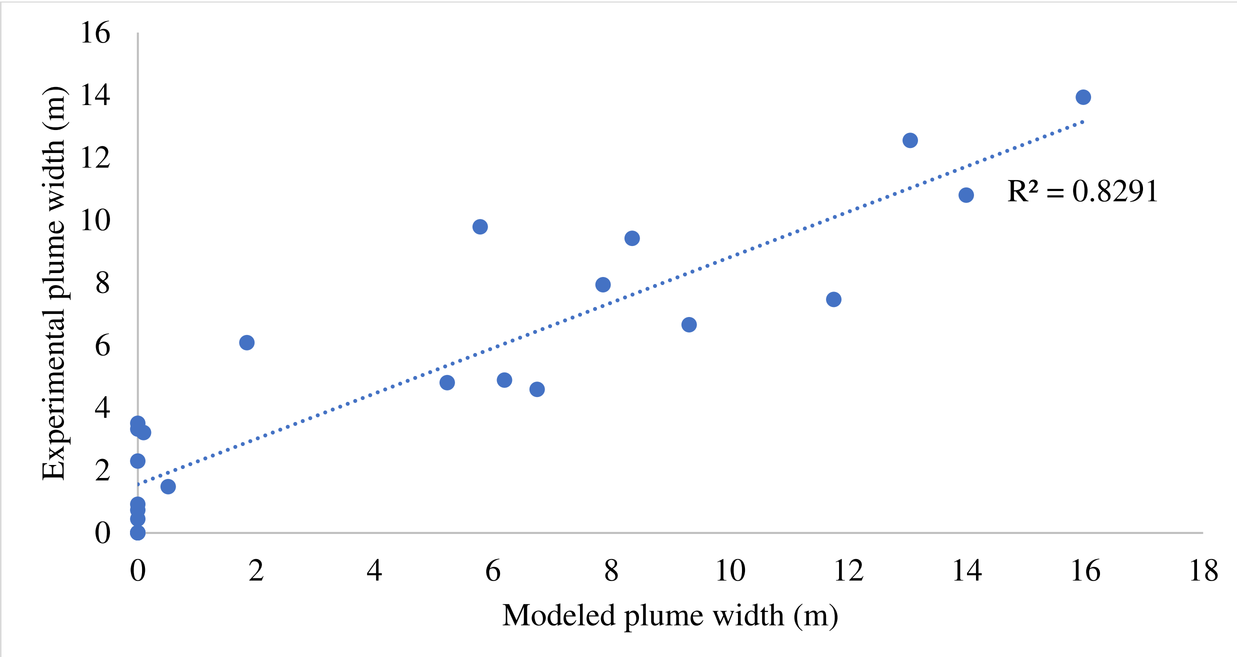

Figure A41 Experimental vs. modeled plume width

A4.2 Gas compositions of different flowlines/gathering lines

Table A2 Gas compositions of largest production basins in the USA (Kennedy, 2015). G denotes the percentage gas composition. V denotes the volumetric flow rate (slpm) of each component based on a total gas emission of 10 slpm, and ρ is the gas density (g/L).

		CH_4	C_2H_6	C_3H_8	C_4H_{10}	C_5H_{10}	C_6H_{12}	C_7H_{14}	NG density
Fayetteville Shale, Arkoma Basin***	G (%)	97.3	1.0	0	0	0	0	0	
	V (slpm)	9.73	0.1	0	0	0	0	0	
	ρ (g/L)								0.66
Haynesville Shale, North Louisiana Salt Basin***	G (%)	95	0.99	0	0	0	0	0	
	V (slpm)	9.5	0.1	0	0	0	0	0	
	ρ (g/L)								0.66
Barnett Shale, Fort Worth Basin**	G (%)	88.4	5.0	2.2	1.0	0.4	0.22	0.08	
	V (slpm)	8.84	0.5	0.22	0.1	0.04	0.022	0.008	
	ρ (g/L)								0.75
Marcellus Shale, Appalachian Basin*	G (%)	80.8	11.0	4.1	1.6	0.7	0.8	0	
	V (slpm)	8.08	1.1	0.41	0.16	0.07	0.08	0	
	ρ (g/L)								0.83
Permian, Permian****	G (%)	66.3	13.4	10.3	4.7	1.7	1.0	0	
	V (slpm)	6.63	1.34	1.03	0.47	0.17	0.1	0	
	ρ (g/L)								1.01

A4.3 Effect of gas density on plume width compared to leak rate and depth

$$\Delta\frac{W}{\rho} = -34.8$$

$$\Delta\frac{W}{r} = -1.29$$

$$\Delta\frac{W}{d} = -31.1$$

$$\Delta\rho = -0.04\Delta r$$

$$\Delta\rho = -0.89\Delta r$$

A5 Methane Oxidation

Methane oxidation by methanotrophic bacteria is a phenomenon that has been tested. Methanotrophs have unique ability to grow on CH_4 as their sole source of carbon and energy (Murrell, 2010). Methanotrophs oxidize CH_4 in aerobic and anaerobic environments. The enzyme responsible is CH_4 monooxygenases (MMOs). The lack substrate specificity results in the fortuitous metabolism of a very large number of compounds including xenobiotic chemicals. MMOs utilize two reducing equivalents to split the O-O bonds of dioxygen. 1 O_2 atom is reduced to form H_2O, and the other incorporated into CH_4 forming CH_3OH (Hanson & Hanson, 1996). The required power for CH_4 metabolism is produced by oxidation of formaldehyde to CO_2.

A6 List of abbreviations and acronyms

NG	Natural gas
US	United States
EIA	Energy Information Administration
IEA	International Energy Agency
PHMSA	Pipeline and Hazardous Materials Safety Administration
CH_4	Methane
C_2H_6	Ethane
C_3H_8	Propane
C_4H_{10}	Butane
C_5H_{12}	Pentane
C_6H_{12}	Hexane
CO_2	Carbon dioxide
GWP	Global warming potential
THC	Total hydrocarbon
LDAQ	Leak detection and quantification
AGL	Above ground level
METEC	Methane Emissions Technology Evaluation Center
UAVs	Unmanned aerial vehicles
ROWs	Rights-of-way
PGSC	Pasquill-Gifford stability class